Orthopädische Klinik und Poliklinik, Universitätsmedizin Rostock

(Direktor: Prof. Dr. med. Wolfram Mittelmeier)

Electro-stimulating Implants for Bone Regeneration:

Parameter Analysis and Design Optimization

Dissertation

zur Erlangung des akademischen Grades

Doctor rerum humanarum (Dr. rer. hum.)

der Medizinischen Fakultät der Universität Rostock

vorgelegt von

Yukun Su, M.Sc.

geb. in Gansu, China

Rostock, 12. 2015

Tag der Einreichung: 23.12.2015
Tag der Verteidigung: 16.05.2017

Gutachter

Prof. Dr. med. Dipl.-Ing. Rainer Bader, Universitätsmedizin Rostock

Univ.-Prof. Dr. med. Thomas Mittlmeier, Universitätsmedizin Rostock

Priv.-Doz. Dr. med. Dr. phil. Maik Stiehler, Universitätsklinikum Carl Gustav Carus Dresden an der Technischen Universität Dresden

Contents

1   Introduction

Bone regeneration is a complex physiological process of bone formation and it is involved in continuous remodelling throughout adult life. It can be seen during normal fracture healing. However, when the regenerative process is compromised, bone diseases, like avascular necrosis, atrophic non-unions and osteoporosis may occur. Electrical stimulation therapy is considered as one of common methods to enhance an insufficient bone regeneration process.

1.1   Motivation

Electrical stimulation is a method that introduces electric fields into target bone sites to heal bone fractures and other bone diseases, such as avascular necrosis of the femoral head. It has been used as an orthopaedic bone healing treatment more than several years. Both, invasive and non-invasive electrical stimulations are used as an adjunct to enhance bone regeneration. Non-invasive electrical stimulation generates a weak electrical current within the target bone site using either pulsed electromagnetic fields, capacitive coupling, or combined magnetic fields. Invasive electrical stimulation needs to surgically implant electrodes in the bone and the cathodes are located at the target bone site.

Electrical stimulation has also been found to be an effective tool for bone healing in various orthopaedic conditions such as aiding internal and external frication [1], enhancing delayed or non-union fractures [2] and osteotomies [3], improving the efficacy of bone grafts [4], treating fresh fractures [5], and aiding femoral osteonecrosis [6]. It has been found that applying electric fields can regulate the expression of genes in connective tissue cells for structural extracellular matrix (ECM) proteins and increase production of cartilage and bone [7].

Although electrical stimulation is successfully applied in many clinical situations and has become a common therapy for bone healing, the understanding of its mechanisms of action in the bone is still not well studied. Moreover, the knowledge on the effects of the electro-stimulating implant parameters and electrical stimulation parameters, including implant size, electric potential, signal wave form and frequency, on the bone regeneration is also still scarce, as well. Experiments in vitro and in vivo, both in animal and human, are used to get a deeper understanding of these mechanisms and effects. In recent years, due to advances in computational methods development numerical simulation of bone electrical stimulation draws attention to predict the effect of bone electrical stimulation.

The widely used computational methods are finite element method (FEM) and finite integration method (FIT). Medical image processing and computer aided design (CAD)

software help to reconstruct the computational models. Measurements of the electric properties of bone tissue support the numerical simulation for bone electrical stimulation.

1.2 Aim of the dissertation

The aim of this dissertation is to analyse relevant parameters of electro-stimulating implants and their respective impact on bone regeneration in order to optimize the implant's design and stimulating parameters. Analysis and optimization will be approached through computational simulations. Hence, numerical simulation software is used to analyse the electric field distribution in relevant bones. Furthermore, optimization software is used to optimize the design of the implant. The aim of the dissertation is reached in three different sections, numerical simulation in the human femoral head, in cell experiments and in animal testing.

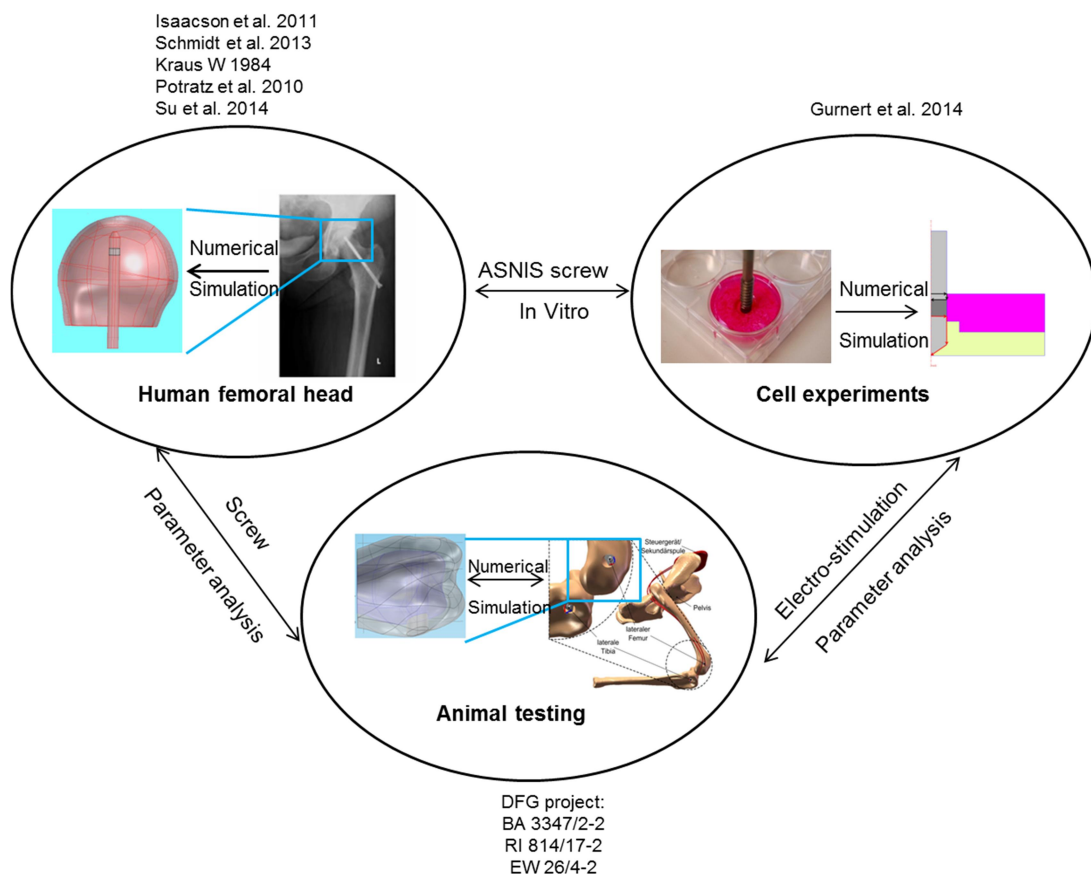## 1.3 Structure of the dissertation

Fig. 1.1 Concept for the dissertation

Figure 1.1 shows the concept of this dissertation. There are three different sections:

numerical simulation in the human femoral head, cell experiments and animal testing. The first section analyses how the screw implant's parameters influence the electric field distribution in the human femoral head. Bone cell experiments should investigate electro-stimulation parameters for different electrostimulative implants, such as screw implants for the human femoral head and specifically designed implants for animal testing. Animal testing should evaluate electro-stimulation parameters and implant parameters in animal bones in order to see their impact on bone regeneration.

The main contributions in these three sections are listed below.

In the human femoral head

- First, evaluation of the electric field distribution caused by the Asnis s-III series screw in the human femoral head
- Optimized screw implant position in the human femoral head

In cell experiments

- First, using numerical simulation in cell experiment design and validating the model
- Presenting a convenient method to optimize the cell experiment design

In animal testing

- Using numerical simulation to design animal electrostimulative implant
- Automatically calibrating animal bone dielectric properties at 20 Hz

In chapter 2 the basis of bone regeneration and bone electrical stimulation is introduced. The bone structure and bone remodelling, three different bone electrical stimulation methods including direct current, capacitive coupling and inductive coupling stimulation are reviewed in detail. This dissertation is based on one clinical study that uses the Asnis III s-series screw system to treat avascular necrosis in the patients' femoral head. Therefore, the Asnis III s-series screw system is explained in detail, and human femoral anatomy, bone disease, avascular necrosis in femoral head, are also elucidated.

Chapter 3 introduces the background of bone electrical stimulation modelling. Maxwell's equations and electro-quasistatic (EQS) equation used for electric field calculation, FEM, bone dielectric properties and model generation are explained specifically. As an example, the human femoral head modelling is presented.

In chapter 4, the numerical simulation of bone electrical stimulation in the human femoral head is introduced. The Asnis III s-series screw parameters in the human femoral head according to clinical study are numerically analysed. First, the femoral model used in simulation is experimentally validated and the electric field distribution in the bone depending on different implant parameters is evaluated. Then, the automatic approach to find an optimized implant position in the human femoral head is also presented. The limitations and

an outlook are also discussed.

In chapter 5, the numerical simulation of bone electrical stimulation in the vitro testing is shown. Three systems for cell experiments are introduced in this chapter. The vitro testing setup for the Asnis III s-series screw in clinical study of human femoral head is also experimentally validated for simulation. The electric field distribution in chamber setup is numerically analysed and the design of the vitro testing setup for electro-stimulating implant in the animal testing is optimized.

Chapter 6 introduces numerical simulation in the animal testing. Two designs of the electro-stimulating implants are numerically compared according to the electric field distribution on the surface of the electrodes and an optimized one is suggested. Dielectric properties of one animal bone are automatically calibrated and the procedure is explained in detail. The automatic approach and the implant designs are discussed and a short outlook for the animal testing is presented.

2 Electrical stimulation of bone regeneration

2.1 Bone properties and bone regeneration

Bone tissue is specialized connective tissue in the body. It is made mostly by collagen and it contains almost all the calcium of the body. Collagen is a protein that provides a soft framework, and calcium phosphate is a mineral that adds strength and hardens the framework. With the combination of collagen and calcium, bone can support functional organs, protect highly sensitive body parts and resist load.

There are two types of bone in the human body – cortical and cancellous. Cortical bone, synonymous with compact bone, is denser, harder, stronger and stiffer than cancellous bone. It facilitates the bone's main function and accounts for up to 80 percent of the weight of a human's skeleton. It can mostly be found in the shaft portion of long bone, such as bones in the arms and legs. Additionally, it can also be found in the outer shell around the cancellous bone at the end of the joints. Cancellous bone (trabecular bone) forms the inner layer of the bone and has a spongy, honeycomb-like structure. It can be found on the edges of long bones, such as femur. Although cancellous bone is not as hard as cortical bone, it is more flexible and it is really useful in the joint bones. Most importantly, it contains many blood vessels and red bone marrow. The red marrow in cancellous bone supplies osteoprogenitor cells and helps the new bone to form and grow.

In 1892, Julius Wolff first proposed that bone adapts its structure accordingly to bone loading [8]. This bone adaptation function principle is named 'Wolff's Law'. It can be found in bone growth [9], after fracture healing [8], and in implant incorporation [10]. During bone adaption, bone is due to continuous resorption and formation. Frost defined these two processes as bone modelling [11] and bone remodelling [12], respectively. Modelling and remodelling are based on the separate actions of bone resorbing cell osteoclasts and bone forming cells called osteoblasts. At the cellular level, bone modelling and bone remodelling do not have many differences. The remodelling starts from a quiescent bone surface with the appearance of osteoclasts. Osteoclasts have been shown to be able to damage mineralized bone under physiological conditions. They are large multinucleated cells that form by fusion of mononuclear precursors of haematopoietic origin [13]. To resorb the bone tissue, osteoclasts first attach to the bone matrix and form a ruffle border at the bone interface that is completely surrounded by a 'sealing zone'. In this way, the osteoclast creates an isolated microenvironment. Subsequently the osteoclast acidifies the micro-environment and dissolves the organic and inorganic matrices of the bone [14]. Shortly after the bone resorption is accomplished, osteoblasts appear at the same surface site. Osteoblasts derive from mesenchymal stem cells in the bone marrow, periosteum and soft tissue. They are

specialized bone forming cells. After synthesizing bone matrix and regulating mineralization, finally they differentiate to osteocytes, mature bone cells. The growth factors which influence the bone modelling and remodelling are platelet derived growth factor (PDGF), insulin-like growth factor (IGF), bone morphogenetic protein (BMP) and transforming growth factor beta (TGF /ß) [15-18]. Once the resorption process is finished by osteoclasts, the growth factors are released into the bone fluid to activate osteoblasts to refill resorption cavities.

Unlike in other tissues, the majority of bony injuries (fractures) can heal with no scar, because bone can be regenerated with its pre-existing properties largely restored, and the newly formed bone is eventually indistinguishable from the adjacent uninjured bone [19]. Although bone can be regenerated by itself during the lifetime, there are still some cases where bone regeneration is required in large quantity. For example, skeletal reconstruction of large bone defects caused by trauma, infection, tumor resection and skeletal abnormalities, as well as in the case of compromised bone regeneration, like avascular necrosis or osteoporosis [20]. There are lots of different ways which can be used either alone or in combination for augmenting the impaired or insufficient bone regeneration process. The standard approaches which are widely used in clinical practice are distraction osteogenesis and bone transport [21,22], and different bone graft methods, such as autologous bone grafts, allografts, and bone-graft substitutes or growth factors [23]. In addition, non-invasive methods, such as low intensity pulsed ultrasound and pulsed electromagnetic fields (PEMF), are also commonly used to enhance bone regeneration [24].

2.2   Avascular necrosis in the human femoral head

In this dissertation, one of the electrical stimulation systems combining with bone graft is introduced to treat early stages of avascular necrosis in the femoral head. For clarity, a brief introduction of avascular necrosis is given in this section, including etiology, methods of diagnosis, classification and treatments.

Avascular necrosis, often named osteonecrosis, is a bone disease caused by death of bone cells. It primarily affects weight-bearing joints. Figure 2.1 shows a picture of avascular necrosis in the femoral head. It is clear to see that the fatty tissue, necrotic lesion, in the femoral head causes bone collapse in the femoral head. Typically it occurs in young patients between the age of twenty to forty [25].

Besides traumatic causes such as subcapital fracture or hip dislocation, the exact factors that affect the progression of avascular necrosis in the femoral head are still not fully understood. One of the most common risk factors for avascular necrosis of the femoral head is the use of corticosteroids [26]. But the corticosteroid dose of use that becomes a risk is still disputed. Many reports show evidence of a corticosteroid dose-related risk of avascular necrosis for

the femoral head in patients with severe acute respiratory syndrome (SARS) [27] and renal transplant [26]. Moreover, smoking and alcohol have also been implicated a risk factors for avascular necrosis of the femoral head [28].
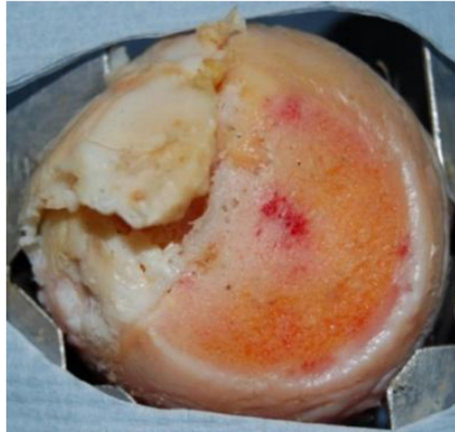

Fig. 2.1 Avascular necrosis in the femoral head – bone turns to fatty tissue and collapses.

Compared to other radiographs, magnetic resonance imaging (MRI) is the best diagnostic method for avascular necrosis in the human femoral head, because MRI is particularly sensitive to the soft tissue structures in the body and it is a safe technique without radiation. It has been found to be 99% sensitive and 89% specific for avascular necrosis in the femoral head [29]. In figure 2.2, avascular necrosis in the patient's femoral head was detected by MRI. The abnormal dark areas in the femoral heads (red circles) are the necrotic lesions.
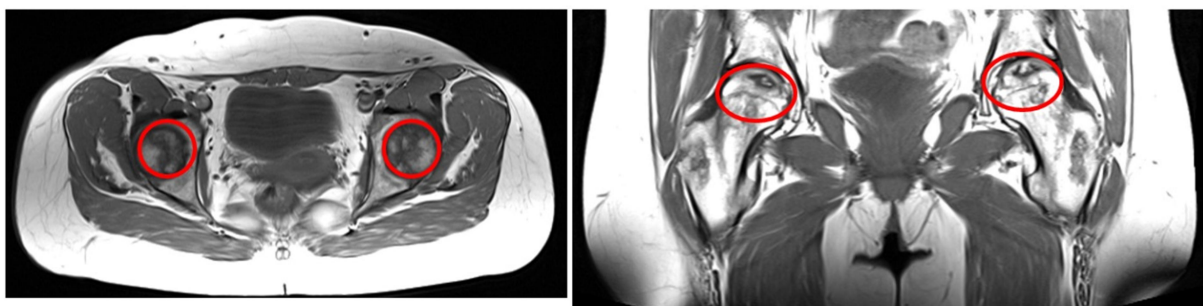
Fig. 2.2 MRI of avascular necrosis in patient's femoral heads, horizontal view (left) and lateral view (right). The areas in the red circle are femoral head, in which the dark black areas are necrotic lesions.

The treatment of avascular necrosis in the femoral head is based on the stage of the lesion. Before defining the stage, the volume of part of the femoral head involved in the necrotic lesion has to be calculated. Many reliable and reproducible methods have been described to measure the size of a lesion using MRI [30] or radiographs [31]. To evaluate the evolution of avascular necrosis, the Ficat classification [32] is commonly used. It describes a four stage (I

through IV) classification system based on standard radiographs. In Stage I the radiographs show normal. In Stage II the contour of the femoral head is normal but the radiographs show evidence of bone remodelling including cystic and sclerotic areas. Stage III involves flattening of the femoral head. In Stage IV, there is joint space narrowing with secondary degenerative changes in the acetabulum. Steinberg classification [30] is one of the common modifications of Ficat's. It expands the Ficat system by dividing Stage II into femoral with and without collapse or hip with acetabular involvement (Fig. 2.3). The missing parameters in Ficat classification, the size and location of the necrotic area, are extended in another modification, the Association Research Circulation Osseous (ARCO) classification [33].
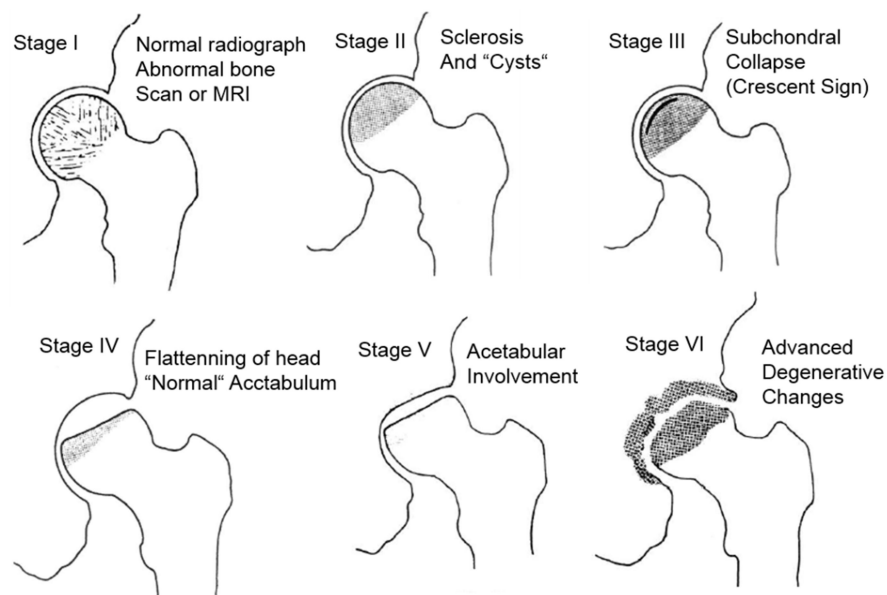
Fig. 2.3 Steinberg classification for avascular necrosis in the femoral head based on Steinberg [30].

According to the stage of the avascular necrosis, the treatment can be proposed differently. For the early stage of the avascular necrosis (less than Stage IV in Steinberg classification), the operative treatment includes core decompression [34], osteotomy [35], bone grafting [36] and electrical stimulation [37]. For the higher stages of avascular necrosis (Stage IV and higher in Steinberg classification) in the femoral head, limited femoral resurfacing arthroplasty or total joint replacement are indicated as the femoral head has collapsed and the hip joint has degenerated such that the articulation is compromised.

2.3   Bone electrical stimulation

Electrical stimulation is a common method used for bone regeneration. Electromagnetic

stimulation of bone fractures and other bone diseases, such as avascular necrosis of the femoral head, has been studied for more than half a century. The bone electrical stimulation theory has been summarized by Habel [38] into a simple schematic (Fig. 2.4). Exogenous bone mechanical deformation can transduce an endogenous electric field in the bone. As the electric potentials play an important role in early callus development and the remodelling stages of bone healing, the endogenous electric fields in the bone can inspire bone remodelling to regenerate the bone and accelerate bone growth.
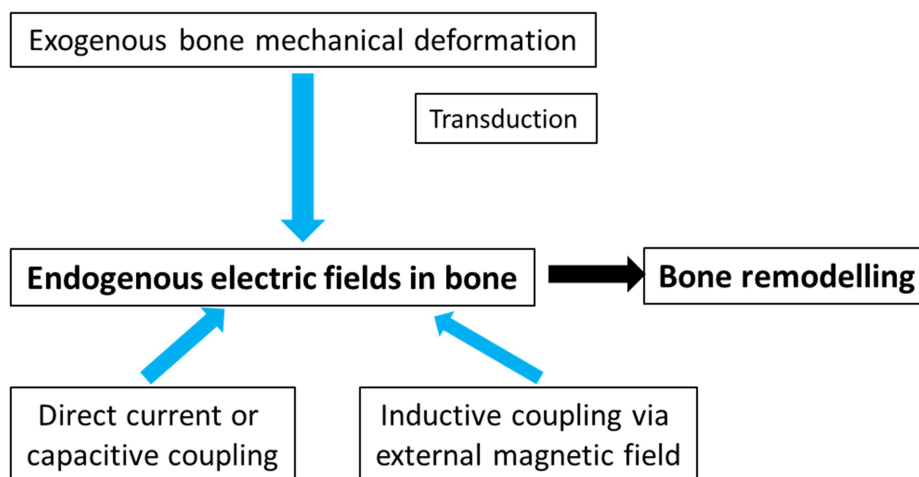

Fig. 2.4 Schematic of bone electrical stimulation theory based on Habel [38].

The underlying biological mechanism has been presented by many research groups. Fukada et al. in 1957 [39] revealed that bone has piezoelectric properties; i.e. stress-generated potentials, that can be created by the shear forces in the collagen. The compression side produces a negative potential, while the tension side has a positive potential [40]. Since 1957, the electric properties of bone material have been widely investigated. Friedenberg and Brighton [41] reported that a bio-electric potential can be generated by healthy bone. It is believed that electric signals in bone tissue is important in the bone modelling and remodelling [42,43]. The electric signals in the bone are generated either from piezoelectricity or from streaming potential. Experiments have shown that, the behaviour of bone cells can be influenced by externally applied electric energy [44]. Recently, Soda et al. [45] showed that applying low frequency electromagnetic fields on the bone can increase collagen synthesis in osteoblasts. Aaron et al. [7] reported that electric and electromagnetic fields can regulate the expression of genes in connective tissue cells for structural extracellular matrix proteins. Hence, using electrical stimulation can lead to the production of more bone-forming cells by the osteoprogenitor cells [46]. Consequently, bone healing can be accelerated by augmenting the development of extracellular matrix.

Basically there are three ways to therapeutically induce electric current into bone, direct current (DC), capacitive coupling (CC) and inductive coupling (IC).

2.3.1   Direct current (DC)

DC is an invasive technology [47], which involves the surgical placement of electrodes (Fig. 2.5). A cathode is placed at the site of the bone defect and an anode is in the soft tissue nearby [48]. The advantage of using DC for bone stimulation is the constant stimulation of the desired osseous area, with increased patient compliance, so that optimization of the position of the electrodes is possible over time [49] . Due to the invasive nature of the procedure, DC stimulation has a risk of infection and tissue reaction although bone growth has been demonstrated using direct current devices [50].
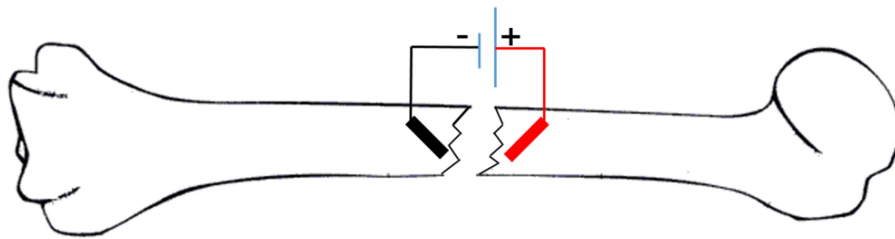

Fig. 2.5 Electrical stimulation method: DC using two electrodes and a battery. Two electrodes are implanted to the bone fracture area.

Osteogenesis has been shown to be stimulated at the cathode using currents between 5 and 100 μA and varying the number of electrodes between 2 and 4 [48]. The stimulator is implanted to the bone and the treatment is continuous until the bone healing occurred, then it will be removed. Although DC has the risk of bone infection, tissue reaction and soft tissue discomfort [51], an 86% clinical healing rate of nonunions after 16 weeks of use of DC has been reported by Brighton et al. [52]. In the patients who did not achieve union, the authors suggested that failure was due to either the proper placement of cathodes or the premature discontinuation of cast immobilization.

Many in vitro studies were carried on to illustrate the cell mechanism of action of DC. It is widely thought that DC stimulating osteogenesis by an electrochemical reaction at the cathode referred to as faradic products [48,53-60], which results in consumption of dissolved oxygen concentration and the pH value increased by the production of hydroxyl ions at the cathode [54]. Therefore, bone resorption is prevented and bone formation is increased by increasing osteoblast and decreasing osteoclast action [54]. Another faradic product which formed at cathode is hydrogen peroxide [54]. This enhances osteoclast differentiation [60]. The bone formation is triggered by the osteoblast due to the resorption by the osteoclasts. It

is also found that the DC's stimulatory effect may be due to an increase in growth factor synthesis by osteoblasts, in particular bone BMP -2,6,7 [59].

2.3.2 Capacitive coupling (CC)

In CC stimulation [61], electrodes are applied externally to the skin above the area to be stimulated. A power source is usually attached to the patients cast and connected to the electrodes to generate an electrical field within the fracture site (Fig. 2.6). The big advantage of CC is that it is non-invasive. Many studies showed evidence of successfully treating bone non-unions using CC. In [62], 77% successful fracture union by CC in 22 non-unions was found, in which, all the patients were treated for an average of 22.5 weeks without an effect on infection, previous recalcitrant non-union, or prior internal fixation hardware. One study showed that CC could also be safely used in athletes with stress fractures [63]. Aaron et al. [64] have found that the electric field from 1 to 100 mV/cm which generated from electric potential 1 to 10V at frequencies between 20 Hz and 20 kHz in CC, has shown to be efficient for bone stimulation. Even though, the therapeutic results depend on patient compliance. Due to the high voltages and frequencies in CC, it may cause irritation [65].
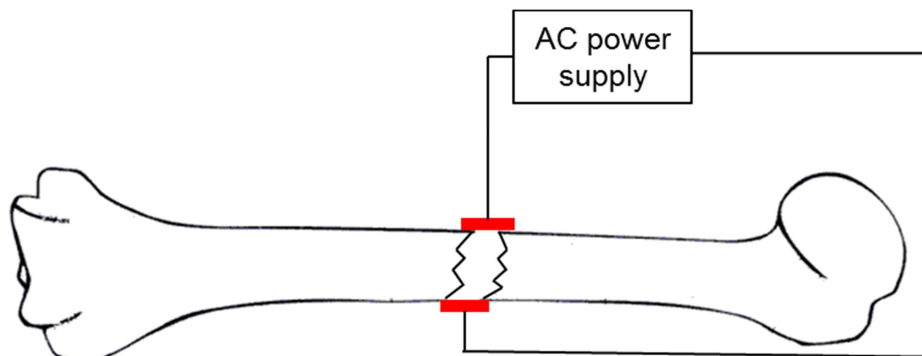

Fig. 2.6 Electrical stimulation method: CC using two capacitor plates.

Molecular pathways and growth factors have been shown in CC to enhance proliferation and differentiation of the osteoblast [66].The mechanism by which CC stimulates bone formation is commonly thought to be calcium translocation via voltage-gated calcium channels [66,67]. Calcium is unregulated by CC, which is important in bone healing because calcium has a role in the mineralization of bone and conducts the communication between cell surface receptors, antibodies, and hormones for DNA synthesis needed for bone healing [68].

2.3.1 Inductive coupling (IC)

In IC [69], often referred to as PEMF, a magnetic field is produced by forcing electric current through a wire coil placed over the lesion (Fig. 2.7). Bassett et al. [70,71] were the first to

report on the use of oscillating electromagnetic fields to treat non-unions. Pulsed electromagnetic fields can affect endochondral bone formation [72,73], connective tissue repair [74], osteoporosis [75,76], and various other conditions [77-80]. The frequency of PEMF devices for the bone healing is either at a relatively high frequency (1 – 10 kHz) or at relatively low frequency (1 – 100 Hz) [81]. The induced electric field at a low frequency (lower than 120 Hz) has been found to have has the most effect on bone modelling activity [82]. From the investigation of using a sinusoidal varying electric field to stimulate bone remodelling activity, the electric field frequency in the range of 15 to 30 Hz has been found to have remarkable sensitivity for preventing bone loss and inducing new bone formation [83]. However, negative results of electromagnetic stimulation tested on several animal models have been reported [63,84-86] and there is the continuing question of how particular waveform characteristics influence the biologic results [87].
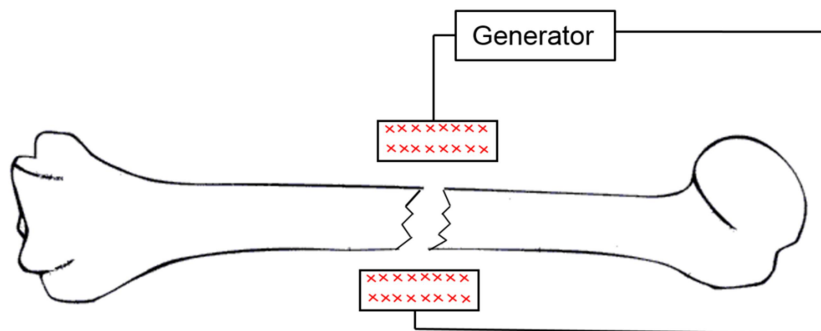

Fig. 2.7 Electrical stimulation method: IC using coils.

Kraus and Lechner developed an application of low frequency for PEMF. It consists of a primary coil at a frequency of 0.2 to 20 Hz with a magnetic flux of 2 to10 mT. The primary coil is located outside of the bone defect to stimulate bone regeneration [88]. The induced electric field in the bone from the primary coil is really low, smaller than 0.1 V/m, which has no significant stimulation effect on bone healing [89]. Therefore, the magnetic induced electrical stimulation system was presented to improve the bone healing outcome by Kraus and Lechner [89]. This system is based on the interplay of two coils and two electrodes. One coil is placed outside of the body where the two electrodes are implanted, the so-called external primary coil, and is used to generate the sinusoidal oscillating magnetic fields. The second coil is an implanted transducer coil, which is used to receive induced currents from the external alternating magnetic field and connected to two electrodes. One electrode was placed in the bone to be healed, and another one in the immediate proximity. Figure 2.8 shows the principle of the Kraus and Lechner system in treatment of avascular necrosis in the human femoral head. Two electrodes are designed as screws.

It has been found that the frequency refractures after leg lengthening can be diminished after carrying out the Kraus and Lechner system [90]. Although the effectiveness of the system has been tested in vitro and animal experiment [91], whether a low frequency magnetic field itself in this system has a big influence on the bone regeneration is still a debatable issue. Kraus [92] presented that the low frequency magnetic field (0.2 to 20 Hz) alone promotes bone healing by way of accelerated blood vessel development and bone remodelling. These positive effects are more apparent in magnetically stimulated bones than in control bones or in electrically stimulated bones. However, Blümlein [93] examined the effect of pure magnetic fields (30 Gauss and 22 Hz) on vascularization and bone formation in dogs non-unions and found that there was no positive effect of the magnetic field in the animal model. Also the same result was found by Gerber et al. [94]. They used the same magnetic field and found no effect on the growth of embryonic bones. Similar results were revealed in our previous cell culture study [95]. That is exclusive magnetic stimulation showed similar but non-significant tendencies in metabolic activity and cell viability and collagen type 1 synthesis compared to experiments of control, electrically stimulated and electromagnetic stimulated.
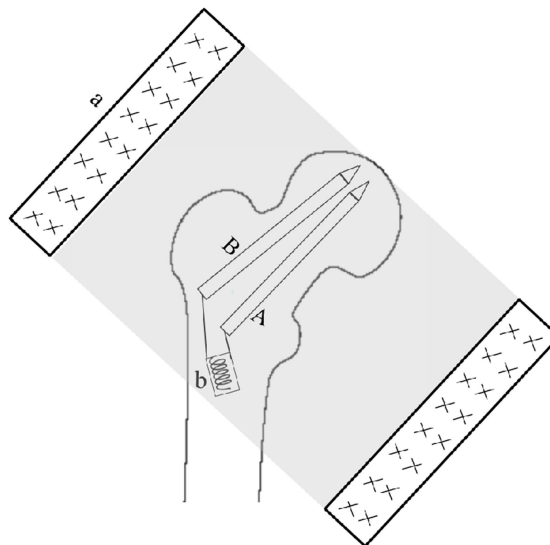

Fig. 2.8 Kraus-Lechner system, (a) the primary coil is placed outside of the femoral head and generates a magnetic field. This magnetic field induces a current in (b), the secondary intra-corporeal coil. The secondary coil is connected to (A) and (B), the two electrodes. This generates an electric field between the two connected electrodes.

Practically the Kraus and Lechner system has some disadvantages. For example the fatigue failure of the connecting wires and mechanical disconnections at the contact elements because of friction against the bordering tissue, additional implants (separate transducer system with cables) and minimum two osteosynthesis parts (e.g. two screws) . Therefore, to

improve the technique, based on the approach of Kraus and Lechner, Mittelmeier et al. [96] proposed a bipolar induction screw system (BISS), the depicted Asnis III s-series screw (Stryker Trauma, Kiel, Germany) (Fig. 2.9) with integrated coil and two electrodes. In this system, the transducer coil is embedded into the screw, thus there are no extra wires to be implanted. This reduces the failure risk of electro-stimulation caused by wire disconnection. Furthermore, it is also much easier to insert the implant and to remove e.g. after three months of treatment. Besides, it has a more consistent arrangement of electrodes to each other to guarantee a correct and reproducible handling of the system compared to the Kraus-Lechner system [96].
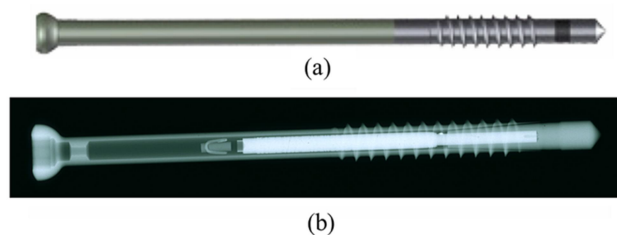

(a)

(b)

Fig. 2.9 Asnis III s-series screw: (a) screw implant, (b) X-ray of screw implant. The internal coil is connected both to the tip and the shaft of the screw, which are isolated from each other.
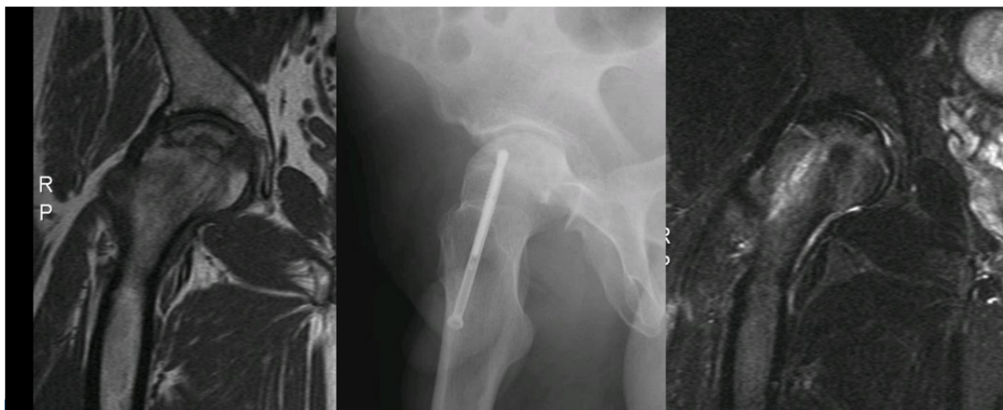
Fig. 2.10 (left) patient pre-operative MRI data, (middle) X-ray of patient data with Asnis III s-series screw, (right) patient post-operative MRI data.

Ellenrieder et al. [37] performed a retrospective clinical observation of 53 patients (59 hips) treated with the Asnis III s-series screw. In this study, none of the patients had undergone an intertrochanteric osteotomy in the past, and none of their avascular necrosis state was higher than stage III, according to the Steinberg classification [97]. This is because the screw implant is only suggested when treating early stages of avascular necrosis in the femoral

head. For later stages, higher than stage IV of the Steinberg classification, a total hip replacement will be considered. Avascular necrosis in the patients' femoral heads was diagnosed using MRI before the operation. After the surgery, the screw implants stimulated the weak bone in the femoral head for 5 to 12 weeks. The patients were asked to wear an extracorporeal coil around the body for 45 minutes three times a day and the implants were removed after three months. Another MRI check was used to assert the outcome of the treatment. Patient pre- and post-operative MRI data and X-ray with Asnis III s-series screw in the patient's femoral head are shown in figure 2.10. The preliminary results of the study showed that 86% of the patients had a significantly improved medical condition.

3 Computational modelling of bone electrical stimulation

3.1 Electro-quasistatic model

The electro-quasistatic (EQS) formulation can be used to compute the voltage response in the stimulated target area of bone electrical stimulation. This formulation is a simplification of Maxwell's equations. For electromagnetic fields that are slowly varying and have a negligible magnetic induction, the EQS approach may be applied [98].

3.1.1 Maxwell's equations

In 1865, James Clerk Maxwell presented a set of differential equations which became a foundation of electromagnetic theory [99]. This set of differential equations describes all macroscopic electromagnetic phenomena reflecting the relations between the characteristic quantities of electromagnetic fields, the space- and time-dependent electric and magnetic field strength ($E\ (V/m)$ and $H\ (A/m)$). The governing equations of the bone electrical stimulation phenomena in this thesis can also be formed by Maxwell's equations. The following four differential equations (3.1. to 3.4) describe the interrelation of the electric field E, the electric displacement $D\ (As/m^2)$, the magnetic induction $B\ (Vs/m^2)$ and the magnetic field H,

$$div\ D = \rho \qquad\qquad \text{(Gauss' law)} \quad (3.1)$$

$$div\ B = 0 \qquad\qquad \text{(Gauss' law for magnetism)} \quad (3.2)$$

$$curl\ H = J + \frac{\partial D}{\partial t} \qquad\qquad \text{(Ampère's law with Maxwell's extension)} \quad (3.3)$$

$$curl\ E = -\frac{\partial B}{\partial t} \qquad\qquad \text{(Faraday's law of induction)} \quad (3.4)$$

whereas ρ is the volume density of free charges, and J is the density of free currents. Gauss' law describes the source of the electric displacement field. Written in integral form, it states that the total outward electric displacement flux over any closed surface is equal to the total free charge enclosed in the surface. Gauss' law for magnetism describes the absence of magnetic monopoles. The origin of electromagnetic waves can be found in the coupling of Ampère's law and Faraday's law [100]. Ampère's law indicates that a time-varying electric field will give rise to a magnetic field, even in the absence of a current flow. The additional term $\frac{\partial D}{\partial t}$ is called displacement current density, and its introduction in the $curl\ H$ equation was one of the major contributions of Maxwell. Faraday's law describes how a time varying magnetic field induces an electric field.

The set of constitutive relation equations in the following is extended to determine the electromagnetics in media. These additional material equations are valid for linear, isotropic, non-polarised or -magnetised media [101]

$$D = \varepsilon E \tag{3.5}$$

$$B = \mu_H H \tag{3.6}$$

$$J = \sigma E \tag{3.7}$$

with electric permittivity ε, magnetic permeability μ_H and electric conductivity σ. J is the electrical conduction current density in a conductive medium.

In reality, the material properties of biological tissue like bone or cartilage are normally anisotropic and frequency dependent. Therefore, in the numerical analysis and simulation, the dielectric properties of bone have to be clearly defined. Details of the dielectric properties of bone can be found in section 3.3.

3.1.2 Electro-quasistatic fields

Slowly varying electromagnetic fields play an important role in many applications in bio-systems and medical engineering. The introduction of electro-quasistatic fields in this subsection is based on van Rienen [98] .

Electro-quasistatics (EQS) gives a reasonable approximation for low-frequency fields which can be thought to be free of eddy currents (i.e. the time derivative of the magnetic flux density may be neglected and thus $curl\, E \approx 0$), while the effects of the displacement current, which is the time derivative $\frac{\partial D}{\partial t}$ of the electric flux density, are dominant.

A harmonic time-dependence of the electric field can be expressed as

$$E\,(r,t) = Re(E(r)e^{j\Phi}e^{j\omega t}) = Re(\underline{E}(r)e^{j\omega t}) \tag{3.8}$$

with the angular frequency ω, the phase angle Φ and the phasor $\underline{E}(r) = E(r)e^{j\Phi}$.

Therefore, the time harmonic electro-quasistatic equations can be described as

$$div\,\underline{D} = \underline{\rho} \tag{3.9}$$

$$div\,\underline{B} = 0 \tag{3.10}$$

$$curl\,\underline{H} = i\omega\underline{D} + \underline{J}_E + \underline{J}_C \tag{3.11}$$

$$curl\,\underline{E} \approx 0 \tag{3.12}$$

17

where the current density $\underline{J}$ is separated into a conduction current density $\underline{J}_C$ arising from conductive materials and an impressed current density $\underline{J}_E$.

Since the electric field is assumed to be free of eddy currents, the electric phasor $\underline{E}$ can be derived from a scalar potential function:

$$\underline{E} = -grad\ \underline{\varphi} \tag{3.13}$$

in which the complex potential $\underline{\varphi}$ is equal to the amplitude of the real, time harmonic potential: $\underline{\varphi} = Re(\varphi e^{i\omega t})$.

Using the time-harmonic electro-quasistatic equations (3.9) to (3.12), after a few steps, the electro-quasistatic equations can be reformulated as the following potential equation, i.e. one single differential equation.

$$div([\sigma + j\omega\varepsilon_0\varepsilon_r]grad\underline{\varphi}) = div\underline{J}_E \tag{3.14}$$

In bone electrical stimulation, since the bone has a relatively low conductivity, the induced eddy currents in the bone are several magnitudes smaller than the currents generated by the coils that are integrated in the screw implant. Therefore, impressed currents can be neglected and the electro-quasistatic potential equation results in

$$div([\sigma + j\omega\varepsilon_0\varepsilon_r]grad\underline{\varphi}) = 0 \tag{3.15}$$

The EQS formulation in equation (3.15) is solved in a volume conductor model of the bone, which forms the computational domain Ω, by applying conditions to the exterior boundaries $\partial\Omega_i$, $i = 1,\ldots,N_b$ of the model, where N_b is the number of boundaries with different conditions. Dirichlet boundary condition applies a potential

$$\underline{\varphi}\,\big|\,\partial\Omega_i = V_i e^{j\phi_i} \tag{3.16}$$

with the constant amplitude V_i and phase ϕ_i to the surface of the electrode contacts and ground in the model. Homogeneous Neuman boundary condition applies to the perfect insulator, where the gradient of the solution $\underline{\varphi}$ is orthogonal to the normal component $\boldsymbol{n}$ of each boundary element

$$\boldsymbol{n} \cdot \nabla\underline{\varphi}\,\big|\,\partial\Omega_i = 0 \tag{3.17}$$

to the exterior boundary of the bone model as well as the electrode insulator.

3.2 Finite Element Analysis (FEA)

In many biological applications, complex geometries are included. As the geometry is not regular, it is often impossible to analytically compute the electric and magnetic field distribution in the studied biological tissue. Numerical simulations are often used as an approximate solution to the problems. For instance, in this thesis, the electric field caused by electrical bone stimulation can be computed numerically by the Finite Element Method (FEM) even though the computation of the bone model is complex. Numerical discretisation techniques subdivide the complex bone configuration into small elements and each of the small elements is assigned its own material properties, such as conductivity and relative permittivity. The small elements can also be set as sources as needed. Then, the electromagnetic equations are solved for the collection of small elements to obtain the fields in each element and thus in the whole configuration.

FEA is a favourite approach for the numerical solution of electromagnetic field problems due to the reason that FEA has a strong capability to deal with complex geometry [102]. It is used to solve boundary and initial value problems of partial differential equations on discretised geometries, called meshes. To get the approximate solution of the problem, the so-called Galerkin method is often used. The weak formulation of the partial differential equation is used to discretise the boundary value problem into finite elements and the solution on each finite element is interpolated by local basis functions and put into the derived (weak) formulation. The finite element meshes include triangles and quadrilaterals in two-dimensional space and tetrahedral, prisms, pyramids and hexahedra in three-dimensional space. The interpolation degrees can also be varied from linear, quadratic to cubic. In [102], chapter 6, the use of the Finite Element Method (FEM) to solve Maxwell's equations is given in more detail.

Various software tools are based on a FEM implementation. In this work, the software COMSOL Multiphysics® (Comsol AG, Göttingen, Germany) is used. The finite element computations of the bone electrical stimulation model used in this thesis were carried out using this commercial software, COMSOL Multiphysics®, version 4.3b. It offers an easy to control graphical user interface for geometry generation and many mesh algorithms and adaptive refinement techniques are contained. Anisotropic material parameters can be accessed in many ways. For both, linear and nonlinear problems, various direct and indirect solvers are available. A very essential feature of COSMOL is that it has an application interface to MATLAB (Mathworks, Ismaning, Germany) and allows MATLAB to control COMSOL via script files and functions.

3.3 Bone dielectric properties

To evaluate the electric field distribution in the bone caused by electrical stimulation, electric properties of the bone and the electro-stimulating implant, like relative permittivity ϵ_r and electric conductivity σ are crucial parameters. The implant geometry, its position in the bone and the stimulation parameters substantially influence the voltage response in the stimulated target area of the bone in bone electrical stimulation. Titanium alloy is a common material for orthopaedic and dental implants due to its high biocompatibility [103]. Thus, the electric properties of an electro-stimulating implant are directly provided by the manufacturer. Unlike the electro-stimulating implant, bone tissue is the most variable resistive medium in the body. It is an inhomogeneous composite material with fluid-filled pores and it is anisotropic in its structure [104]. Hence, its dielectric properties are varying at different frequency ranges.

The dielectric properties of any material can be obtained from its measured complex relative permittivity $\varepsilon_{(\omega)}$, written as

$$\varepsilon_{(\omega)} = \varepsilon' - j\frac{\sigma}{\varepsilon_0 \omega} \tag{3.16}$$

where ε' is the relative permittivity of the material and $\frac{\sigma}{\varepsilon_0 \omega}$ is the out-of-phase loss factor, σ is the total conductivity of the material, ε_0 is the permittivity of free space and ω is the angular frequency of the field.

The dielectric properties of biological tissues result from the interaction of electromagnetic energy with the tissue constituents at the cellular and molecular level [105]. As early as in 1957, Schwan [106] described that there are three distinct regions for the conductivity and relative permittivity of biological tissue as a function of frequency and that the relative permittivity occurs to have an 'enormous value' in the order of millions at low frequencies. These three regions are called the α, β and γ dispersion, respectively (Fig. 3.1) and an example of a biological tissue's dielectric properties in different frequency ranges is shown in figure 3.1 which is based on Schwan [106].

Dispersion is the corresponding concept to relaxation in the frequency domain [107]. The different dispersion regions specify the non-symmetrical distribution of the relaxation times in biological tissue and result from dielectric effects at the membranes of the tissue, which has the following origins [106]:

- α-dispersion, (mHz-Hz): associated with ionic diffusion processes at the outer cell membrane
- β-dispersion, (kHz-MHz): due to the polarization at the poorly conductive membranes, resulting in cellular membrane capacitance

- γ-dispersion, (GHz): due to the polarization of water molecules in the tissue

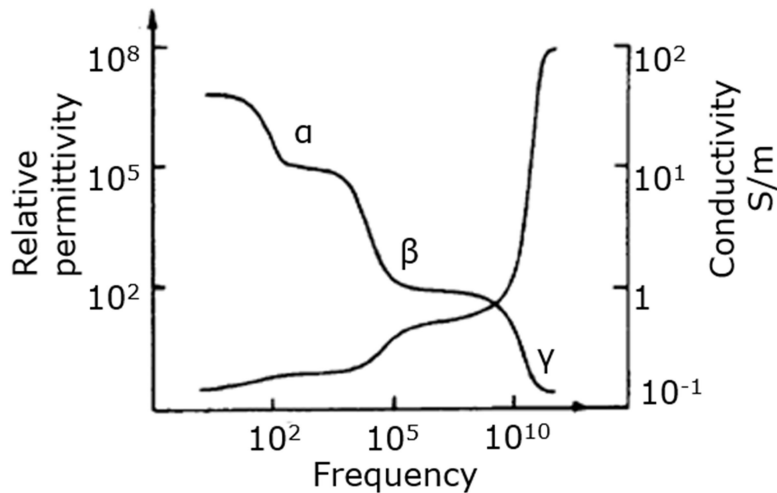Fig. 3.1 Example of relative permittivity (decreasing) and conductivity (increasing) of biological tissue within the three dispersions region α, β, γ (based on Schwan [106]).

In 1996, Gabriel et al. [108] systematically reviewed almost half a century's literature available at that time in terms of dielectric properties of tissues over ten frequency decades. Later, an extensive experimental study was carried out on a large number of biological tissues at body temperature with three different measurement techniques in the frequency range of 10 Hz to 20 GHz [105]. They found good agreement between the experimental results and the data from three experimental setups in the overlapping frequency ranges, as well as the data from the literature [105]. Finally, Gabriel et al. [109] created a parametric model to characterise the electrical properties of various biological tissues as a function of frequency. The conductivity and relative permittivity of cortical bone and cancellous bone in a frequency range from 10 Hz to 100 MHz after the parametric model that is explained below, is shown in figure 3.2.

To parameterise the conductivity and relative permittivity of the investigated tissue, the previously reported experimental data, complemented by the data surveyed in the literature, and a mathematical model characterising the four dispersion regions was used [109]. The frequency dependence within each region was expressed as a Cole-Cole term. The Cole-Cole relation derives its name from Cole and Cole [110,111]. They noted that the frequency dependence of the electric permittivity in a range of different experiments could all be summarized by a particularly simple mathematical relation in the complex plane.
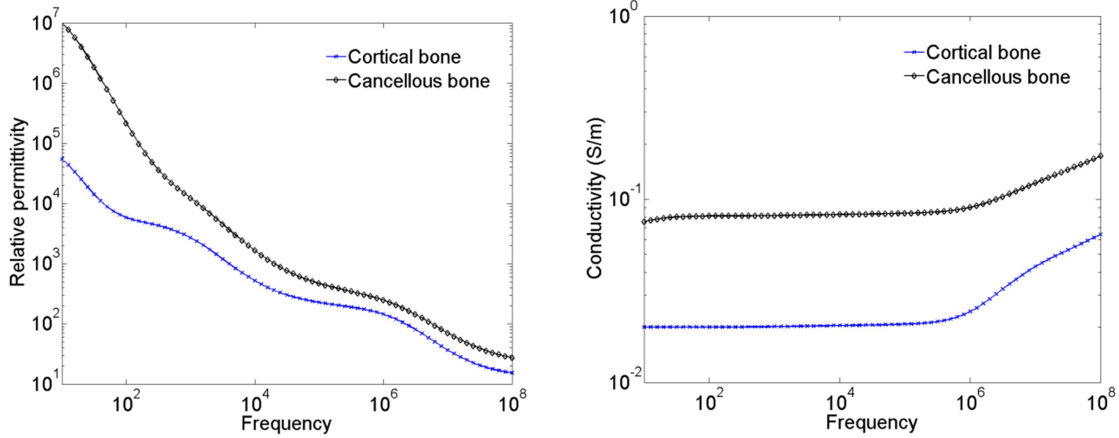
Fig. 3.2 The conductivity and relative permittivity of cortical bone and cancellous bone in a frequency range from 10 Hz to 100 MHz. Image based on the Cole-Cole dispersion parameters by Gabriel et al. [109,112].

The Cole-Cole model parameters can be found in [112] and have been widely used. With this mathematical model, the frequency dependent complex relative permittivity $\varepsilon_{(\omega)}$ can be calculated by

$$\varepsilon_{(\omega)} = \varepsilon_\infty + \sum_{n=1}^{4} \frac{\Delta\varepsilon_n}{1+(j\omega\tau_n)^{(1-\alpha_n)}} + \frac{\delta_i}{j\omega\varepsilon_0} \qquad (3.17)$$

where ε_∞ is the relative permittivity at high frequencies, $\Delta\varepsilon_n = \varepsilon_{sn} - \varepsilon_\infty$, ε_s is the permittivity at low frequencies with $\omega\tau \ll 1$. τ_n is the relaxation time, and δ_i is the static ionic conductivity. ε_∞ and α_n are the Cole-Cole-parameters found experimentally for every Cole-Cole equation [109]. In figure 3.2, the values of the relative permittivity of cancellous bone and cortical bone are extremely high (10^6 to 10^7) at low frequencies and decrease to diminish when the frequency increases. This phenomenon has been described by Schwan [106]. The relative permittivity of a biological tissue may reach an 'enormous value' in the order of millions at low frequencies (below 100 Hz). The reason why the electrical permittivity in biological tissues decreases with increasing frequency is that the different electrical charges are not capable to follow the changes in the applied electrical field. The distinct dispersion regions mentioned in [106] can be easily detected from the cancellous bone and cortical bone in the data [109].

The parametrical model described by Gabriel et al. [105,109] is used to predict the dielectric data that is in line with that contained in the vast body of literature. It is based on experimental data. Due to the errors in the different references, the relative permittivity values in [109] from the parametrical model below 100 Hz can be affected by up to a factor of two or three. The dielectric properties of bone are important to understand the generation

22

and distribution of electrical current in the body caused by external electrical fields.

Although a wide range of values for bone impedances has been reported in the literature, the results are still difficult to compare due to the lack of a standard normalised representation of the bone impedance. Saha et al. [113] investigated the environmental condition factors which can affect the measurement of the dielectric properties of bone. In [113], bone specimens, standardised rectangular cortical bones, were chosen from the shaft of adult beef cattle femurs. Measuring the dielectric properties of bone in living animals or humans still presents difficulties. Therefore, the bone specimens were stored at -20 °C. Before the experiment, the bone specimen were thawed and brought to room temperature. Based on [113], care has to be taken regarding the environment during the measurements. The preserving solution's pH value and temperature have to be specified when presenting the results on the electrical properties of bone as it may induce a relative big change in resistance, conductance and capacitance of the bone specimens. The bone specimen exposure time has to be short and the measurement has to be taken immediately after the bone sample was removed from the solution to avoid loss of moisture content and consequent errors.

The sample of the investigated biological tissue is critical to the measured results of dielectric properties because biological tissues are inhomogeneous. It shows considerable variability in dielectric properties. In addition to the factor in [113], the electrical properties of bone are likely to depend on the microstructure and the chemical composition of the specific bone sample. The structure and chemical composition of bone samples depend on age, sex, species and the direction and location of the bone; therefore, these are also factors which influence the dielectric properties of the bone. Peyman [114] reviewed that dielectric properties of tissue varied with the biological tissues' age and a significant decline in both, relative permittivity and conductivity as a function of age for some tissue, such as brain (white matter), long bone, skull, skin, muscle and bone marrow, has been found. Interrelationships between electrical properties and microstructure of human trabecular bone have been investigated by Sierpowska et al. [115] in 2006. They found that dielectric parameters of trabecular bone, especially relative permittivity and dissipation factor, were significantly and specifically related to a trabecular microstructure as characterized with micro-CT. Moreover, the effect of human trabecular bone composition on its electric properties has also been researched by Sierpowska et al. [116] and a strong linear correlation is found between the relative permittivity at 1.2 MHz and trabecular bone fat content. In addition, the relative permittivity measured at 200 Hz served as a good predictor of water content. Phase angle, specific impedance and especially conductivity were strongly related to the trabecular bone density and water content.

3.4 CAD modelling

In general, the construction of a CAD model for a specific tissue often starts from the acquisition of anatomic data from an appropriate medical imaging modality [117]. The CAD modelling has to be capable to produce three-dimensional views of anatomy, differentiate heterogeneous tissue types, display the different structures and generate computational tissue models for analysis and simulation.

3.4.1 CAD model generation

Three major steps are basically involved in CAD model generation: non-invasive image acquisition, imaging processing and three-dimensional reconstruction to form a voxel-based volumetric image representation, and the construction of a CAD-based model [117].

The commonly used imaging modalities in tissue modelling are computed tomography (CT) and MRI. Each has its own advantages and limitations. CT exposes a sample to small quantities of ionizing radiation and detects and images it according to its radiation absorption. The result of a CT scan is a series of 2D images which display a density map of the sample. The big advantage of CT as an imaging modality is its reasonably high resolution. The limitation of CT scanning is that it could not be ethically justified to create image models for each and every organ, due to the reason that radiation dosage is administered. The advantage of MRI is that it is capable to show subtle differences in soft tissue anatomy without the harmful effects of ionizing radiation present in CT. It is superior in differentiating soft tissue types and in recognizing border regions of tissues with similar density. The disadvantage of using MRI is that the patient is required not to move during the scan.

To reconstruct a three-dimensional anatomic model from CT/MRI, the images have to be integrated using 2D segmentation and 3D region growth. 2D segmentation means extraction of the geometry of the CT scan data set [118]. In CT scans, the grayscale value of each voxel determines the tissue density. In order to differentiate the tissue in CT scans, contrast segmentation can be used. Although CT is inferior to MRI in differentiating soft tissue with similar density, it has the advantage that it is more effective to segment hard tissue and tissue with sharp density changes, for instance the interface between bone and soft tissues. Segmentation can be accomplished either manually or automatically. In spite of the fact that the manual segmentation method is time consuming, it is still often used since it offers whole user-control and all anatomical knowledge can be applied in the segmentation process [117]. Therefore many algorithms have been designed only to segment the region of interest automatically. To evaluate segmentation methods for a particular model, important factors should be considered, such as running time, accuracy, reproducibility and generality. There is no gold standard to evaluate the accuracy of a segmentation algorithm. In general, it is

evaluated by comparison with a manual segmentation by an expert. The accuracy of automatic segmentation can be evaluated by volume difference measures, overlap measures and geometrical measures [119].

The 3D voxel model from the region growth algorithm normally cannot be effectively used in numerical simulation [117]. CAD models, represented as boundary representations and mathematically described as Non-Uniform Rational B-splines (NURBS), need to be carried out for model design, analysis and simulation. Kluess et al. [120] presented a convenient approach to generate a CAD model from medical imaging data. In their method, first, the 3D voxel model is converted to a stereolithography (STL) file and this STL file is then imported into a reverse engineering software for surface refinement and NURBS surface generation. This method has also been mentioned in [117]. The bone CAD models in the present thesis are generated using this method. Moreover, the reverse engineering interface approach is a method that first converts the 3D voxel model to point data form and loads the points into reverse engineering software. Then, one generates a triangulate faceted model from the points and creates a NURBS surface from this faceted model. Besides this method, some commercial programs that can construct a CAD-based model directly from medical images were also introduced in [117]. For example, MedCAD (Materialis, Belgium), a standard module of medical image processing software, directly exports data from the imaging system to the CAD platform through either the International Graphics Exchange Standard (IGES), the Standard for Exchange of Product (STEP) or in STL format.

3.4.2 Human femoral anatomy

In this thesis, the Asnis III s-series screw is used to treat avascular necrosis in a patient's femoral head. Therefore, this bone's modelling is given as an example. To clarify the human femoral structure, the anatomy of human femur based on Gray [121] is introduced in this subsection.

As the interest of biology and the functional mechanism of the human femur is not the focus of this work, it will not be explained here. More information about the biology and functional mechanism of the human femoral can be found in [119].

Figure 3.3 shows the left and right femur structure. The femur is the longest and strongest bone in the human skeleton. As in figure 3.3, it is almost perfectly cylindrical in the greater part of its extent. The femur consists of a body, and two extremities. The upper extremity is divided into a head, a neck, a greater and a lesser trochanter. From the mechanical point of view, the inner structure and outer form of the femur are governed by the conditions of maximum stress where weight is transmitted to the femur head through the acetabulum [121].

Figure 3.4 shows an upper extremity of a right femur viewed from behind and above. The

femur head is globular and forms a hemisphere. The head surface is smooth and coated with cartilage in the fresh state. Fovea capitis femoris is from ovoid depression and attaches to the ligamentum teres. The neck connects the head with the body and forms with the latter a wide angle. The greater and lesser trochanter is prominent bone structures which afford leverage to the muscles that rotate the thigh on its axis.
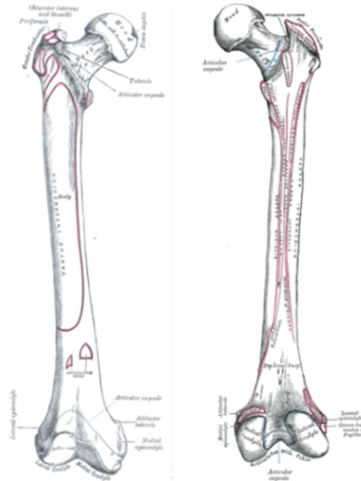

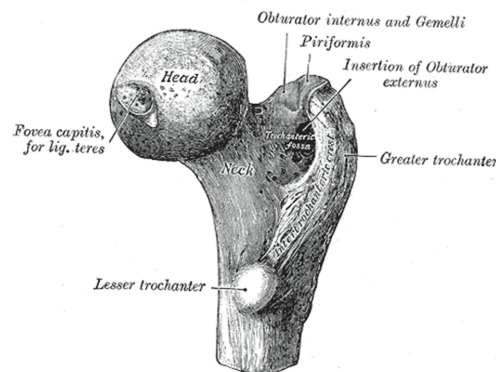Fig. 3.3 Posterior surface of left femur (left) and right femur (right) (anatomy from Gray [121]).

Fig. 3.4 Upper extremity of right femur viewed from behind and above (anatomy from Gray [121]).

3.4.3 Human femoral head modelling

The process of human femoral head modelling is shown in figure 3.5. A femoral head which is used for the CAD model reconstruction is from a patient undergoing total hip replacement. Basically, these software tools are involved in the human femoral head modelling:

- Segmentation: Amira 5.4 (Mercury Systems, Chelmsford, MA, USA)
- CAD-reconstruction of faceted surfaces: Geomagic (Geomagic, Morrisville, NC, USA)
- FEM solver: COMSOL Multiphysics

There are alternatives to these choices. They can be replaced by similar software with the same functions. For example, the segmentation software Mimics (Materialise NV, Gilching, Germany) can replace Amira to segment the human femoral head. The numerical simulation

software COMSOL can be replaced by CST studio (CST STUDIO SUITE, Darmstadt, Germany) or others. Although COMSOL and CST both have pre-processing and post-processing functions for the simulation, those have many limitations and are not sufficient for some special requirements. That is why some special pre- and post-processing software tools are needed. For example, to achieve a more precise mesh for the simulation, commercial pre-processing software Altair HyperMesh (Altair Engineering, Inc., Hamburg, Germany) can be used before the simulation to get a customized mesh. Then, the generated fine mesh can be directly imported to the simulation software to calculate the results. The results of the simulation from the FEM software can be exported in txt format and can be analysed in MATLAB.
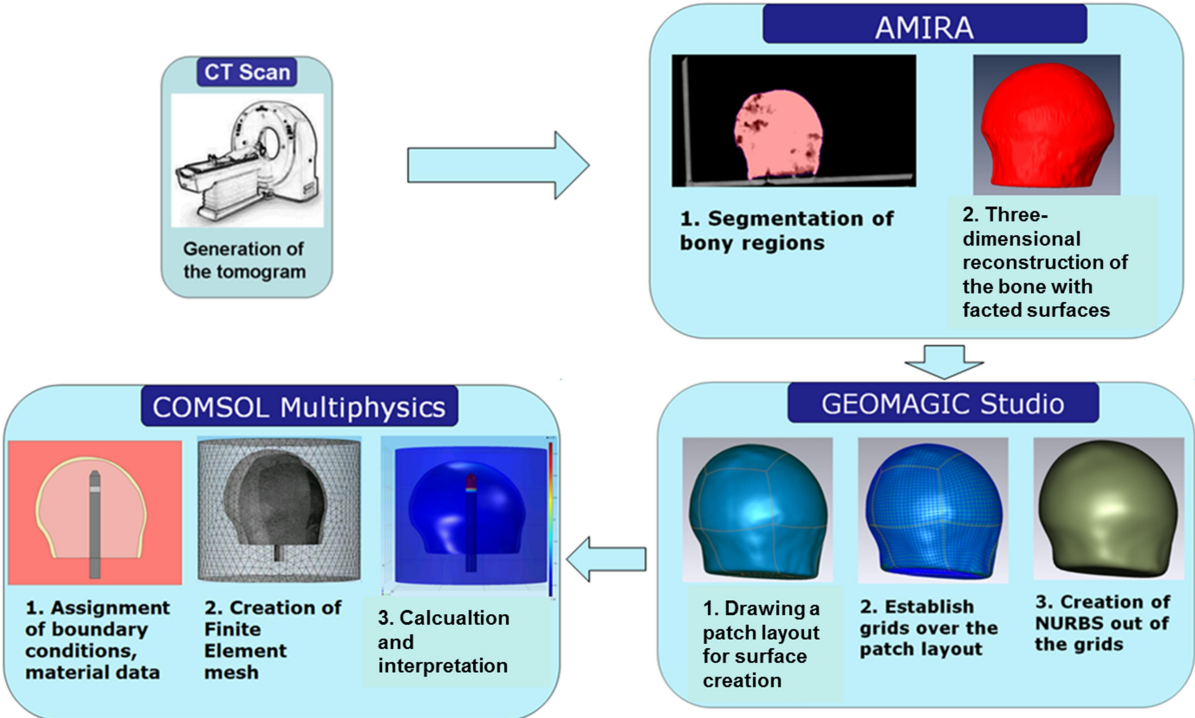
Fig. 3.5 Human femoral head modelling process according to Kluess et al. [120].

The first step of human femoral head modelling in this thesis is to get a medical image of the human femoral head. After the CT scan of the human femoral head specimen, the DICOM images are loaded into the software Amira. It is used to segment the bone tissue (cortical bone and cancellous bone) from the human femoral head CT data set and convert the 3D voxel model to STL files in American Standard Code for Information Interchange (ASCII) format. It is clear to see from the CT scans of the human femoral head that the cortical bone of the femoral head is just a really thin layer on the articular surface of the head. The inner part of the femoral head is cancellous bone. The segmentation can be done both manually and automatically in Amira depending on the type of material that needs to be segmented.

27

The automatic segmentation is a convenient approach for separating areas with highly contrasting colour and it can be applied to one or all slices. It separates between selected and unselected voxels based on a threshold colour value. As the cortical bone is a relatively thin layer on the surface of the femoral head and it is hard to set a threshold colour value for automatic segmentation, the whole segmentation process of the human femoral head in this thesis is done manually.

The STL files of the human femoral head, both cortical bone and cancellous bone, are imported into reverse engineering software Geomagic and the surface of the cortical femoral head bone structure and cancellous femoral head bone structure were both refined. Then, the patch layout is drawn for surface creation and grids are established over the patch layout to generate NURBS CAD models. In order to control the model generation accuracy, the tolerance for the differences between the input STL files and the output CAD STEP file can be calculated and adjusted during the CAD model generation in Geomagic.

The femoral head CAD models are imported to the software COMSOL Multiphysics to calculate the electric field distribution in the model. In COMSOL, the AC/DC module was used, specifically the module for electric currents in the frequency domain, to compute the electric potentials within the volume conductor model. When the computation module was set in COMSOL, basically there are three steps involved to get the results: assign the boundary conditions and material parameters for the whole computation domain, create the finite element mesh, solve the resulting linear problem and interpret the results. The material properties of all subdomains are set according to either material data sheets or experimental measurements. The boundary conditions for all subdomains are defined according to the problem that needs to be solved. The mesh in COSMOL Multiphysics can be generated either automatically or customized. The linear solver for the calculation includes as iterative solver the conjugate gradient solver. In the end, the results of the electric field distribution in the model can be represented through COMSOL post-processing.

4 Numerical simulation in human femoral head

The Asnis III s-series screw system is used to treat avascular necrosis in patients' femoral head. To better understand this clinical effect the electric field caused by Asnis III s-series screw in the human femoral head should be evaluated. To evaluate electric field distribution in electromagnetic stimulation of human femoral head, we considered two aspects. In this work one is analysing the influence of the implant parameters on the electric field distribution of the human femoral head, another is optimizing the implant position parameter in the femoral head.

To better design an electro-stimulation implant for electrical stimulation therapy, it is necessary to know how the implant parameters influence the electric field distribution in the femoral head. The implant parameter which has the most influence on the electric field distribution in the bone tissue dominates the implant design. The implant parameters which have minor influence on the electric field distribution in the bone tissue can be neglected the implant design decision making. The effect of implant parameters on the electric field distribution in the femoral head can be numerically studied by FEA.

Although use of the Asnis III s-series screw for internally-applied electrical stimulation of the bone healing process is a common clinical application, the optimum screw position in the human femoral head has not so far been investigated. It is important to realise that the implant position may be crucial to the outcome of the electro-stimulation treatment. Patients may have different reactions to the same surgery. Most notably example is that treat tibia fractures with electrical stimulation in the research of Jorgensen et al. [122], one patient refused to continue treatment because of heat and pain in the affected limb. In order to improve the outcome of the electro-stimulating screw implant and to predict the optimum position of the screw in the femoral head before surgery, how screw positioning influences the electric field distribution in the femoral head is really necessary to know. Therefore, it is important to analyse the effect of implant position on electric field distribution in the femoral head, and to optimize implant position in the femoral head. Moreover, to design customized electro-stimulating implants for the specific patients, patients' personal requirements need to be considered. For example, the size and location of the weak tissue within the bone, e.g. necrotic lesions, are varied from patients to patients. Therefore, the position and the design of the electro-stimulating implant need be customized defined for the specific patient. Due to this considering, as a prior study, an optimized electro-stimulation screw implant position in one patient femoral head is numerically defined by combining FEA and optimization algorithm.

4.1 Material and methods

In this subsection, the material and methods used in electro-stimulating implant parameter analysis and screw position optimization process are explained respectively.

4.1.1 Implant parameter analysis in the femoral head

Reconstruction of coordinate system

The key of validation is that to keep the same coordinate system in the experiment and numerical simulation. Only the coordinates of measuring points are the same in both experiment and simulation, the validation results can be trustable and numerical simulation model can be reused in the parametric study. Therefore, we created one reference frame for the human femoral head model. This reference frame consists of three perpendicular boards and it was used in the validation experiment to get the coordinate of the measurement points by measuring arm. It was also used to reconstruct the coordinated system in the numerical simulation.
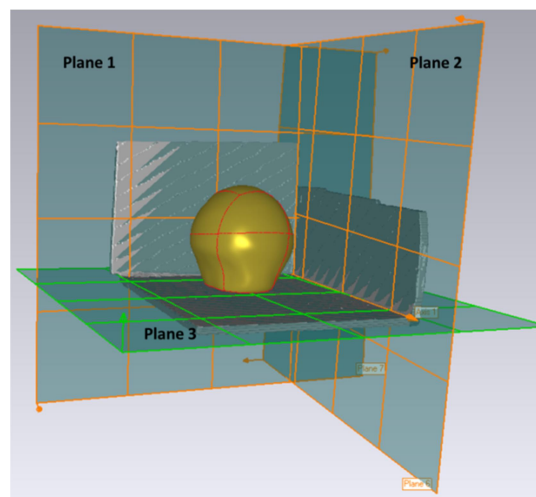
Fig. 4.1 Coordinate system reconstruction in Geomagic.

To reconstruct the coordinate system from the reference system, we segmented the reference frame from the CT scans by Amira 5.4. Unlike bone CAD model reconstruction, the STL surface file was imported to Geomagic not for surface refinement and NURBS model generation, but for datum generation. Three planes which matched surfaces of three perpendicular boards were created in the Geomagic. According to these three perpendicular planes, original point (0,0,0) was set as crossing point of three planes and x, y, z direction in coordinate system was defined (Fig. 4.1).

As the Geomagic cannot directly set the CAD model using the new coordinate system, the IGES file which include the coordinate system information was imported to the CAD

software PTC creo (PTC, Inc., Needham, MA, USA). The position information between human femoral head CAD and reference frame was kept the same when human femoral head step file and reference frame IGES was imported to Geomagic. New coordinate system of the human femoral head could be set by saving the CAD model with the new coordinate system in PTC creo. The newly saved human femoral head CAD model in this moment had the same coordinate system as in the validation experiment and could be directly import to COMSOL to do numerical simulation.

Model Generation

Reconstruction of human femoral head model from CT scans of bone specimen has been explained in detail in subsection 3.4.3. Figure 4.2 shows the reconstructed human femoral head CAD model from CT scans with reference coordinated system. In reality, the human femoral head bone is surrounded by kinds of the soft tissues, such as muscle, fat and skin. But because the surrounding tissues of the femoral head have a high complexity and are of minor interest for the electric field distribution inside the femoral bone, the surrounding tissue was first substituted by blood in the simulation of screw parametric study. To consider close to a real patient situation, the surrounding blood cylinder in the simulation had a radius of 100 mm and a length of 100 mm. The human femoral head was located in the middle axis of the cylinder.
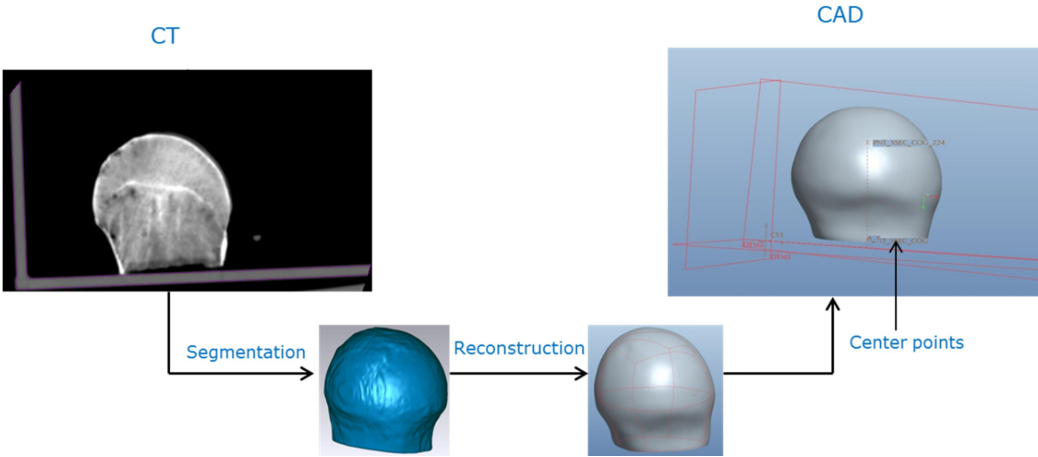
Fig. 4.2 Femoral head model reconstruction workflow.

Although the bone surrounding tissues have high complexity, to better understand how the electric field in the femoral head was influenced by tissues around the bone, the surrounding tissues in the simulations were also represented by three cases, like only muscle tissue, muscle combination with fat, muscle combination with both fat and dry skin. The blood cylinder around the femoral head was replaced by muscle in the case of surrounding tissue only muscle. In other two cases, surrounding tissues were muscle combination with fat and muscle combination with both fat and dry skin, the thicknesses of the fat and the skin above

the muscles were 4 and 1 mm, respectively. Moreover, a designed sphere-shaped lesion was located in the femoral head to get close to the real case. In numerical simulation, lesion was categorized into two cases: lesion as fat and lesion as blood. This because that in the surgery, when the lesion was moved out from the patient´s femoral head, the blood was filled into the gap.

The CAD model of the Asnis III s-series screw in the simulation (Fig. 4.3) was created in the Solidworks 2008 (Dassault Systemes Deutschland, Hamburg, Germany) which was based on CAD datasets of the screw from the manufacture. There was one simplification of the screw CAD model generation. The thread of the implant screw was not taken into account in the numerical simulation because it could increase the computational and mesh generation complexity.
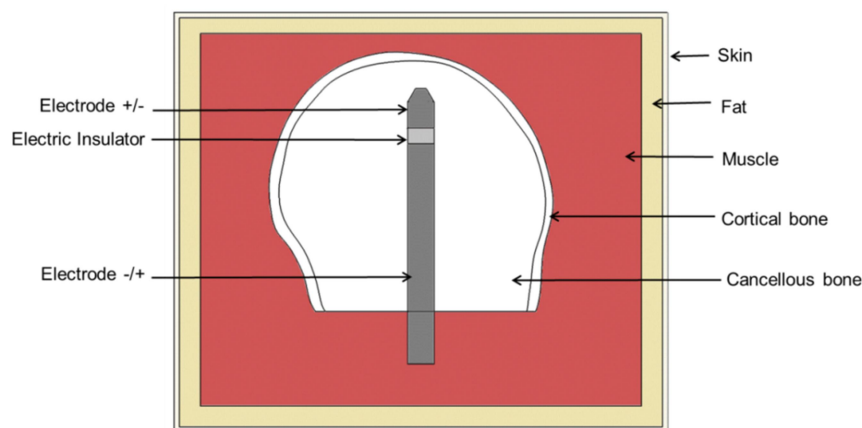
Fig. 4.3 The model of a human femoral head with muscle, fat and skin.

Finite element simulation

The numerical simulation of the human femoral head was performed using COMSOL Multiphysics Version 4.3. In COMSOL, at first was to choose the proper module for solving the current physical problem. In current study, the AC/DC module was used, specifically the module for electric currents in the frequency domain, to compute the electric potentials within the volume conductor model. The second step was to import or create the volume conductor model. In present study, the femoral head model and the screw implant model were imported and the bone surrounding tissues in the numerical simulation was created in COMSOL.

Consequently, the third step was to set material properties for all the domains and the boundary conditions for all the desired boundaries. As the bipolar induction screw system is made of titanium alloy Ti6A14V and the insulation layer is based on epoxy resin, the material properties of the screw implant in the numerical simulation were according to the data sheets from manufacture. All the human tissues in the present simulation, such as cancellous bone,

cortical bone in the femoral head, blood, muscle, fat, and skin, were all simplified to homogenous and isotropic. As the dielectric properties of the bone at a frequency of 20 Hz have not been widely studied, in present study, the electric properties derived from Gabriel et al. [105,109] were used to calculate the electric field distribution in biological tissue [123]. The comparable data to those of Gabriel et al. was found in the research of Sierpowska et al. [124]. They investigated the dielectric properties of human trabecular bone at a frequency of 50 Hz. The conductivity and permittivity of the tissues from Gabriel et al. [105,109] at 20 Hz frequency in present simulation can be seen in Table 4.1. As the surrounding tissue composition has a high complexity, the surrounding tissues of the human femoral head were replaced by blood or muscle, fat, and skin in the numerical simulation.

Table 4.1. Electric properties of screw implant and tissue (according to [105,109]) used for numerical simulation

Material	Conductivity σ [S/m]	Relative permittivity ε_γ
Ti6A14V	$7.407 \cdot 10^5$	1
Epoxy	10^{-12}	4
Cortical bone	0.020045	25119
Cancellous bone	0.078902	4020200
Muscle	0.20742	24306000
Fat	0.015477	5032800
Skin (dry)	0.0002	1136
Blood	0.7	2560

The boundary conditions in the simulation had Dirichlet boundary condition and Neuman boundary condition (equations 3.16, 3.17). Dirichlet boundary condition was considered to impose an electric potential on the surface of the screw implant electrodes. The insulating surfaces of the screw implant and the exterior boundary of the model were set to the Neumann boundary condition.

After the boundary conditions and material properties were defined, all the domains needed to be discretized to finite elements to calculate electric potential on all the nodes. Therefore the fourth step of the numerical simulation was to discretize all the domain of volume

conductor models into small elements. In present study, all models had the free tetrahedral mesh and were adjusted manually (Fig. 4.6). The triangular element size on the surface of the electrode was set based on the results of parametric study about the triangular element length. This parametric study was to ensure the simulation had sufficient computational accuracy. The objective of the parametric study was to find the triangular element length on the screw surface that could keep the alteration of the integral of the current density over the surface area of the simulation electrode to a value below 2%. To the end, the screw implant surface was meshed using triangular elements and the maximum element length was 0.5 mm. Due to the limitation on computational consumption, the human femoral head was meshed using free tetrahedral elements and maximum element length was 0.8 mm. The resulting model for each implant parameter variation consisted of three million mesh elements. The model was discretized with four million degrees of freedom (DoF).

The last step of the numerical simulation was to choose the proper solve in COMSOL to calculate the electric potential on the all the nodes. An iterative solver with the generalized minimal residual method (GMRES) was used to solve the resulting system of equations. The iteration was stopped when the 2-norm of the residual was below ten to the power of minus six to insure the enough accuracy of computation.
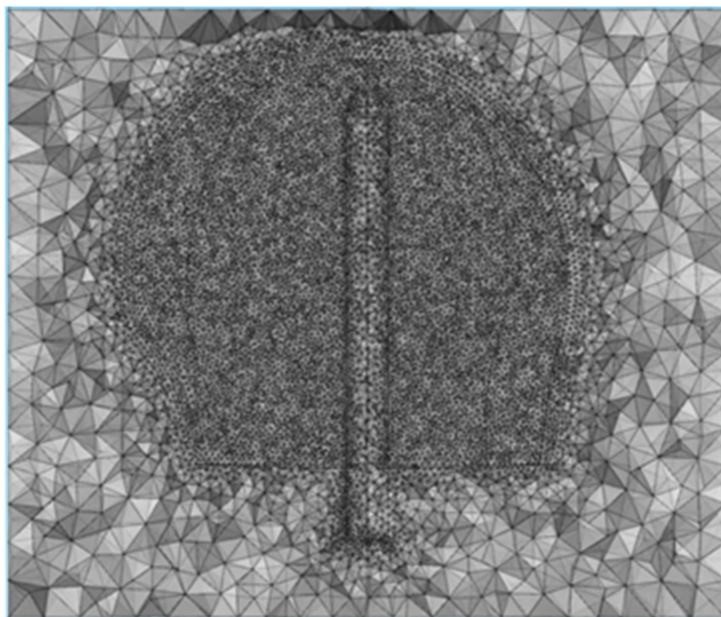
Fig. 4.4 The mesh in the femoral head model.

Moreover, since the conduction current in the femoral head is several orders of magnitude higher than the displacement current, for the purpose of reducing the computational complexity, the influence of the permittivity of the cortical and cancellous bone at a frequency of 20 Hz could be neglected theoretically. But in order to keep the same stimulation

parameters (electric voltage 700 mV and frequency 20 Hz) as the clinical situation, the numerical simulations were still solved in the frequency domain. To investigate the influence of surrounding tissue on the electric field distribution in the femoral head, three different layers (muscle, fat and skin) in the simulation were carried out.

Electric field computation

The electric potential inside of the femoral head was solved based on the assumption of the outer boundaries of the surrounding tissue were isolated and zero Neuman boundary conditions were applied on these boundaries. 20 Hz frequency and maximum secondary root mean square (RMS) voltage 700 mV on the surface of the screw were used in the numerical simulation. Due to the reason of that the induced eddy currents in the relatively low conductivity of the cancellous bone are several orders of magnitude smaller than the currents generated by the coils which are integrated in the screw implant at 20 Hz stimulation frequency, the induced eddy currents in the femoral head were neglected in the simulation. Therefore, the Maxwell equations in current model can be considered as time harmonic electro-quasistatic equation

$$div([\sigma + j\omega\varepsilon_0\varepsilon_r]grad\underline{\varphi}) = 0 \qquad (3.15)$$

in which $\underline{\varphi}$ is the electric potential, σ is the conductivity, ε_r is the relative permittivity, and $\varepsilon_0 \approx 8.854 \times 10^{-12}$ As/Vm is the electric field constant. To keep the same conditions as in the clinical study, the influence of permittivity of cortical and cancellous bone at frequency 20 Hz was not neglected in the current simulation even though that is relatively small. Therefore in COMOSL, study type frequency domain but not stationary was chosen for our simulation.

To quantify the deviation electric field distribution amount all different kinds of screw implant parameters, an efficient approach to evaluate this influence is to determine the volume of tissue activated (VTA). The VTA considered in the simulation is based on one experiments [89]. The activated tissue electric field interval in the femoral head was 5 to 70 V/m [89]. The VTA was calculated in COMSOL with MATLAB version R2011b by the grid method. The 2-norm of the electric field on each grid node was interpolated from the nearest point in MATLAB. To maintain the balance between computational accuracy and computational time consumption, the grid size was chosen to be 2 mm in numerical simulations. In order to quantify the VTA changes according to different screw parameters, the volume fraction was calculated. It is written as

$$volume\ fraction = \frac{VTA}{Volume_{femoral\ head}} \times 100\%$$

Validation experiment

For evaluating the electric field distribution in electromagnetic stimulation of the human femoral head, the numerical model has to be validated. Validation is a really important step in the numerical simulation of complex biology tissue model due to the reason that to ensure the accuracy of simulation results. If the simulation results and validation experiment data have the acceptable difference, the numerical simulation results can be considered reasonable in the real system. The context in this subsection is based on Su et al. [125].

As validating is utilized to determine if the numerical model is an accurate representation of the real system, we set up on validation experiment with the same human femoral head and the screw implant as in the screw implant parametric study in the femoral head model. Due to the reason that in the numerical simulation, the electric potentials at each mesh nodes are numerically calculated by FEA software, to verify the numerical data, the electric potential was determined experimentally using a bone specimen and compared with the numerical data. The validation experiment (Fig. 4.1) was set up according to the clinical application of Asnis III s-series screw system.

The human femoral head used for the experimental validation and numerical simulation was retrieved from an osteoarthritic patient undergoing total hip replacement due to the lack of sources of fresh femoral heads from patients with early stage avascular head necrosis. The early stage avascular femoral head necrosis normally can be totally healed after the certain treatment. Although the cartilage lesion of the femoral head has a relatively small lesion, it should not result in relevant discrepancies between numerical simulation and experimental measurement. Many factors can influence the electric properties of the bone tissue, such as time of exposure or moisture [113]. To minimize the kinds of influences, in our study the bone specimen used was refrigerated at –20 °C from post-surgery until the experiment. Although freezing is commonly recognized as a method of preserving bone samples for electrical measurements [126], the influence on the electric bone properties is not known so far. Moreover, the femoral bone was moistened by sodium chloride (NaCl) solution during the experimental measurements in our study to avoid drying of the thawed specimen.

The validation experiment process comprised the following steps. The first step was to carry out a CT scan of the bone specimen with a reference frame to reconstruct the CAD model of the bone for numerical simulation before setting up the validation experiment. The second step was to prepare the experiment setup (Fig. 4.5). In the setup, a 3D coordinate measuring

arm, MicroScribe G2x (Solution Technologies, Oella, MD, USA) was used to determine the coordinates of the measuring points, which should be kept consistent in the numerical simulation. The primary coil generates the same oscillating (20 Hz) magnetic flux density as in the clinic study, 5 mT. The bipolar induction screw system (Asnis III s-series screw) was implanted into the centre of the bone. One care was taken that, before the screw was implanted into the bone, the root mean square (RMS) voltage on the surface of the screw needed to be measured, which was 500 mV. Because this electric potential was also the one used into the numerical simulation and the results from the numerical simulation was compared to the experimental ones. The third step was to measure the RMS voltage on the surface of the bone and approximately 5 mm into the bone (see Fig. 4.6). The recorded results needed to be compared with those in the numerical simulation. The last step was to take X-ray scans of the bone specimen after the validation experiment. This step was used to refine the position of the screw in the simulation as the position of the screw in both the numerical simulation and the validation experiment has to be kept consistent.
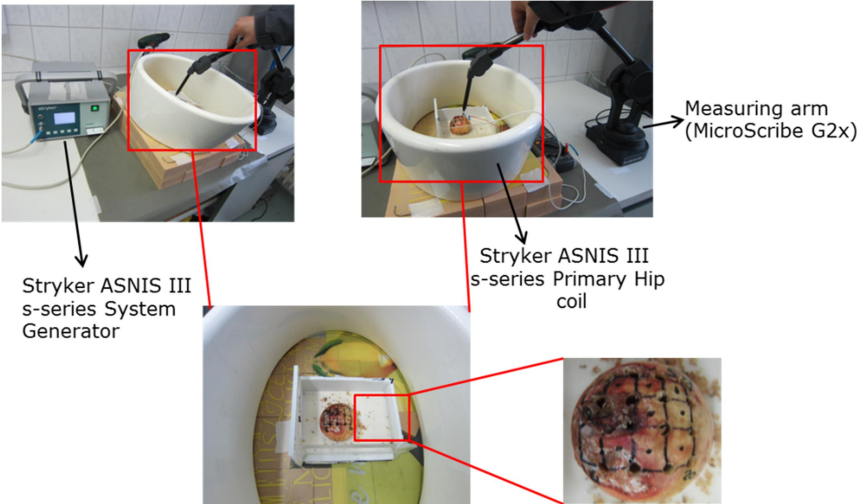
Fig. 4.5 Human femoral head model validation experiment setup.

- Blue - Measuring points 5mm in the bone
- Black – Measuring points on the surface of the bone
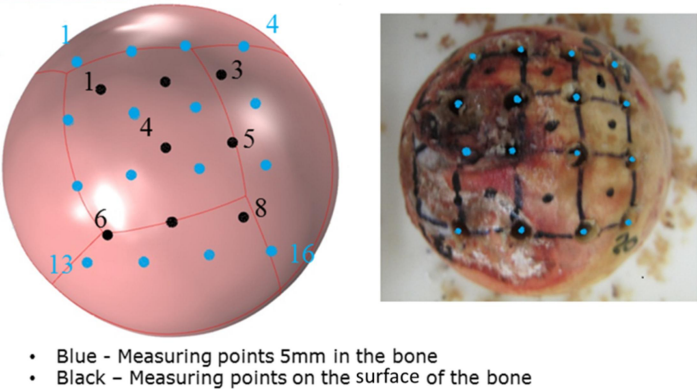
Fig. 4.6 Measuring points in validation experiment (right) and in numerical simulation model (left).

Screw implant parametric study

In the numerical simulation the screw implant was located in the centre axis of the human femoral head model in accordance to the validation experiment. There are three kinds of parameters were investigated in implant parametric study: screw tip design, screw insulation length, and screw positioning. Besides the original tip, a round and a flat tip were considered. The screw was positioned, one step at a time, further into the femoral head dome or out of the femoral head in the simulation model to analyse the influence of screw position on the electric field distribution. In order to keep the screw tip and shaft length proportionately the same, the screw insulation length was varied in both the screw tip and the shaft direction. Furthermore, to investigate how the tissues surrounding the bone influence the electric field in the femoral head, the surrounding tissues were considered as in three cases: muscle only, muscle with fat, and muscle with fat and dry skin. One designed lesion in the sphere shape was located in the femoral head to consider the real clinical condition. The tissues surrounding the bone in the lesion cases were considered as muscle with fat and dry skin. As in reality, when weak bone tissue is removed from the bone during surgery, blood fills up in the open space. Therefore, lesion materials were considered as fat and blood respectively in the simulation.

4.1.2 Optimization of the implant position in the femoral head

Asnis III s-series screw system is only suitable for early stage of the avascular necrosis in the femoral head (Steinburg Stage I to III). Due to the reason that MRI was used to diagnose early stage of avascular necrosis in the patients and to assess the outcome of the treatment, only patient MRI data (pre-operative and post-operative) is available for the optimization process. To determine the optimum position of the electro-stimulating screw implant within the femoral head, the first is to set up the numerical model of implant and femoral head before optimization techniques could be applied. The second step is to apply this numerical model into FEM software to calculate the electric field distribution in the femoral head. The third step is to include numerical simulation into the optimization algorithm and calculate the optimum position of screw in the patient femoral head.

Numerical modelling

Model reconstruction

To numerically analyse the screw implant optimization in the patient femoral head, a typical patient who suffered from avascular necrosis (Steinberg Stage III C) was chosen. The pre-operative patient MRI data was used to reconstructed the proximal femur model according to the procedure described by Kluess et al. [120]. Two software tools were used in the model reconstruction. First the proximal femur and the lesion in the bone of the patient were

manually segmented from the pre-operative MRI data using Amira 5.4 software (Mercury Systems, Chelmsford, MA, USA) , and converted to STL files in ASCII format. Then the STL of the femur was transferred to the reverse engineering software Geomagic (Geomagic, Morrisville, NC, USA) and lesions were refined and generated to a NURBS CAD model for numerical simulation. To keep the same as reality, the proximal femur model was divided into sections of cortical and cancellous bone. But as the MRI patient data had relevant large slice sickness, the contrast between thin cortical bone and cancellous bone in the patient femoral head MRI data were not all the time clear. Due to this reason, the full volume of the femur was scaled down and then subtracted from the original volume in Geomagic. To verify the ratio of the scaling, the patient model (in 4.1.1) was reconstructed from CT scans. As a result, the inner subtracted volume represents cancellous bone, whereas, the outer layer represents cortical bone.
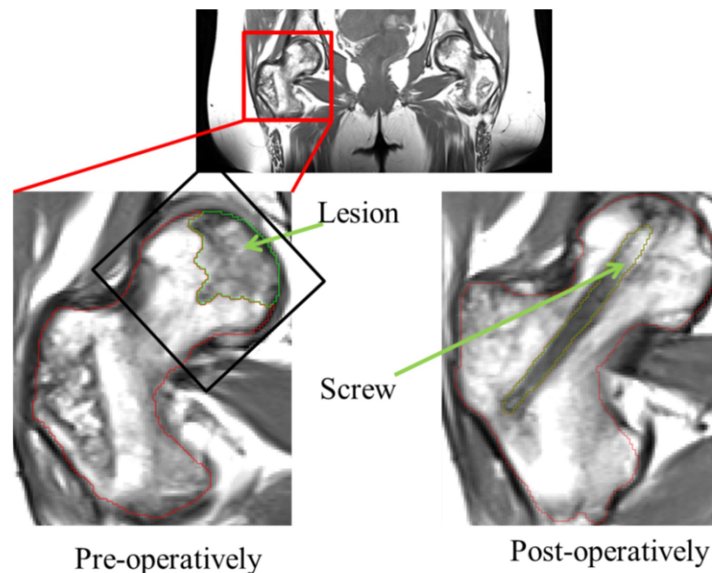
Fig. 4.7 Patient femoral MRI data. The pre-operative (left) and post-operative (right) femoral head under the area of the black rectangle is used to reconstruct the femoral head model for the simulation.

To define the initial position of the screw in the femoral head, the post-operative MRI patient data was used (Fig. 4.7). As first, the screw was manually segmented using Amira 5.4. The screw datum which included screw position information was reconstructed using Geomagic. In the end, the screw has to be translocated from the post-operative into the pre-operative femur model. To do the screw translocation, the post-operative femur model was reconstructed from the post-operative MRI data. The transformation matrix which included the best-fit alignment of the post-operative femur to the pre-operative data was created. The screw datum was translocated to the pre-operative femur model by loading the

transformation matrix.

The screw model was created according to the screw datum in the pre-operative femur model and the size of the screw was obtained from the manufacturer's datasheet. The thread of the implant was not taken into account in the numerical simulation due to the reason to reduce computational and mesh generation complexity.
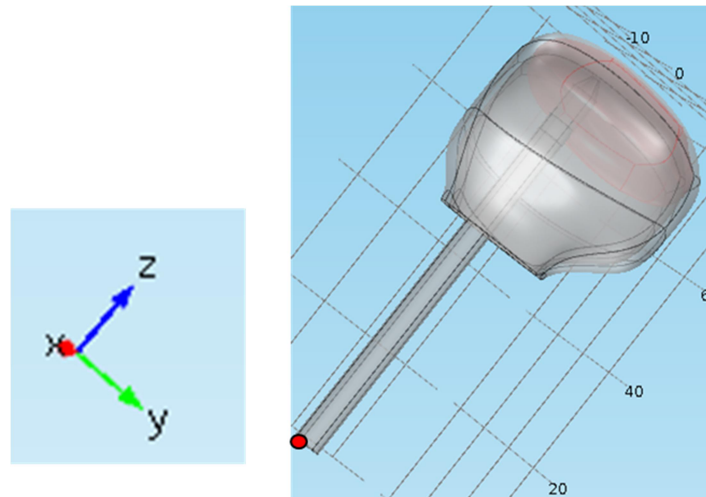
Fig. 4.8 Patient femoral head model. Femoral head with lesion and screw implant, where the (0, 0, 0) point is the bottom centre point of the implant.

To decrease computational effort, the proximal femur model (Fig. 4.8) in the numerical simulation was reduced to the femoral head as depicted in figure 4.7 by the black frame. Another reason for this considering is that the electric field caused by screw implant should only affect the volume inside the femoral head. The surrounding tissue of the femoral head was substituted by blood in the present simulation since the surrounding tissues of the femoral head are highly complex and are of minor interest for the electric field distribution inside the femoral head. The surrounding blood cylinder has a radius of 100 mm and a length of 120 mm. In order to reduce mesh complexity, the thread on the surface of the implant was not taken into account to simulation.

Due to the lace source of the dielectric properties of bone are available, the conductivity and relative permittivity of bone tissue and blood were taken from Gabriel et al. [105,109]. The material properties of the screw implant in the numerical simulation were according to the data sheets from manufacture. Dirichlet boundary condition and Neuman boundary condition were applied in the simulation (equations 3.16, 3.17). Dirichlet boundary condition was considered to impose an electric potential, RMS 700 mV, on the surface of the screw implant electrodes. Neumann boundary condition was applied to the insulating surfaces of the screw implant and the exterior boundary of the model.

Mesh generation

In all calculation domains of the femoral head model simulation, the tetrahedral mesh was implemented and adjusted manually. To ensure sufficient computational accuracy, triangular elements with a maximum element length of 0.5 mm was used to mesh the screw implant surface and free tetrahedral elements with a maximum element length of 0.8 mm was used to mesh the human femoral head. The resulting model for each implant positioning consisted of 1.68 million mesh elements and 2.2 million DoF was existed in the model computation.

Optimization platform

An optimization platform was developed to optimise the implant position in the femoral head model. MATLAB software and finite element COMSOL Multiphysics 4.3b software were integrated through use of the iSIGHT software (Dassault Systemes Deutschland, Hamburg, Germany) interface. Figure 4.9 shows the general approach of design optimization process. To optimize the designed model, input parameters for the model should be automatically adjusted according to different optimization algorithm and output results from the simulation should be automatically determined if that is optimized or not. Moreover, the model simulation should be automatically started with the adjusted input parameters. All these function are available in iSIGHT .iSIGHT supplies a desktop solution which provides a visual and flexible tools for creating simulation process flows, integrating varies of CAD and CAE commercial software, in order to automate the exploration of design alternatives and identification of optimal performance parameters. It also combines different classes of optimization algorithms to exploit the particular aspects of these algorithms to address specific aspects of a design problem.
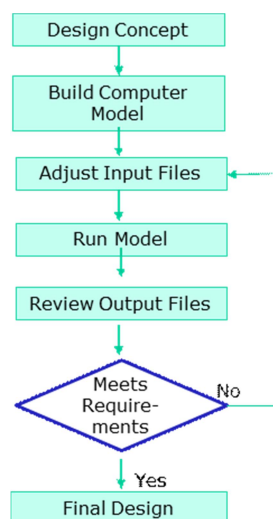
Fig. 4.9 General optimization approach.

Software integration

As COMSOL is not supported application in iSIGHT, this software package has to be integrated first into iSIGHT. Process integration is important in simulation and optimization, as it automatically adjusts the variables at the end of every cycle and starts the new simulation with the adjusted variables. As shown in figure 4.10, the patient's femoral head model based on the screw position is built in COMSOL. Moreover, in COMSOL the model is discretised into small elements for numerical analysis, boundary conditions and electric properties to all materials are applied and the electric field in all domains is calculated. The VTA in the femoral head is calculated in MATLAB according to the COMSOL calculation result of the electric potential. The result of VTA is saved into output files after the VTA calculation. Finally, the input screw position is adjusted according to the response of the output VTA results by the iSIGHT optimization. Variables and objectives from the input and the output files will be parsed by the optimization platform respectively. To integrated COMSOL into iSIGHT, the batch model with a SimCode component was used and was named as 'CallComsol' in iSIGHT. In additional, the input parameters and output parameters are monitored in iSIGHT to analyse how the input parameters influence the output parameters. This is really important to better understand the model design.
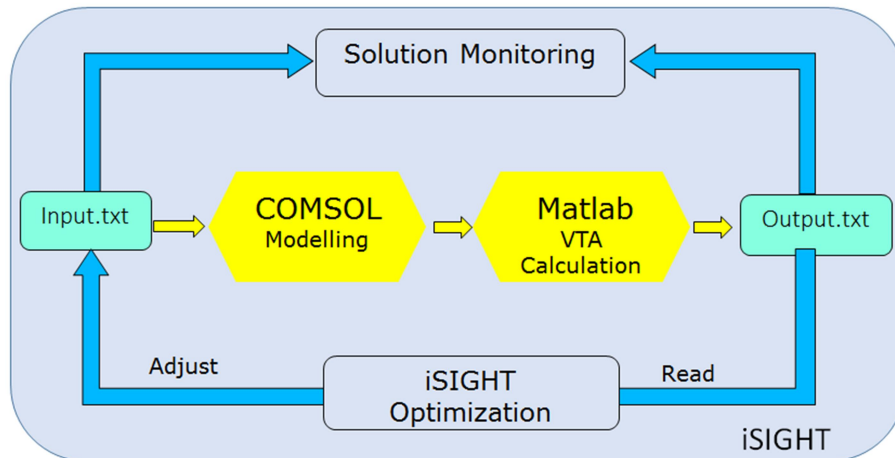
Fig. 4.10 Integration scheme.

Optimization strategy

The optimization was based on the femoral head simulation. It is a process of hundreds of simulation cycles and optimization searches. Besides the optimization efficiency and precision, the time consumed by each step is one of the most important factors in optimization process. The grid size of the VTA calculation was chosen to be 3 mm to

maintain a balance between optimization efficiency and computational accuracy.
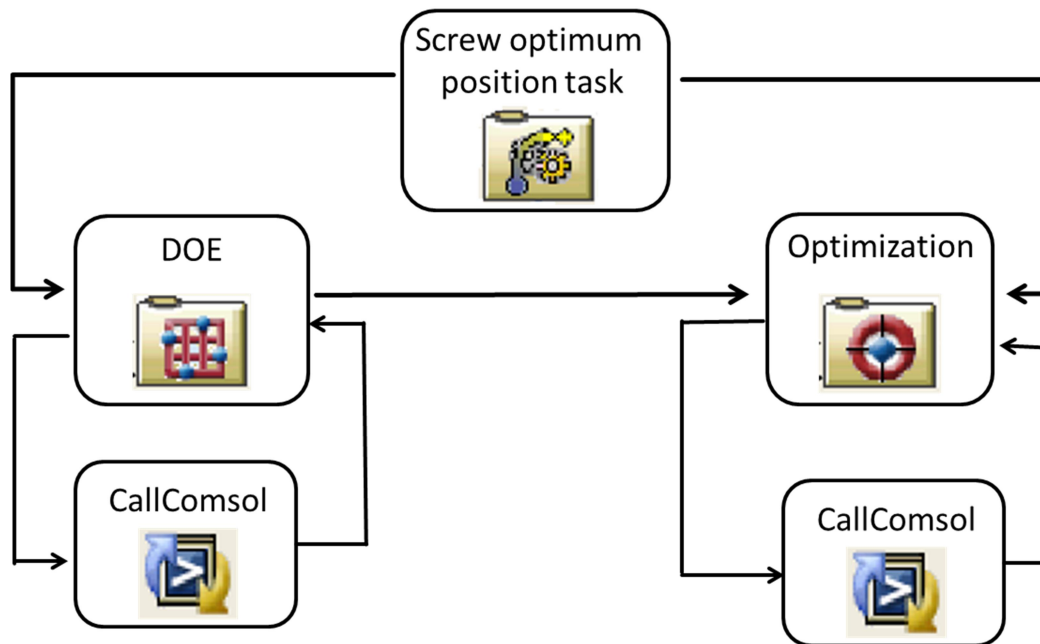
Fig. 4.11. The workflow in iSIGHT.

There are two components in our global optimization strategy, one is design of experiment (DOE) and another one is optimization. The reason to run DOE before the optimization is to better understand how each parameter influences the final design. It is normally a preferred approach to find the global optimization for the model design. DOE screens the design space and then results in an estimated optimum result. In order to balance the run time and accuracy, in our optimization process, the screw position parameters in model simulation were sampled using the *optimal Latin Hypercube technique* with 100 points. The estimated optimum screw implant position was found by DOE. The optimization algorithm in the workflow does not have to start from scratch or randomly at some points in the design space. Instead, the optimization uses the results of the DOE to start the search intelligently in the vicinity of the estimated optimal point. In practice, the optimizer starts where the DOE left off. As the current study is a single objective application, the single objective optimization method '*sequential quadratic programming technique* [127]' was chosen in the optimization process. This method explores the local area around the initial design point and rapidly obtains a local optimum design. It builds a quadratic approximation to the Lagrange function at each iteration. On each iteration, a quadratic programming problem is solved to find an improved design until the final convergence to the optimum design. A considerable reduction in the number of optimization iterations to convergence is achieved and the global optimal solution was found. Figure 4.11 shows the workflow of the optimization process in iSIGHT.

Variables and objectives:

The variables, objective and constraints of optimization can be shown following.

Variables: screw position in the x direction (spx) (mm),

               screw position in the y direction (spy) (mm),

               screw position in the z direction (spz) (mm),

Objective: maximum volume of tissue activated (VTA) in the femoral head (mm^3)

Constraints: screw position in the x direction (spx) (mm), -3<spx< 3

               screw position in the y direction (spy) (mm), -3<spy<3

               screw position in the z direction (spz) (mm), -15<spz<3

Three parameters of screw position was defined, screw position in the x, y and z direction respectively. The objective of the optimization was to find the optimum position of the screw that delivers the maximum VTA to the femoral head. The screw position in the femoral head should be considered as reasonable for surgery. Therefore, there were some constraints on the screw positions in the x, y and z directions.

4.2   Results

4.2.1 Implant parameter analysis in the femoral head
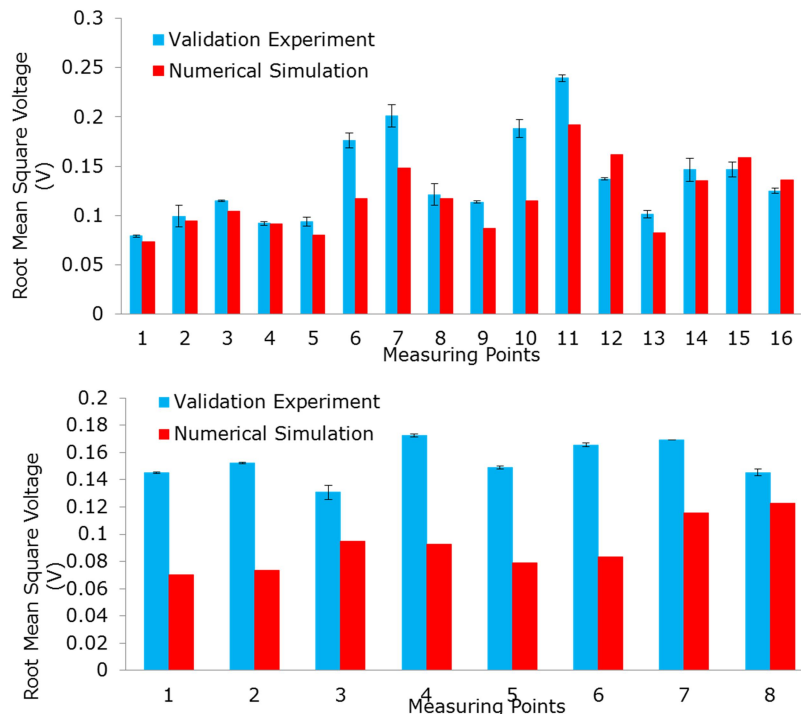
Fig. 4.12 Results of validation experiment, where the measuring points are (top) approximately 5 mm depth in the femoral head and (bottom) on the surface of the femoral head: blue bars are the RMS voltages in the validation experiment; and red bars are the RMS voltages in the numerical simulation.

Validation results

Figure 4.12 reveals that the results of the validation experiment are close to those of the numerical simulation when the measuring points are at 5 mm depth in the femoral head and on the surface of the bone. The tolerances between the numerical simulation data to experiment data on all measuring points were calculated. On average, 24% difference can be found when the measuring points are on the surface of the bone. When the measuring points are at 5 mm depth in the bone, this percentage decreases to 19%. In total, average 20 % tolerance can be found in all the measuring points. Also we considered that the tolerance is acceptable for the validation of numerical simulation.

Screw implant parametric study

To simplify the models in the screw implant parametric study, the surrounding tissue of the femoral head in whole screw implant parametric study is only blood. The activated tissue electric field distributions in the human femoral head under different screw parameter variations are shown in the following figures. Contour lines of the field for a 2D cutting plane of the human femoral head are presented to give an insight into the activated tissue electric field distribution in the femoral head.

Tip design parameters
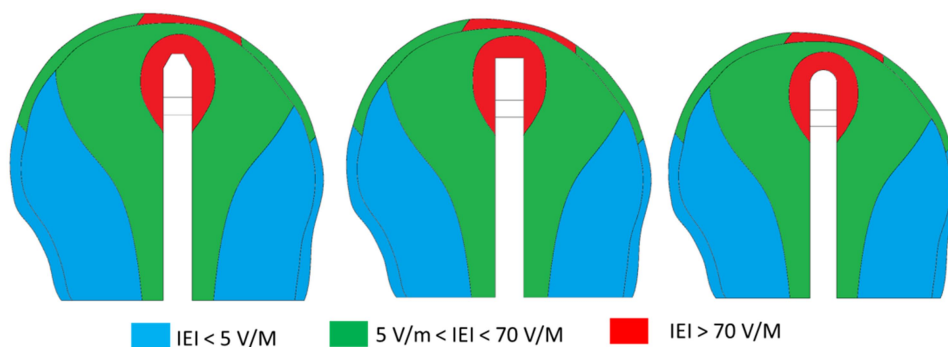
Fig. 4.13 Numerical simulation of electric field distribution: testing three screw tip designs. The electric field in blue and red areas provides regions of < 5 and > 70 V/m, whereas the green areas are optimal activated regions for bone tissue growth.

Figure 4.13 shows that, the original tip and the round tip designs have similar electric field distributions under the condition of keeping the screw in the same position. But in the flat tip design, the electric field shows a minor difference around the screw tip. This tiny changing is caused by the edge effect.

The results of the volume fraction can be found in figure 4.14. It shows that there is only 0.2% electric field change in the human femoral head of between the original tip and the round tip designs. But this difference rises to 1.4% when the tip design is changed to flat. The linear regression function for simulation of tip designs is also shown in the figure 4.14, which is $f(x) = 0.698\,x + 25.161$ and R^2 is 0.876.
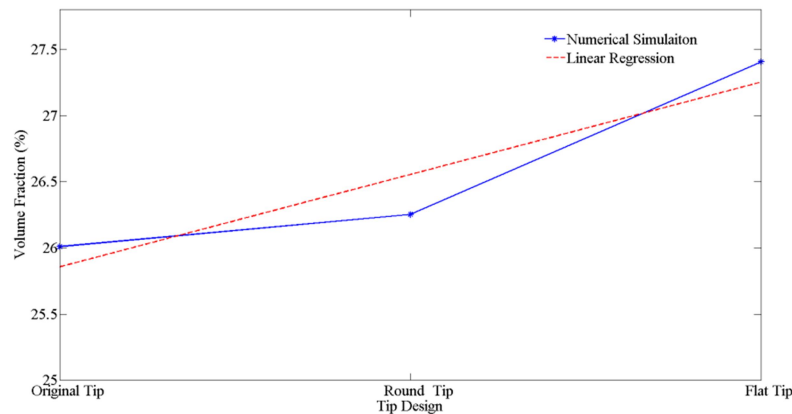
Fig. 4.14 Numerical simulation of screw tip design: results for volume fraction. The line with the star is the volume fraction for each screw positioning parameter and the dashed line without a star is the best fitting linear regression function of the numerical simulation.

Screw insulator parameter results

In the screw insulation length variation, all the screw insulation varied under the condition of keeping the screw position constant and using the original screw tip design. There were two cases of screw insulation length variation. In the first case, the screw insulation was varied while the screw shaft electrode was kept same (Fig. 4.15 (left)). The results show that the tissue area activated by the electric field increased when the screw insulation length decreased. Figure 4.16 (left), shows that this changed has been quantified, that is each 1 mm changed in the insulation length resulted in a volume fraction difference in the femoral head of approximately 1.8%. The linear regression function is $f(x) = -1.738\,x + 31.063$ and R^2 is 0.997.

Figure 4.15 (right) shows the second case of the screw insulation length variation. In this case, the length of the insulation was varied while the screw tip was kept the same. It is clear to see that the larger the screw insulation length in this variation, the bigger the activated tissue electric field distribution area. Comparison to in the first case, the volume fraction increased in the second case only by approximately 1% when the insulation length was increased same amount, 1 mm (see Fig. 4.16 (right)). The linear regression function for the simulation of this kind of insulation variation is $f(x) = 0.973\,x + 23.029$ and R^2 is 0.996.
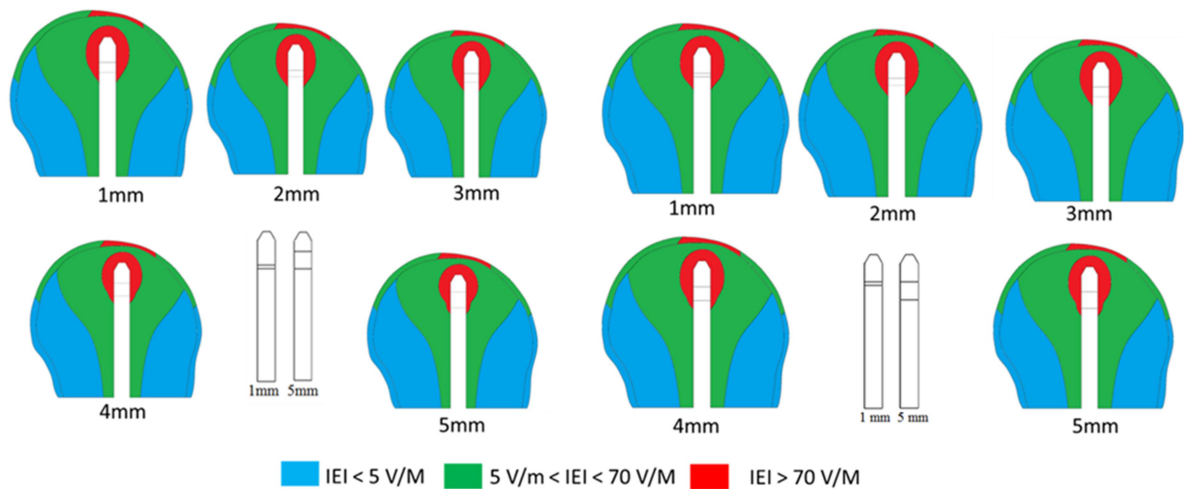
Fig. 4.15 Numerical simulation of electric field distribution: testing different screw insulation lengths, where (left) the length of the screw shaft electrode stays constant and (right) the length of the screw tip electrode stays constant. The electric field in blue and red areas provides regions of < 5 and > 70 V/m, whereas the green areas are optimal activated regions for bone tissue growth.
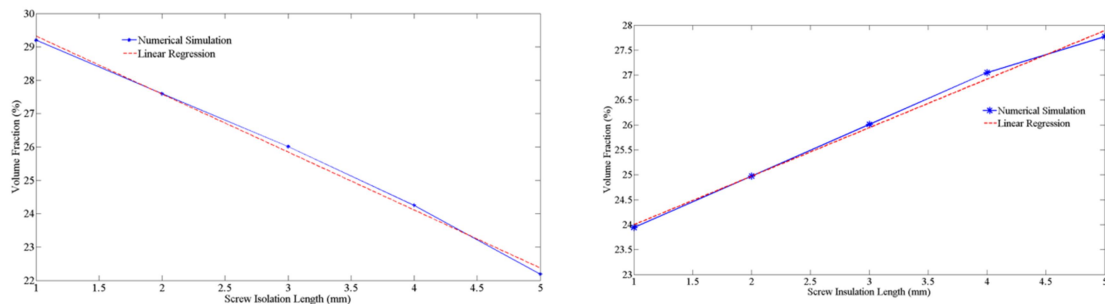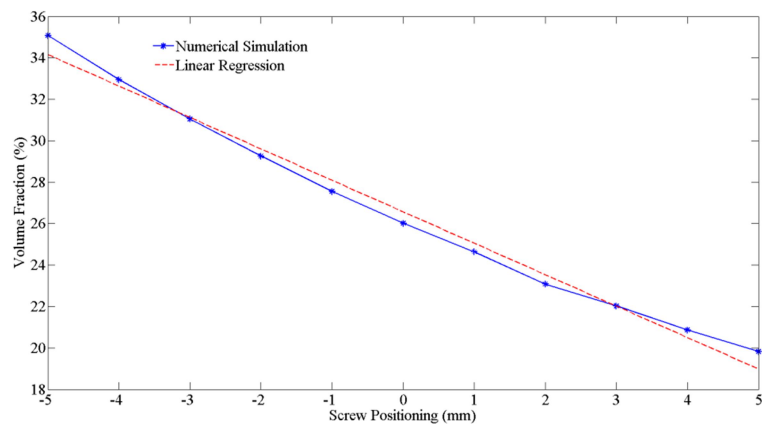

Fig. 4.16. Numerical simulation of screw insulation length, where (left) the length of the screw shaft electrodes stays constant and (right) the length of the screw tip electrode stays constant. The line with the star is the volume fraction for each screw positioning parameter and the dashed line is the best fitting linear regression function of the numerical simulation.

Screw position parameter

Figure 4.17 shows the electric field distribution of the screw positioning in the femoral head under the condition of using the original screw design. The screw moved in the femoral head in two directions, one is forwards, one is backwards. The activated tissue electric field area is increased when the screw is moved backwards and decreased when the screw is moved to the dome of the femoral head. Figure 4.18 demonstrates that an approximately 1.5% change in the volume fraction in the femoral head can be found in each 1 mm change of the screw position. The linear regression function for the simulation of the screw positioning parameter is $f(x) = -1.517x + 26.575$ and R^2 is 0.989.

47

From the volume fraction and electric field distribution in the femoral head for these four parameter variations, it is clear to see that the screw tip design has the least effect on the electric field distribution, and the insulation length and position variations have similar effects.
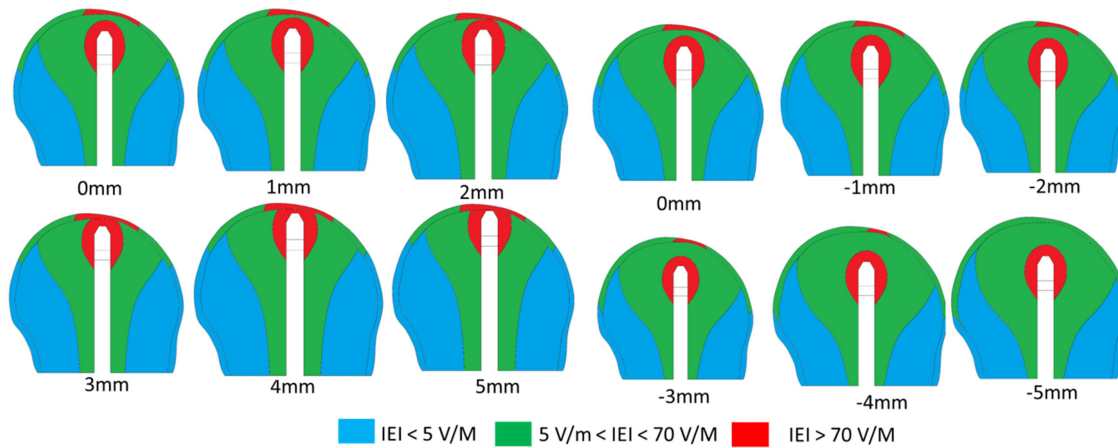
Fig. 4.17 Numerical simulation of electric field distribution: testing (right) screw backward positioning and (left) forward positioning. The electric field in blue and red areas provides regions of < 5 and > 70 V/m, whereas the green areas are optimal activated regions for bone tissue growth.
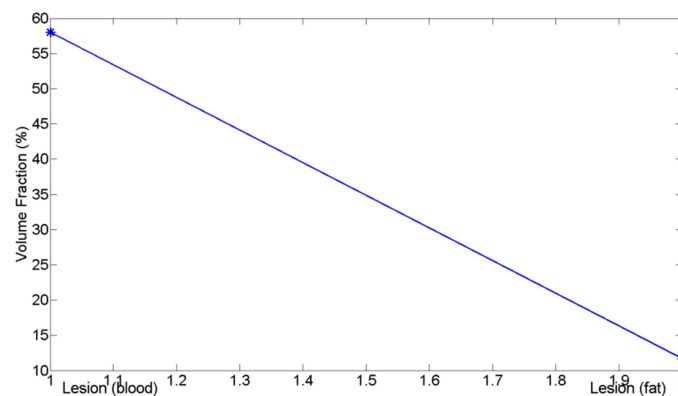

Fig. 4.18 Numerical simulation of screw positioning: results for volume fraction. The line with the star is the volume fraction for each screw positioning parameter and the dashed line is the best fitting linear regression function of the numerical simulation.

Surrounding tissues

Figure 4.19 shows the electric field distribution in the femoral head of the different tissues surrounding the bone under the condition of keeping the screw position and design the same. Significant activated tissue electric field distribution changing can be found between

the case of surrounding tissue is blood and muscle. When the surrounding tissue changed from blood to muscle, the activated tissue electric field area was clearly increased. But comparing only muscle case, to the other two cases - muscle with fat and muscle with fat and skin - the electric field area of the activated tissue remained almost the same as in the case of muscle only. In figure 4.20 these three scenarios are demonstrated by the volume fraction of the electric field in the femoral bone. From the case of blood to only muscle tissue surrounded, 4% volume fraction is gained. But a similar change of the volume fraction cannot be found in the cases of combination, muscle and fat, or muscle with fat and skin.

IEI < 5 V/M   5 V/m < IEI < 70 V/M   IEI > 70 V/M
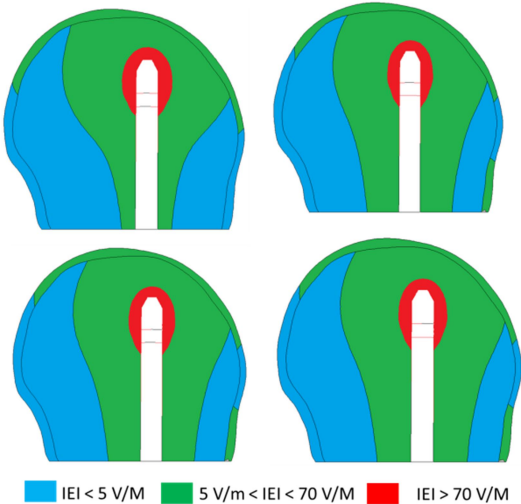
Fig. 4.19. Numerical simulation of electric field distribution: testing different tissues surrounding the bone, where the surrounding tissue is (up left) blood, (up right) muscle, (down left) muscle with fat, and (down right) muscle with fat and skin. The electric field in blue and red areas provides regions of < 5 and > 70 V/m, whereas the green areas are optimal activated regions for bone tissue growth.
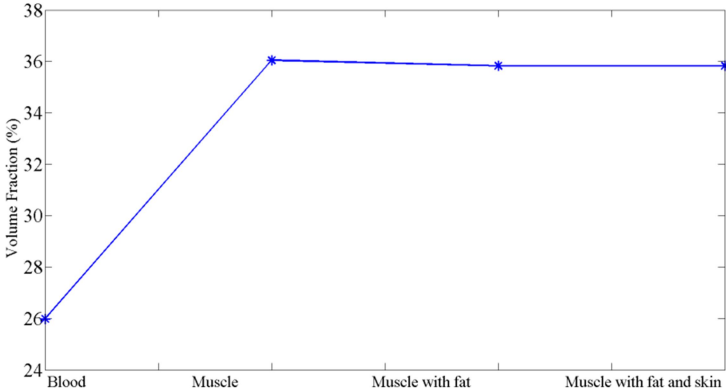
Fig. 4.20. Numerical simulation of tissue surrounding the bone: volume fraction.

Lesion in the femoral head

Figure 4.21 shows the electric field distribution of the different lesion materials under the condition of keeping the tissues surrounding the bone as muscle with fat and skin. The screw position and design are kept the same as well. Two cases of lesion material are considered, one is blood and one is fat. The activated tissue electric field in the femoral head is significantly increased from fat to blood. Similar scenario can be seen in figure 4.22. It shows that comparing to the case of lesion is fat, 46% the volume fraction is gained in the case of lesion is blood.
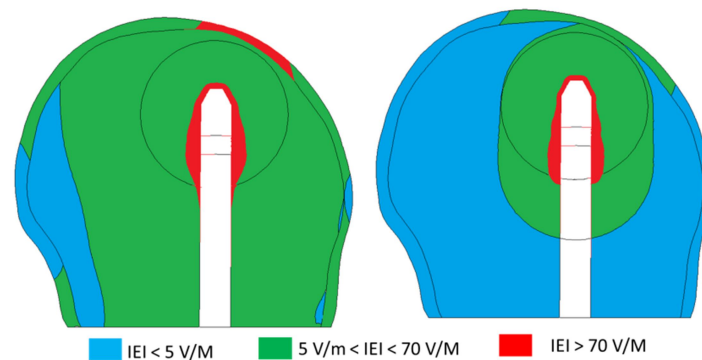
Fig. 4.21 Numerical simulation of electric field distribution: testing different lesions, where the designed sphere-shaped lesion in the bone is considered as (right) fat and (left) blood. The electric field in blue and red areas provides regions of < 5 and > 70 V/m, whereas the green areas are optimal activated regions for bone tissue growth.

Fig. 4.22 Numerical simulation of lesion in the bone (lesion as blood, lesion as fat): volume fraction.

4.2.2 Optimization of the implant position in the femoral head

The results of the optimum position of the screw which delivers the maximum VTA to the femoral head was shown in Table 4.2. Compared to the initial position (based on post-

operative MRI data), deltas of 0.7 mm, 2 mm and -6.1 mm in the x, y and z directions respectively exist on the calculated optimum screw implant position. A pareto plot generated by DOE (Fig. 4.23) in optimization algorithm reveals that how the screw position in the x, y and z directions influences the VTA in the patient femoral head. It shows that the screw positioning in the axial z direction has the largest influence (50%) on the VTA in the femoral head. Screw in the x direction positioning can cause negative effect on the VTA in the femoral head. It means screw positioning in the direction of moving in or out of the femoral can bring out the biggest effect on the activated tissue electric field distribution in the femora head. These results are essential to the implant surgery processing.

Table 4.2. Screw implant position in the femoral head after optimization.

	Optimum position (mm)
spx (screw position in x direction)	0.7
spy (screw position in y direction)	2.0
spz (screw position in z direction)	-6.1
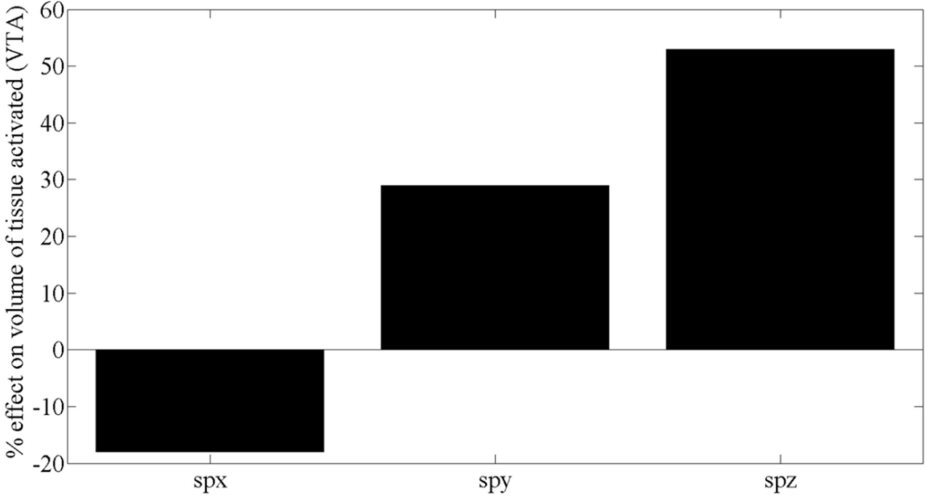
Fig. 4.23 Pareto plot of screw position effects on the volume of activated tissue at different **s**crew positions in the x , y and z directions (spx, spy and spz).

The activated tissue electric field distributions in the human femoral head with both original screw implant position and optimum screw implant position are shown in figure 4.24. To give an insight into the activated tissue electric field distribution, contour lines of the field for a 2D cutting plane of the femoral head are presented. Compared to the screw position in the post-

operative femoral head of the patient (original screw implant position in the numerical simulation), the optimum screw position in the femoral head is located almost outside of the lesion. But comparing to the original screw implant position, the larger activated tissue electric field area in the necrotic lesion can be found.
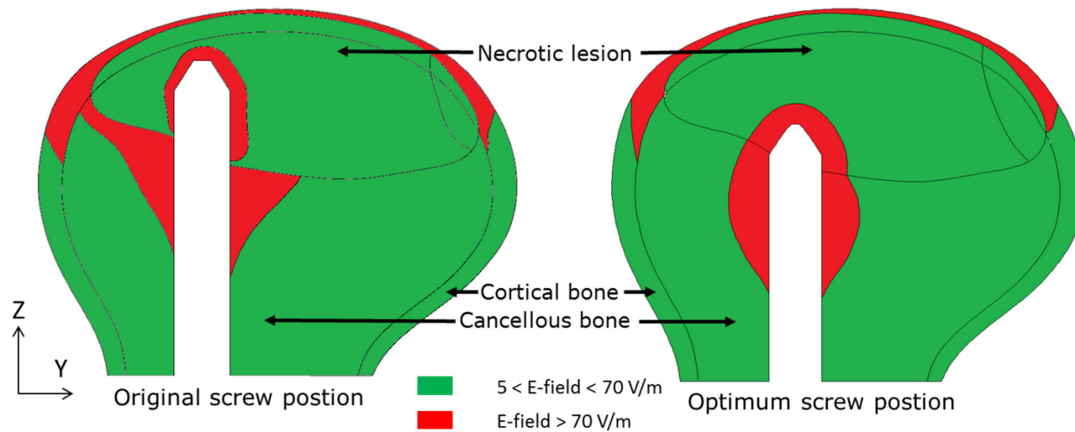
Fig. 4.24 Electric field distribution in the femoral head in 2D ZY cut plane. Screw position in the optimum position (right), and screw position in the patient's post-operative MRI data (left).

To quantify the activated tissue electric field volume changes in the femoral head from original screw implant position to optimum screw implant position, percentage of VTA has been calculated. The result shows that 85% percentage of VTA in the femoral head can be found in the original post-operative position and 88% in the optimum calculated position.

4.3   Discussion

Numerical simulation is a commonly used method of calculating the electric field distribution in biological tissue [123,128-132]. The influence of different parameters of an electro-stimulating implant on the electric field distribution in the human femoral head has been evaluated and an automatic modelling approach [133] was introduced in the present study to find the optimum position of an electro-stimulating implant in the femoral head. iSIGHT in combination with COMSOL was used in the optimization procedure [134]. The numerical simulation model of a femoral head for the implant parameter analysis was experimentally validated and demonstrated that the position of the implant in the femoral head and length of the implant insulation have a significant influence on the VTA in the femoral head compared to the effect from the implant tip design. The effect of screw position in each direction (x, y, z) has been quantified and optimized screw position has been given for the patient specific femoral head in the screw positioning optimization. A very important result for screw implant

surgery was found in the optimization. It is that the screw position in the z direction (moving inside or outside of the femoral head) was found have the most effect on the VTA in the femoral head.

The electric potentials at all measuring points were measured in the experiment and numerically calculated in the numerical simulation. As a result, an acceptable range (average 20%) of tolerance was found between numerical simulation data and experiment data in the screw parameter analysis. Subsequently, series evaluations of the effect of different screw parameters on the electric field in the femoral head were carried out using the numerical model. Nevertheless, the electric properties of the human femoral head in the model were not calibrated according to the experimental validation. The real electric properties of the specific human femoral head are necessary to be calibrated and used in the evaluation of electric field distribution in the femoral head although only 20% difference was obtained when using the electric properties from Gabriel et al. [105,109]. The bone dielectric properties calibration from experiment could be achieved by an automatic optimization process. The objective of the optimization process could be minimizing the difference between numerical data and experimental results.

Although in Kraus [89] the electro-stimulating implant was located in the weak bone and successfully stimulated new bone growth, the sensitivity of the electric field in the bone to the implant was not investigated. Screw positioning, screw tip design, and screw insulation length were analysed in screw parametric study. Our screw implant parametric studies results show that in the current human femoral head specimen, a linear relation has been found between the insulation length of the screw and the change in the activated tissue electric volume in the femoral head. According to the results, there are two possibilities to achieve large VTA in the femoral head by changing the length of the insulation: either increasing the screw insulation length while keeping the screw tip electrode length the same or decreasing screw insulation length while keeping the screw shaft electrode length the same. In the results of screw insulation length parameter variation, keeping the screw shafts same case shows almost two time bigger influence on the VTA than keeping the screw tip same. The influence of each 1 mm screw insulation length on VTA while keeping the screw shafts same and keeping the screw tip same are −1.8% and 1.0%, respectively. Among three parameters, the screw positioning in particular is relevant and important because it can be changed during the implantation process. The numerical data shows that 1.5% VTA change can be found when each 1 mm tiny screw positioning in the femoral head. It reveals an approximated negative linear relation between the screw positioning and VTA in the femoral head. This gives a guidance for intra-operative application when considering the effect of the screw position on the electric field in the bone (for example, by moving the screw implant

outside of the femoral head to get a larger VTA in the femoral head). The screw position revealed the largest effect on the electric field distribution in the femoral head in these three parameters. In present study, the screw position was only investigated without considering a necrotic lesion; however, necrotic lesions are usually removed and filled with fresh autologous bone during surgery [37]. Moreover, comparing to screw insulation variation and screw positioning variation, the relevant low influence on VTA was found from the screw tip designs (0.2% in round tip and 1.4% in flat tip). This demonstrates that the shape of the screw tip design has only a minor influence the VTA in the femoral head.

However, the effect of VTA in the femoral head from the radius of the screw implant was not included due to the reason that the screw radius is mainly decided on the basis of the patient's femoral head size. Therefore, the number of the screw implant and the radius for each implant should be taken from the relevant surgery process and evaluated when designing a patient's specific screw implant. In present work, the mechanical stability of the bipolar induction screw system with different tip designs and insulation lengths was not included. Although in Mittelmeier et al. [96], the mechanical stability of the original Asnis III s-series screw was tested and the BISS screw (which was later named the Asnis III s-series screw) was found has significantly higher mechanical values than normal screw due to a reinforcing effect by the attached electrode. In future studies, in order to produce customised screws for specific patients, their mechanical stability should be considered.

Moreover, the screw parametric study and screw position optimization in the femoral heads are based on various limitations, assumptions and simplifications. As the electric potential on the surface of the screw is relatively low, around 750 mV, electrical double layer (EDL) was not included in the screw parametric study and screw position optimization. But EDL is important to bone electric stimulation [135]. Therefore, in future studies, the electric potential caused by EDL on the surface of the screw in the bone should be calculated like in [135,136] and the femoral head model in the screw parametric study should be revalidated and the optimum screw position in the patient femoral head should be recalculated with the new electric potential on the surface of the screw.

The electrical properties of cancellous bone and cortical bone for the human femoral head simulation were used both isotropic and homogeneous conductivity and permittivity. Because bone density varies between patients, the electrical properties of the femoral bone may also differ from patient to patient, especially for osteoporosis patients. Williams and Saha [137] found that the specific capacity of wet human cortical and cancellous bone depends on bone density. Sierpowska et al. [115] found that the electrical and dielectric parameters of human trabecular bone, especially the relative permittivity and the dissipation factor, were significantly and specifically related to the trabecular microstructure. Therefore, to achieve

patient-specific stimulation modelling, the relationship between bone density and dielectric properties should be taken into account in future studies. Also the material properties of femoral head can be considered as uncertain [138] and the influence of uncertainties in the bone dielectric properties of bone on the probabilistic VTA in the femoral head can be analysed. iSIGHT combining COMSOL by using Monte Carlo application could be one solution for this propose.

In both screw implant parametric study and screw implant optimization study, the electric fields varying from 5 to 70 V/m were only considered to as this interval electric field has been shown the optimum effect on bone growth [89]. But application of excessive current densities to biological tissue can cause tissue degradation [139]. Introducing a specific strength of electric field to the bone tissue is predicted to cause overstimulation of bone tissue. Moreover, Qu et al. [140] explained using a hypothetical model that to effectively stimulate bone remodelling, both the upper and the lower electric field limits were needed. Therefore, minimizing the volume of overstimulated tissue should be an important objective to the optimization process. The overstimulated tissue electric field should also be considered in the screw implant parametric study.

Another simplification in screw parametric study is that the necrotic lesion within the femoral head has not been taken into account in the evaluation of implant parameters until now, although the bipolar induction screw system was used for stimulating the weak bone in the femoral head in the case of avascular necrosis. Moreover, the size of the surrounding tissue of the human femoral head in the simulation model was comparable to reality, but it was simplified by using blood due to the reason that geometric complexity of model reconstruction and lack of knowledge of the electric properties of the soft tissue at a frequency of 20 Hz. Even though, we consider this model simplification is acceptable because from the results of bone surrounding tissues study, the attached tissue surrounding the bone has the greatest influence on the electric field distribution in the numerical simulation. In the future study, cartilage bone can also be considered around the femoral head to get more realistic model for human femoral head.

One care should be taken is that the necrotic lesion in the femoral head cannot be neglected when using numerical simulation to guide a surgical approach as the size, location and material of the lesion have significant influence on VTA in the femoral head. In practical surgery, bone graft and electrical stimulation was combined to treat avascular necrosis. It means necrotic lesion was removed from the patient and health bone and blood were filled in the original lesion place in the patient femoral head. The results showed that considering lesion as blood in the femoral head can significantly increase the activated tissue electric field volume in the femoral head. It numerically proved that the surgical process for screw

implantation is necessary for heal the avascular necrosis in the femoral head.

The limitation in the screw positioning optimization study is that patient MRI data was used to reconstruct the patient specific femoral head model. This because that the screw implant is commonly used to treat early stages of avascular necrosis in the femoral head and MRI is commonly used to diagnose early-stage necrotic lesions in the femoral head [141] due to its sensitivity to soft tissue. But MRI data which was used for proximal femur model reconstruction has a slice thickness of 3 to 5 mm, which is relatively large and results in low geometric accuracy. Also because of this, the cancellous bone in the femur had to be scaled down from the model. A good solution to overcome this limitation involves taking additional CT scans of the patient after diagnosing avascular necrosis and before removing the screw implant. In screw parametric study, the thread on the surface of the screw was not considered in the numerical simulation owing to the complexity of the mesh and long computational time consuming.

Comparing the optimization method used in [132,136], combining COMSOL with iSIGHT is more convenient and easier as iSIGHT has an easy handling user interface. Besides, there are more optimization algorithms available for single and multi-objectives optimization problems in iSIGHT. In future studies, all the single-objective algorithms should be used to solve the current optimization problem and the ability of these algorithms could be evaluated and compared.

In current screw positioning optimization, only the stimulation parameters (700mV and 20 Hz) were used in the optimization process. Further stimulation parameters can be considered in the optimization approach in future studies. For instance, the required frequencies of stimulation are 12 and 20 Hz, depending on the clinical application, and electric potential can also vary. Moreover, when a patient has a very large lesion or more than one lesions in the femoral head, two screws could be implanted. Therefore, depending on the patient-specific location of the lesion in the femoral head, the number of screws can also be considered as a parameter to be optimized. To design the customized electro-stimulating implant for specific patient, CAD design software can be integrated into the optimization approach.

5 Numerical simulation in cell experiments

The objective of in vitro testing is to analyse the effect of electric fields on the growth of human osteoblasts and to allow an optimal cellular stimulation. The cell experiments in this chapter include three systems. System I is designed for the Asnis III s-series screw system. The Asnis III s-series screw system has been successfully used in the clinical treatment of avascular necrosis in the femoral head. But the underlying understanding of bone cell growth in this system has not been studied so far. Therefore, bone cell growth was evaluated in system I in three different conditions: electromagnetic field, electric field and controlled. System II is a designed chamber system. This system's aim is to analyse the bone cell growth under conditions of an applied electric field. System III is designed for an electro-stimulating implant in animal testing. The optimized design of cell experiments for this system is numerically found by applying FEA.

Through the cell experiments, the optimal stimulation parameters for both, clinical study of avascular necrosis in the femoral head and the animal tests, should be found. Designing and establishing the setup of each electro-stimulating implant were very time-consuming. Numerical simulation is a convenient tool for analysing electrical stimulation in biological tissue. Therefore, numerical simulation is used to calculate the electric field distribution in the designed domain and optimize the setup design before the cell experiment process. Moreover, the numerical model of the cell setup model can be experimentally validated to ensure numerical simulation accuracy.

5.1 Material and method

5.1.1 Cell experiment system I

Grunert et al. [95] designed a 3D test setup for the Asnis III s-series screw system (Fig. 5.1). They did series experiments on human osteoblasts on three-dimensional scaffolds in the Asnis III s-series screw system, including electric magnetic stimulation and exclusive magnetic stimulation. Prior to the cell experiments, numerical simulations of the test setup, as well as experimental validation via measurements of the electric potential induced by the screw system were conducted. Here, only the numerical simulation and experimental validation in [95] are shown in this chapter, more details about the cell experiment can be found in [95].

3D test setup for cell experiments

A custom made polystyrole inlay was designed [95] for 6-well cell culture plates (BD Bioscience, San Jose, CA, USA) to facilitate stable alignment of the screws and to elevate

the circumjacent calcium phosphate and collagen scaffolds in the well plate (Fig. 5.1). Three kinds of scaffolds were used to seed the human osteoblasts in the cell experiments, ß-tricalcium phosphate (TCP) scaffolds, BONITmatrix scaffolds (DOT, Rostock, Germany) and collagen scaffolds. The results of the osteoblasts' growth in each scaffold were compared to each other in [95]. The diameter of the holder was 37 mm, the height at the scaffold level was 3.5 mm and 5 mm at the screw, with a centre cut-out of 5 mm. The screw was positioned in the centre of the scaffold and screw holder by screwing it through a pre-drilled hole in the cover plate of the cell culture plate (Fig. 5.1 (left)). The surrounding magnetic field was generated by a Stryker Asnis III s-series hip coil (Stryker GmbH & Co. KG, Duisburg, Germany).

Numerical simulation of the 3D test setup

Cell experiment setup   Sketch of experiment setup
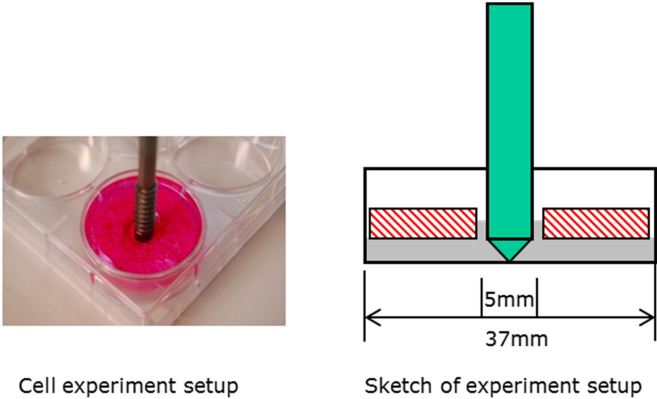
Fig. 5.1 3D cell experiment setup (left) and sketch of experiment setup.

Material	Conductivity σ [S/m]	Relative Permitivity εr
DMEM	1.5	80
Ti6A14V	$7.407 \cdot 10^5$	1
Epoxy& Screw holder	10^{-12}	4
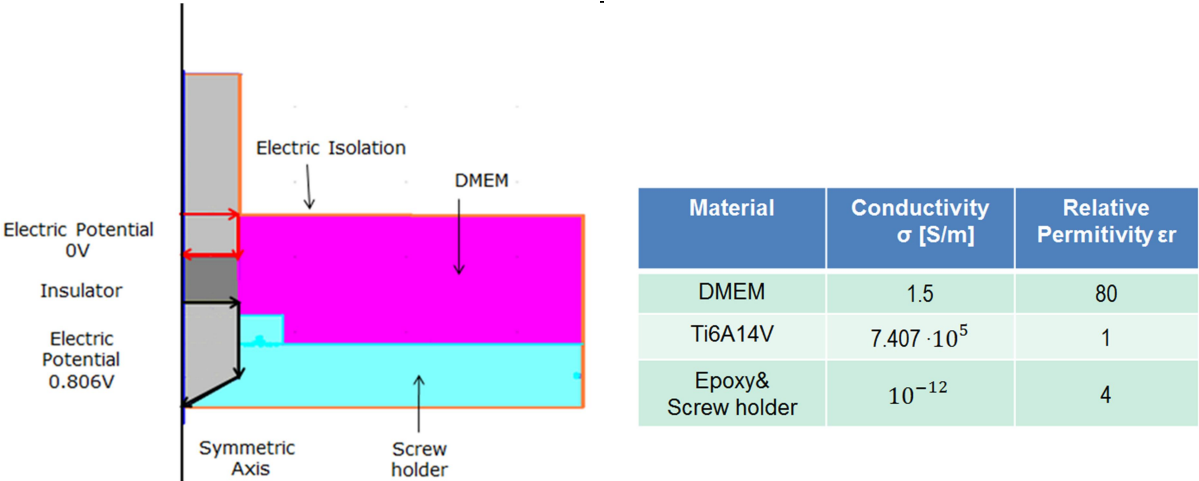
Fig. 5.2 Schematic design of the model geometries in COMSOL and their material properties used for numerical simulation.

The numerical simulation of the test setup was carried out by FEM using the software COMSOL Multiphysics 4.3b. FEM was used to calculate the electric field distribution in the cell culture well caused by the Asnis III s-series screw. The AC/DC module was used; specifically, the module for electric currents in the frequency domain, to compute the electric potentials in the model. The conjugate gradients iterative solver was used to solve the resulting system. To reduce the model complexity, the scaffold was not involved in the numerical simulation. When ignoring the scaffold in the numerical simulation, this cell experiment setup was a totally symmetric system. Therefore, a symmetrical 2-dimensional model was applied (Fig. 5.2) in the numerical simulation. To reduce the mesh complexity, the thread on the surface of the screw was not taken into account in the numerical simulation. The chosen sizes of the screw holder, Asnis III s-series screw and well plate were the same as their real sizes in the simulation. The 2D model in COMSOL and the material properties used for electric potential calculation are shown in Fig. 5.2. The stimulation parameters (Frequency 20 Hz, peak electric potential 800 mV) were taken from experimental measurements of the Asnis III s-series screw system.

In the simulations, a Dirichlet boundary condition and a Neuman boundary condition were available (equations 3.16, 3.17). A Dirichlet boundary condition was applied to impose an electric potential, on the surface of the screw electrodes. A Neumann boundary condition was considered for the insulating surfaces of the implants and the exterior boundary of the cell experiment model.

Experimental validation
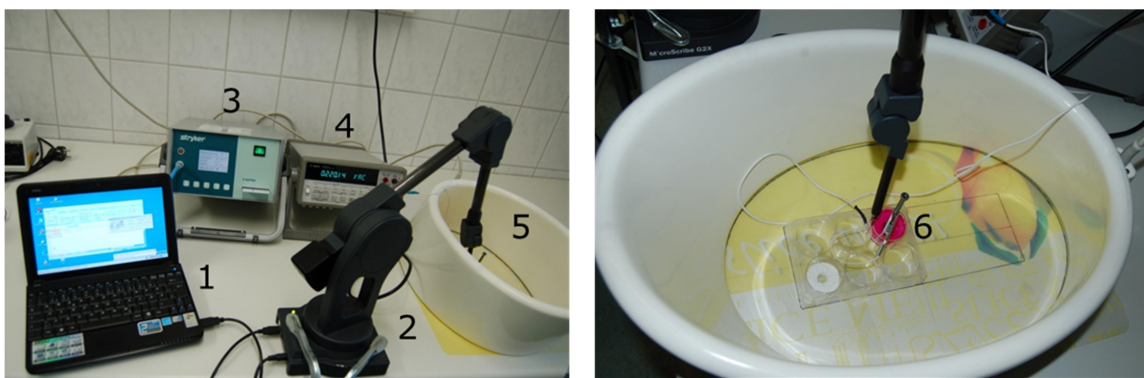
Fig. 5.3 Setup of validation experiment. 1) Computer to process the coordinates of measuring points. 2) Measuring arm (MicroScribe G2x). 3) Stryker Asnis III s-series System Generator 1900-0800. 4) Agilent Multimeter 34410A for electrical potential measurement. 5) Stryker Asnis III s-series Hip coil 1900-0860, 6) Asnis III s-series screw in cell experiment setup.

To prove numerical simulation accuracy, the validation experiment (Fig. 5.3) was set up according to the cell experiment. The measuring arm was used to get the coordinates of the measuring points in the experiment. These coordinates for the measuring points should be kept constant in the numerical simulation (Fig. 5.3). The primary coil generates an oscillating (20 Hz) magnetic flux density of 3 mT. The Asnis III s-series screw was fixed by a screw holder in the well plate and the scaffold was placed on the screw holder. A volume of 6 ml DMEM (Biochrom, Berlin, Germany) containing 10% fetal calf serum (FCS), 1% Amphotericin B, 1% Penicillin-Streptomycin and 1% Hepes-Buffer (all: Gibco® Invitrogen, Darmstadt, Germany) was used. Before the Asnis III s-series screw was fixed in the well plate, the default electric voltage on the surface of the screw was measured and then used in the numerical simulation to compare the results to the validation experiment. The validation was done by measuring the electric potential on the surface and bottom of the scaffold (Fig. 5.4). The results of the validation were compared to the numerical simulation.
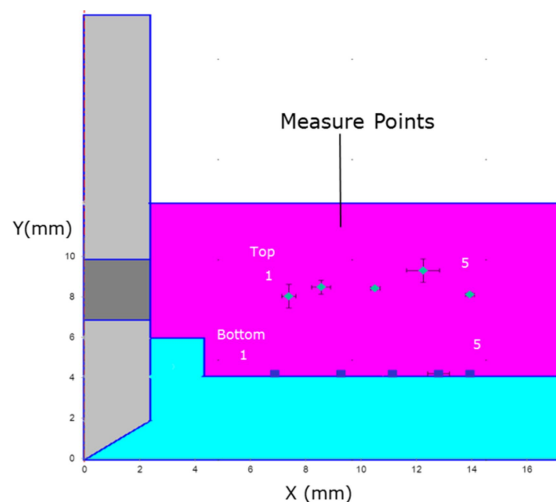
Fig. 5.4 Measuring points in the cell validation experiment.

5.1.2 Cell experiment system II

Although the test setup designed by Grunert et al. [95] can be successfully used for the in vitro experiment, there was a disadvantage for this system. The primary coil, generating the 20 Hz magnetic field to induce the current into the secondary coil in the Asnis III s-series screw, can increase the temperature in the incubator which results in a negative impact on the survival of human osteoblasts. For this reason, Hiemer et al. verified the test setup for in vitro tests of human osteoblasts in the Asnis III s-series system. How the human osteoblasts' growth has been influenced by the electromagnetic field and electric field has also been compared and similar results have been found on the effect of metabolic cell activity at the end of the cell experiment. Therefore, a verified chamber setup only contains the electric field

in the cell experiments and the numerical simulations related to this setup are carried out in this subsection.

Chamber design for cell experiment

The novel *in vitro* test setup, a so called stimulation chamber, was based on the concept of the Asnis III s-series screw system and was designed in cooperation with the Fraunhofer Institute for Ceramic Technologies and Systems (IKTS), Hermsdorf, Germany. Two electrodes were aligned horizontally for cell culture experiments (Fig. 5.5). The stimulation chamber consists of six divisions with equal dimensions (5.4 cm x 5.4 cm x 2.4 cm), inserting a custom made holder, to ensure a stable arrangement of several components. A DMEM medium was contained in the chamber. After closing the cover with pre-drilled holes and connecting the electrodes to the power supply, the chamber was incubated at 37 °C and 5% CO_2 in a humidified atmosphere for 24 h before starting the electrical stimulation (Fig. 5.5).

Numerical simulation of chamber setup

The electrodes in the original chamber setup were cylindrical shapes and the diameters of the cylinders were the same as the Asnis III s-series screw's. To better visualize how the human osteoblasts grew on the surface of the electrodes after the cell experiment, triangular-shaped electro-stimulating implants for animal testing were used for designing the new electrodes. The triangular-shaped electrodes were located in two positions: flat side up and flat side down. The length of the triangular-shaped electrodes and insulator were kept as in the cylinder design. Numerical simulation was used to calculate the electric field distribution in the chamber caused by different types of electrodes and to compare how the shape of the electrode influences the electric field distribution on the bottom of the box and on the surface of the electrodes.

Fig. 5.5 Chamber setup system for vitro experiments.

The electrical stimulation of the chamber was performed using a waveform generator which

developed a sinusoidal wave alternating current with an electric peak voltage of 700 mV and a frequency of 20 Hz. The two designed electrodes were located in the same position of the setup. DMEM was filled in the box, 5 mm higher than the top surface of the electrodes. The calculation model and solver in COMSOL Multiphysics 4.3b were the same as in [95]. Figure 5.6 shows a chamber setup model with triangular-shaped electrodes in the numerical simulation.
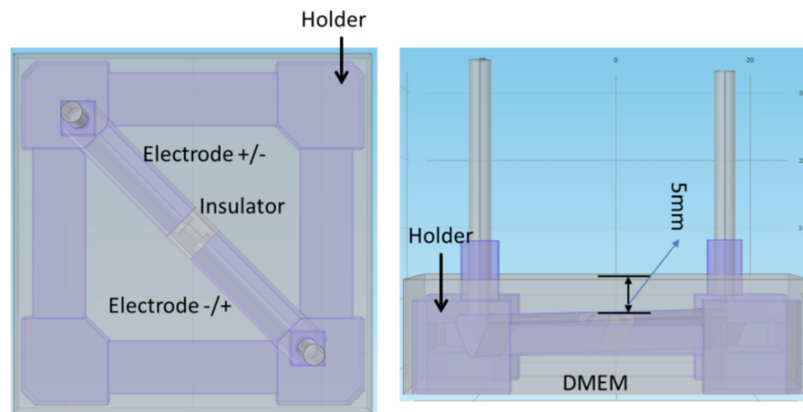
Fig. 5.6 Chamber setup model with triangular-shaped electrode in simulation
where the flat side is up.

5.1.3 Cell experiment system III

In chapter 6 electro-stimulating implants were designed for the animal testing. To find the optimal stimulation parameter for animal testing with electro-stimulating implants, a series of cell experiments should be carried out. Therefore, the in vitro setups for electro-stimulating implants need to be designed. Again, numerical simulation is the prior step for the in vitro setup design.

In vitro setup for implant design 1

To see how electro-stimulating implants stimulate the osteoblasts' growth in the cell chamber and on the surface of the scaffold, we need to design a vitro setup of implant design 1 in animal testing for cell experiments. The scaffold used here will be the same as in [95]. Numerical simulation was used to find an optimized in vitro setup which produces the best electric field distribution in the cell chamber and on the surface of the scaffold. This optimization problem means that both the activating electric field volume in the cell chamber and the activating electric field area on one specific surface in the cell well should be maximized. It can be accomplished by combining iSIGHT with FEA software.

Numerical simulation model

The size of the cell well in figure 5.7 is taken from the standard 12 cell wells. Implant design 1 is designed to be fixed in the cell well by one implant holder. DMEM fills the cell well during cell experiments. The electric field distribution in the cell well is calculated by the FEA software COMSOL Multiphysics 4.3b.

Optimization parameters

Constraints: 2 mm < d < 4 mm

$\qquad$ 0.5 V < v < 0.4V

d is the height of the scaffold and v is the electric voltage on the surface of the implant.

Objectives: - maximum volume of activated tissue electric field norm (5 – 70 V/m) in cell chamber

$\qquad$ - maximum area of the (5-70 V/m) on the surface of the scaffold
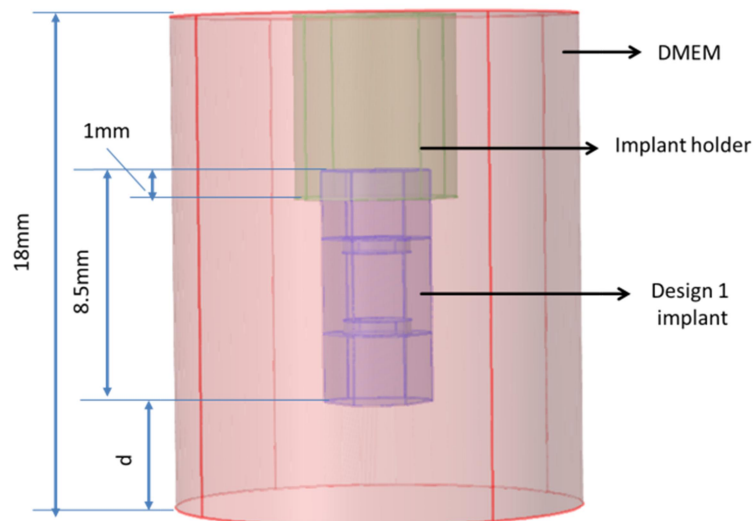
Fig. 5.7 Cell chamber setup for implant design 1.

Optimization process

The model of the cell well setup in vitro was created in COMSOL and integrated into iSIGHT to accomplish the optimization (see 4.1.2). Since COMSOL is not one of the directly supported applications in iSIGHT, a SimCode component in iSIGHT was used to execute COMSOL through a command line interface. The modelling in COMSOL was launched through a batch mode in MATLAB (Mathworks, Ismaning, Germany). After the COMSOL modelling had been integrated into iSIGHT, the initial constraints on d and v were saved in the input file. Maximum volume of the electric field (5-70 V/m) in the cell well and the area of the electric field (5-70 V/m) on the surface of the scaffold were the objectives in the optimization algorithm.

The optimization workflow included a two-step optimization plan: design of experiment (DOE) and the optimization algorithm (see 4.1.2). DOE was used to screen the design space and find an estimated optimal design. The *optimal Latin hypercube technique* with 100 points was chosen to sample the variables in the whole data space. The optimization uses the results of the DOE to start the search intelligently in the vicinity of the estimated optimal point. Furthermore, due to the fact that the current study is a multi-objective application, the *Non-dominated Sorting Genetic Algorithm (NSGA-II)* was selected in iSIGHT to calculate the optimum values for d and v based on the results of the DOE. The whole optimization process is automatic. For each optimization step, the SimCode model was executed by COMSOL, created a new cell well setup model with current d and v and calculated the volume of activated tissue electric field (5-70 V/m) in the cell well and on the surface of the scaffold. After that, the results were imported into the optimization algorithm. When the output of the calculation did not converge, it was not optimal and new values for d and v were created automatically according to the optimization algorithm. Consequently, the input file was updated with new values for d and v and used for the next calculation. The optimization process stopped when convergence was finally reached.

5.2 Results

5.2.1 Cell experiment system I

The numerical simulation results are shown in figure 5.8. In order to compare them with the results of the experimental validation, 6 ml DMEM were used in the experiment and the electrical potential on the ASNIS III s-series screw was measured while using the default setting of the generator. The default electric potential on the surface of the screw, 800 mV, was also used in the numerical simulation. To better view how the activating electric field was distributed in the cell chamber, the contour line of the electric field norm was shown in the range from 5 to 70 V/m because this range of the electric field has the best effect on bone cell growth [89] (Fig. 5.8 (left)). It is clear to see that close to the screw, the electric fields have a higher intensity than 70 V/m, and close to the cell chamber edge the electric fields have a really low intensity, lower than 5 V/m. The desired activate tissue electric field interval, 5 – 70 V/m, was shown to reach from the upper edge of the inlay ring to the middle of the screw holder radius in the well plate.

Figure 5.8 (right) shows the electric potential distribution in the cell chamber. The electric potential showed large variations with potentials ranging from 0.514 V to 0.796 V immediately around the screw implant. But close to the outer edge of the well, the electric potential is around 0.3 V with only small deviations. This electric potential result was compared to the data of the validation experiment. In the experiment, the electric potential of the measuring points on the top and bottom surface of the scaffold has been measured. It is clear to see that in both, numerical simulation and experiment, electric potentials on the top

and bottom surface of the scaffold fall in the range of 0.38 V to 0.43 V (Fig. 5.9). The tolerances between numerical simulation data and validation experiment results, in both top and bottom measuring points, were in the acceptable range. It means the cell experiment setup model for system I is validated by the experiment.
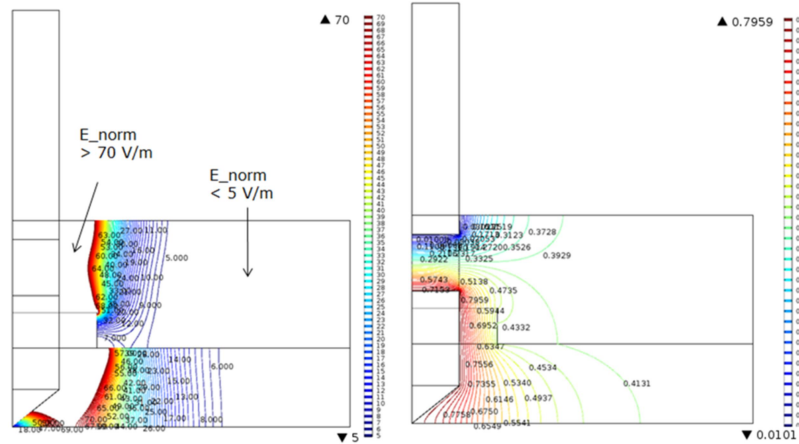
Figure 5.8 (right) Contour line of electric potential (V) and (left) Electric field norm (E-norm [V/m]) in cell.
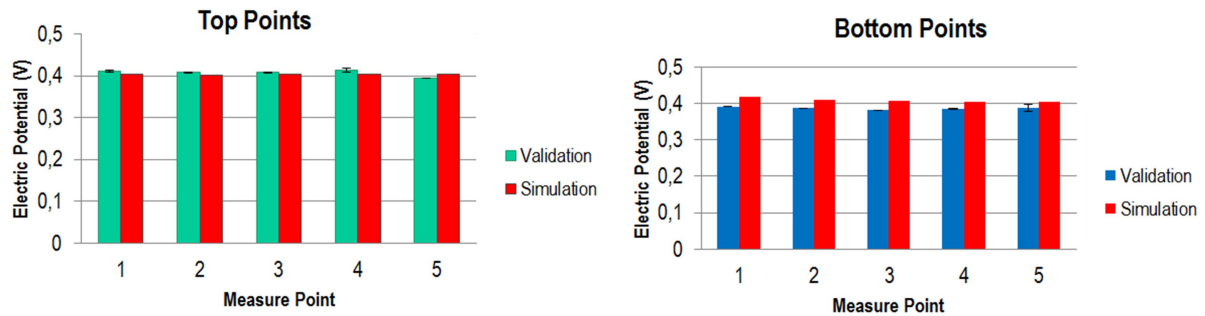
Figure 5.9 Electric potentials of the numerical simulation compared to the cell experiment validation on the top and at the bottom of the experimental setup.

5.2.2 Cell experiment system II

The electric field distribution on the bottom of the box in the chamber setup with two designs of electrodes (cylinder and triangular outer shape) has been shown in figure 5.10. In both cases the electric field distribution on the bottom of the box shows a similar phenomenon. The four corners are covered by the holder. Most of the area of the bottom has the activating electric field interval of 5-70 V/m. In the triangular-shaped electrodes design, locating the electrodes flat side down can get a maximum electric field of 56 V/m, which is still in the range of activating electric field.

Figure 5.11 shows the electric field distribution on the surface of the different electrodes.

65

Similar electric field distributions can be found with the two designs of the electrodes. For each electrode in the three cases, most of the surface on the electrodes is in the range of 5 to 70V/m. Only in the area near to the insulators, the electric fields are higher than 70 V/m. Therefore, in the cell experiment, when the electric peak voltage on the surface of the electrodes is 700 mV, the shape design (cylinder or triangular) and the positioning (locating flat side down or up) of the electrodes in the chamber setup have no relevant influence on the electric field distribution on the surface of the electrodes and on the bottom of the box.
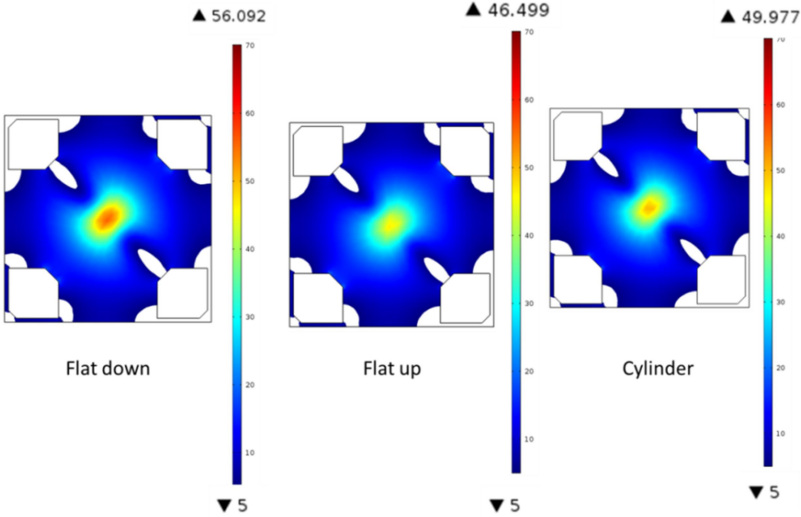
Fig. 5.10 Electric field distribution on the bottom of the box.
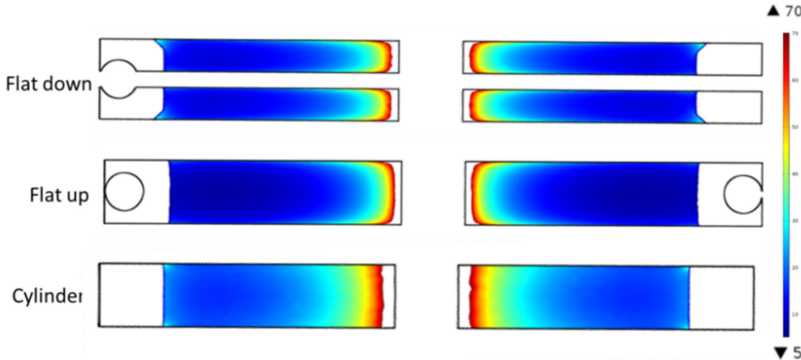
Fig. 5.11 Electric field distribution on the surface of the electrodes.

5.2.3 Cell experiment system III

The optimum scaffold height and the electric potential on the surface of the electrodes are shown in Table 5.1. Comparing the electric peak potential in the animal tests (400 mV) to the cell experiments, the electric potential which leads to the maximum volume of activating electric field in the cell well is 340 mV. The scaffold height is 2 mm.

Table 5.1 Optimization results

d [mm]	*v* [V]	Surface (A) [mm²]	Volume [mm³]
2.034	0.3407	171.01	1100.68
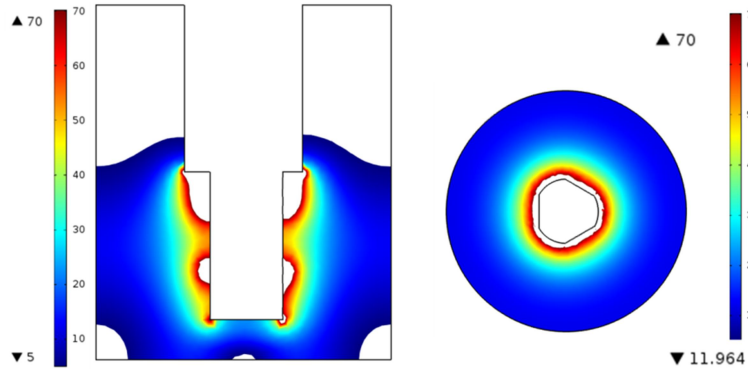
Fig. 5.12 The optimum electric field distribution in the cell chamber in a 2D cut plane (left) and on the surface of the scaffold (right).

The optimum electric field distribution in the cell chamber in a 2D cut plane is shown in figure 5.12 (left). In the cell chamber around the implant the electric fields are higher than 70 V/m. Figure 5.12 (right) shows the electric field distribution on the surface of the scaffold with the optimum scaffold height. On the surface of the implant, only small areas around the implant are not in the activated tissue electric field interval (5-70 V/m), the rest of the surface of the scaffold is all in the activating electric field.
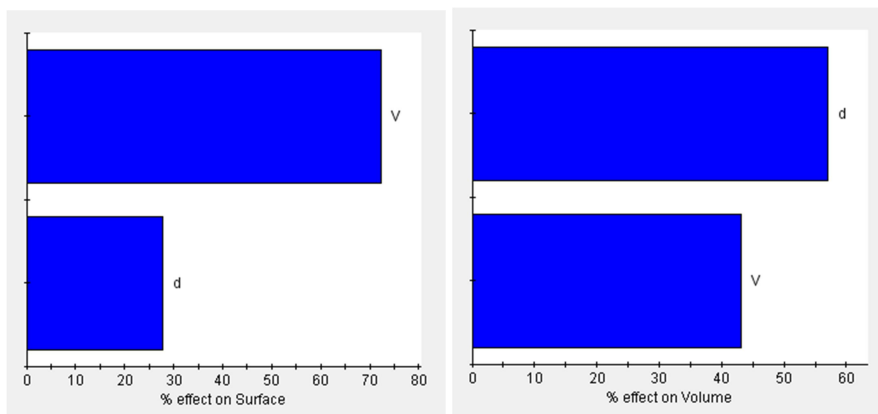
Fig. 5.13 Pareto plots of the effects of the scaffold height and implant surface electric potential on the activated tissue electric field surface of the scaffold (left) and activated tissue electric field volume in the cell chamber (right).

Figure 5.13 shows how the input parameters, height of scaffold and electric potential on the surface of the implant, influence the output parameters, activating electric field area on the surface of the scaffold and volume in the cell well. A 70% effect of electric potential on the surface of the implant can be found in the activated tissue electric field area on the surface of the scaffold. Similar effects (45% and 55%) are shown in the activated tissue electric field volume in the cell well from the electric potential on the surface of the implant and the height of the scaffold.

5.3 Discussion

Prior numerical simulation has been successfully used to design the in vitro setup for cell experiments. This can give an insight into the electric field distribution in the cell chamber. Also, numerical simulation helps to save time in cell experiments, as designing and establishing the cell experiments is a time-consuming, complex process.

One common limitation in all the numerical simulations in this chapter is that electric double layer (EDL) was not taken into account. But EDL is important to cell experiments [135]. Therefore, in future studies, the electric potential caused by EDL on the surface of implant electrodes in cell experiments should be calculated as in [135,136] and used in numerical simulations.

Numerical simulation data and experimental validation results in cell experiment system I showed a good consistency. Only a minimal derivation from the simulation was revealed. This showed the accuracy of the numerical simulation.

Limitations exist in the numerical simulation of the in vitro test setup from cell experiment system I. The scaffold has not been included in the numerical simulation and only one experiment was done to validate the cell experiment model due to the complex structure of the scaffold and validation experiment process. Because the scaffold structure has been neglected in the numerical simulation, the cell setup model was simplified to a two-dimensional model. Even though, the electric potential in the experimental validation on all the measuring points was measured with the scaffold. Because the results were comparable to the numerical simulation, the scaffold was neglected in the numerical simulation to decrease the model reconstruction complexity. But in order to evaluate how the scaffold influences the cell experiment model validation results, more than one experiment should be done to enable the comparison. The thread of the screw has not been involved in the numerical simulation in order to reduce the mesh complexity.

The chamber setup in system II was a verified design based on system I from Grunert et al. [95]. In order to improve the chamber design for the purpose of a better view on the human osteoblasts' growth on the surface of the electrodes in the cell experiment, numerical

simulation was used to compare the electric field distribution on the bottom of the box and surface of the electrodes caused by the two electrode designs and their different positioning in the chamber setup. The likely electric distributions were found in all electrode designs and orientations after the numerical simulation. Although the electric potential has been calculated in cell setup models in system II, the models have not been experimentally validated. To show the accuracy of the numerical simulation in system II cell setup models, it is necessary to carry out an experiment to validate the models in future studies. As in the validation experiment with system I, the electric potential on the measuring points in the numerical simulation and the validation experiment can be compared and the tolerance can be calculated.

Moreover, the cell experiment setups in system I and system II were based on the clinically used Asnis III s-series screw system. The implant parameters and stimulation parameters are not optimized. To improve the outcome of cell experiments, it is necessary to optimize the cell setups for system I and system II. For example, the electric potential on the surface, the size and position of the implants in the cell setup can be optimized by combining iSIGHT with COMSOL.

Combining iSIGHT with a FEA solver is a convenient approach. The optimum in vitro setup for the cell experiment was found after applying an optimization algorithm. However, there is a limitation for system III optimization. Only the activated tissue electric field has been considered in the optimization process. Because of a lack of methods, bone overstimulation has not been involved in the bone cell setup design. Therefore, in cell experiments, the bone cell growth from overstimulation should be analysed by applying a higher electric field intensity to the cell. For example, applying a certain electric potential to the surface of implants can bring most areas of an implant's surface to an electric field intensity of more than 70 V/m. Thus, the outcome of the cell growth after overstimulation could be seen. The electric potential which would be used in the overstimulation experiment can be optimized by combining iSIGHT with COMSOL.

6 Numerical simulation in animal testing

Besides evaluation of the electric field distribution in the human femoral head, investigating the effects of electrical stimulation on bone in in vitro and in vivo models is also important to better understand bone electrical stimulation. This chapter will focus on the in vivo animal testing models. In chapter 5, in vitro models are set up for cell experiments according to the clinical study and the electric field in the bone cell setup model is numerically calculated.

The aim of the animal tests is to evaluate bone growth under the conditions of electrical stimulation in the animal bone. The different stimulation parameters, like duration of stimulation per day, stimulation period, frequency and electric potential, can be analysed in animal tests by connecting a control circuit into all implants in the animal. The results of bone growth in the animal bone can be obtained from a histological analysis to quantify the change of bone structure and to evaluate the effectiveness of the stimulation parameters selected in the animal tests. Moreover, static tests can be used to determine the pull-out forces and the degree of implant ingrowth in the animal bone.

Before the animal tests, a proper animal has to be chosen for the experiments. The next step is to design suitable electro-stimulating implants for the animal tests. To design the electro-stimulating implants, numerical simulation is a necessary tool for predicting the electric field distribution in the designed domain. Therefore, the task in animal testing is to use the numerical simulation to evaluate the electric field distribution in the animal bone and on the surface of the implant and to optimize the animal electro-stimulating implant design numerically.

During the numerical simulation for the animal tests, insufficient sources for the bone dielectric properties were available for the numerical simulation despite numerical simulation already being widely used in electro-stimulating implant design and electric field distribution evaluation in bone tissue. Numerical simulation is a common tool in biomedical research and development. For instance, ultrasound propagation in cancellous bone, a new method for the diagnosis of osteoporosis, can be simulated and the propagation behaviour in the bone can be analysed [142,143] by numerical simulation. A new approach for the enhancement of the bone proliferation rate by electro-stimulation in the acetabular region was investigated by Potratz et al. [132,136], in which numerical simulation was used to compute the electric field distribution in the complex model based on high resolution CT scans of the acetabular area. Clinical application can be improved by analysing the electric field distribution of the bone and the design of electric implants can be also be enhanced through FEA. The model and dielectric properties' parameters of the bone structure decide the precision of the FEA. As a bone model can be accurately reconstructed by using image segmentation and CAD software, bone dielectric properties are especially essential to the outcome of the numerical

simulation. Due to the reason that bone has a complex structure, measuring the electric properties of bone is a difficult task. Therefore, another aim of this chapter is to automatically calibrate the dielectric properties of animal bone from experimental data. An automatic approach was defined to calibrate dielectric properties of animal bone at a frequency of 20 Hz as in the clinical application.

6.1   Material and method

6.1.1 Electro-stimulating implants for animal tests

The animals chosen in the animal tests were female New Zealand white rabbits of 3 — 4 kg weight due to the reason that compared to sheep, this kind of rabbit is easier to handle during the operation and application of electrical stimulation. The designed electro-stimulating implants were planned to be inserted into the rabbit's distal femurs (Fig. 6.1). For implantation, one hole was drilled on one side of the rabbit tibia and a designed implant was inserted into the hole. The gap between the bone and the designed implant was defined as a bone defect in the animal tests. After animal testing, the new bone growth by electrical stimulation in the gap was checked to determine how much the different stimulation parameters influence the new bone growth in the animal bone. The control unit, connected to all the implants and supplying the stimulation parameters for all implants, was embedded in biocompatible silicon and inserted under the skin of the rabbit's pelvis.
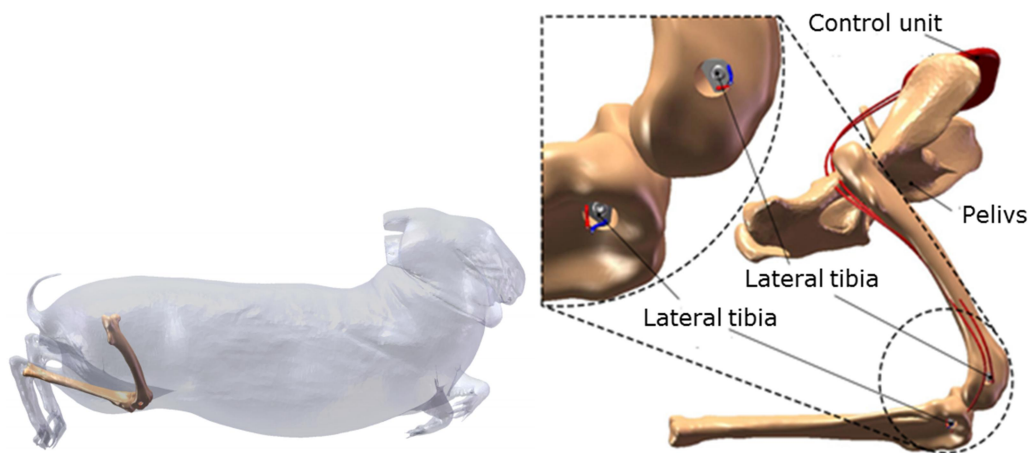
Fig. 6.1 The rabbit's right leg in the rabbit skin STL file (left) and electro-stimulating implant position in the rabbit distal femur (right).

The shape and size of the rabbit distal femur indicated that the electro-stimulating implants should be as small as possible to permit the operation procedure. Two kinds of electro-stimulating implants were designed for the animal tests (Fig. 6.2 and Fig. 6.3). Implant

design 1 consisted of three parts (two electrodes and one insulator). These three parts were connected by two screws and biocompatible gluten from the top and bottoms sides of the implant. Two biocompatible cables were inserted into the implant to connect the two electrodes. Electric power was supplied to these two electrodes by these two cables. The material of the electrodes and insulator were TiAl6V4 and PEEK, respectively. As in the preliminary test, the liquid showed to pass through the gap into the implant interior and caused a short circuit. For this reason, a new, more robust implant design 2 (Fig. 6.3) was developed to improve the ingrowth of bone cells on the implant surface. The outer shape of the implant corresponds to the shape of the first design. At each plane lateral surface, the implant had a slot for the insulator (NOVO sin, Eschen, Germany), in which a wire electrode (Ti6Al4V, length 7mm, Ø 0.3 mm) was integrated into. The three wire electrodes were connected to the cables in the inside of the electrode from a hole on the implant longitudinal axis upwards. The fourth cable was connected with conductive adhesive to the electrode implant body.
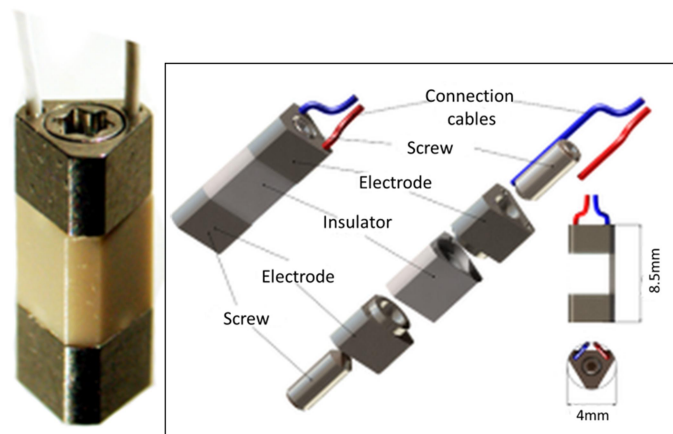
Fig. 6.2 Implant design 1 (left) and its structure (right).
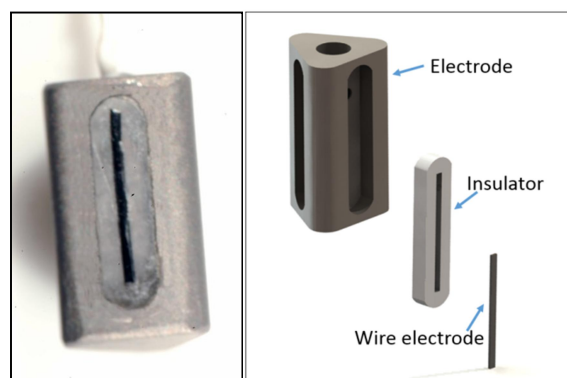
Fig. 6.3 Implant design 2 (left) and its structure (right).

Numerical simulation

Besides the complexity of the construction and difficulties of installation, another important criteria for deciding on the final design for the animal tests is electric field distribution. The design that brings a relatively larger activated tissue electric field on the surface of the implant electrodes and in the gaps between implant and bone, can be used for the final animal tests. COMSOL Multiphysics version 4.3b (Comsol AG, Göttingen, Germany) was used to calculate the electric field distribution caused by the two designs of the electro-stimulating implants in the rabbit distal femur models.

Model reconstruction

As shown in figure 6.4, the construction of the CAD implants was accomplished in 3D-CAD-Software Solidworks 2008. The CAD of the rabbit distal femur models were reconstructed from the rabbit CT scans by using the procedure of Kluess et al. [120]. The position of the implants in the rabbit distal femur models were defined according to figure 6.1. To ensure comparable results, the positions were kept constant for both implants in the rabbit distal femur model. The surrounding tissue of the rabbit distal femur was simplified to being blood in order to decrease the complexity of the model reconstruction. To consider being close to a real rabbit distal femur, the surrounding blood cylinder in the simulation has a radius of 15 mm and a length of 30 mm. The rabbit distal femur was located in the middle axis of the cylinder. In the operation, when the implants were inserted into the holes in the rabbit distal femur, blood was filled into the gaps. After a certain time of electrical stimulation, new bone will grow in the gap. Therefore, in the simulation the material in the gap between the bone and the implants was considered in two cases: the gap is blood and the gap is cancellous bone.
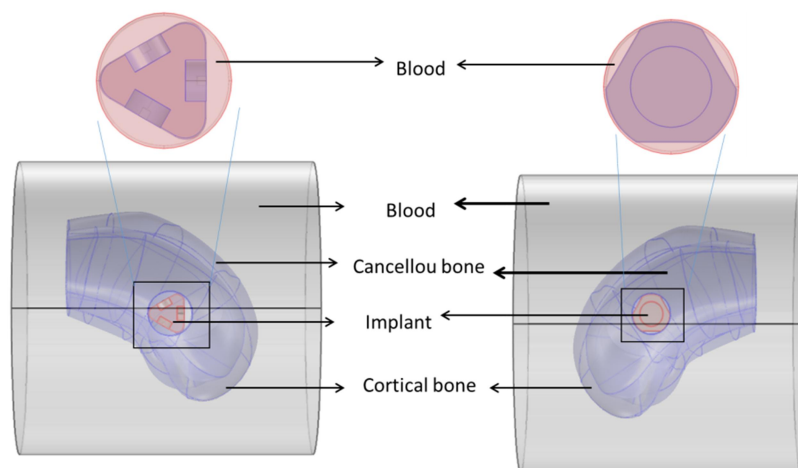
Fig. 6.4 Animal models for both implant designs.

Stimulation parameters

Frequency and signal wave form, are kept constant compared to the human clinical study, i.e. 20 Hz and sinus wave. To ensure that the most area of the implant surface has the optimum electric field interval (5-70 V/m) [89] which activates tissue in the animal bone, one parametric study was carried out for both designed electro-stimulating implants to define the optimized electric potential on the surface of both implants. It showed that 400 mV and 150 mV of peak electric potentials should be applied to implant design 1 and design 2, respectively.

Material parameters

As the dielectric properties of rabbit distal femur are not available in the literature, the conductivity and relative permittivity of cancellous bone, cortical bone and blood were derived from Gabriel et al. [105,108,109] in both implant models. The material properties of the designed implants in the numerical simulation were used according to the data sheets from the manufacturer (see table 4.1).

In the simulations, the Dirichlet boundary condition and Neuman boundary condition were available (equations 3.16, 3.17). A Dirichlet boundary condition was applied to impose an electric potential, 400 mV and 150 mV, on the surface of the designed implant electrodes, respectively. A Neumann boundary condition was considered for the insulating surfaces of the implants and the exterior boundary of the model.

6.1.2 Calibration of the dielectric properties of the animal bone

To develop an algorithm to calibrate dielectric properties, three steps need to be obtained:

- Acquiring an experimental data set
- Accomplishing numerical modelling and simulation
- Calibrating the bone conductivity and relative permittivity

Experiment

Calibration of dielectric properties of animal bone is an optimization process. The first step is to measure the electric potential at specific points in the bone and then compare this experimental result to numerical simulation data. At the end, the minimum difference needs to be found. Therefore, one experiment was set up to acquire the electric voltage at the measuring points in the rabbit distal femur bone.

Bone sample preparation

The hind leg from an eight-week old rabbit was chosen for experimental measurement (Fig. 6.4). The bone specimen was obtained directly after euthanasia of the animal and maintained under refrigeration at – 20 °C until the time of the experiment. Freezing is considered a common method of preserving bone samples for electrical measurements [126]. Moreover, the surrounding soft tissue was not resected before refrigeration to

preserve the moisture of the bone specimen. Before the experiment, the specimen was thawed and the soft tissue was removed. During the experiment NaCl solution was used to keep the bone specimen moist.

Experimental setup

Figure 6.5 demonstrates the experimental setup. To get the coordinates of the measuring points in the experiment measurement, a three-dimensional coordinate measuring arm, MicroScribe G2x (Solution Technologies, Oella, MD, USA) was used. The bone specimen was fixed in a rectangular box to get a datum for the coordinate measuring. The corner and the edges of the box were considered as the coordinate system datum for the experiment. Design 1 of the electro-stimulating implant was inserted into the rabbit distal femur and a generator and two cables were connected to the implant to supply electric power to the implant. A 20 Hz sinusoidal electric signal with a voltage of RMS 400 mV was applied to the implant. The same electric potential was also used in the numerical simulation. To strike a balance between numerical computational and experimental complexity, 25 measuring points were equally distributed on the surface of the bone, and approximately 2 mm into the bone (see Fig. 6.6). The RMS voltage on these measuring points was measured. This data was compared to the results from the numerical simulation. Due to the complexity of the experiment process, only one bone specimen was used in the current study.
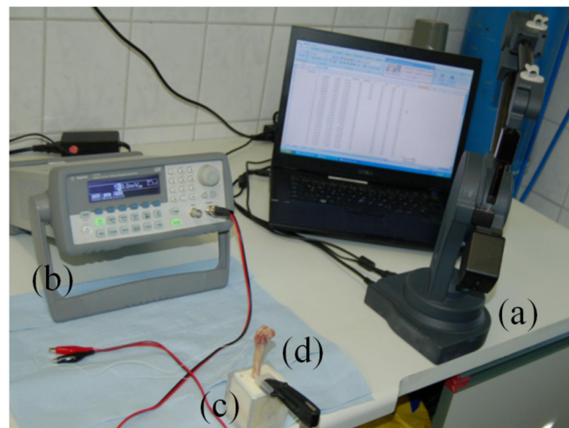
Fig. 6.5 Experimental setup: measuring arm (MicroScribe G2x) (a), Agilent 33220A 20 MHz Function/Arbitrary waveform generator (b), the box for the coordinate system (c) and the bone specimen (d).

Numerical simulation

To compare experimental results to numerical simulation data, a numerical simulation has to be applied to the experiment setup. The model needs to be reconstructed from the bone specimen in the experiment and the coordinates for all the measuring points need to be kept consistent. The electric potentials on all the measuring points will be numerically calculated in the bone specimen model.

Model reconstruction

The geometrical structure of the rabbit distal femur in figure 6.5 (bottom) was based on high resolution CT scans of the bone specimen in the experiment, according to the procedure described by Kluess et al. [120]. To maintain the accuracy of the calibration at a later stage, care was taken to keep the coordinate system in the experiment and in the numerical simulation consistent. Therefore, the rabbit distal femur, fixed in the rectangular box, was placed in the CT scanner again after the experimental measurement. With the same procedure as in the reconstruction of the CAD model of the rabbit distal femur, the datum of the coordinate system in the numerical simulation was reconstructed from the CT scans of the rectangular box. From the CT scans of the bone specimen, the implant position was defined in the numerical simulation.
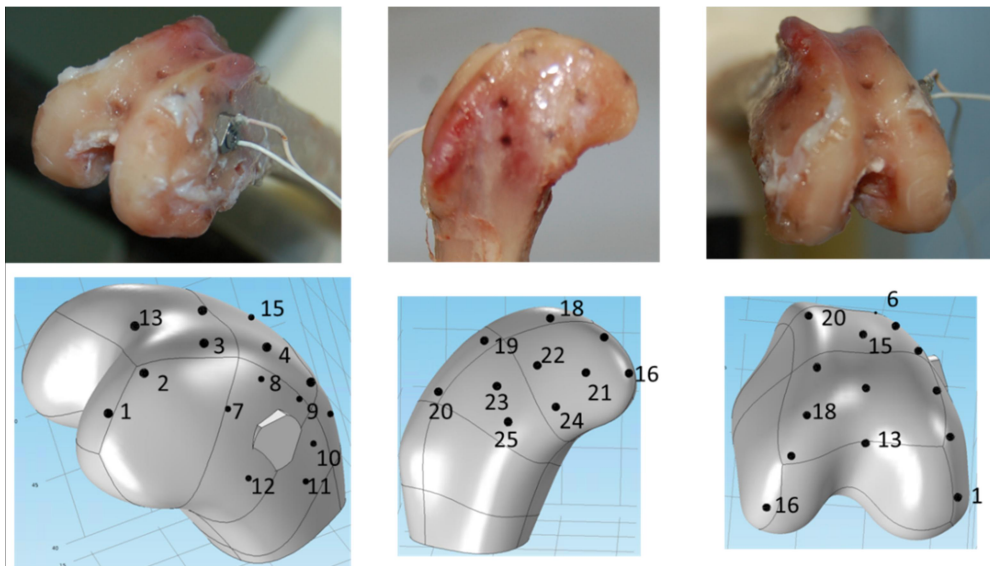
Fig. 6.6 Measuring points in experiment (top) and in numerical simulation (bottom).

Stimulation process

Numerical simulation of the rabbit distal femur was performed using COMSOL Multiphysics version 4.3b. The cancellous and cortical bones in the rabbit distal femur were considered as homogenous and isotropic to reduce the complexity of the calculation. Due to the reason that data of the dielectric properties of the rabbit distal femur were not available in the literature, the initial conductivity and permittivity of the tissues as given in table 6.1 were derived from Gabriel et al. [105,108,109]. The electric potentials at specific measuring points were interpolated from the nearest points in COMSOL. The material properties of the designed implants in the numerical simulation were used according to the data sheets from the manufacturer.

Calibrating the dielectric properties of the bone

Once the electric potentials at the measuring points are available in both, the experimental measurement and the numerical simulation, the dielectric properties can be calibrated. iSIGHT (Dassault Systemes Deutschland, Hamburg, Germany) was used to accomplish the calibration as it has highly capable simulation process automation and design optimization capabilities.

Problem definition

The calibration of the dielectric properties of the rabbit distal femur at 20 Hz was considered as one optimization problem. The optimization techniques were combined with the FEM software COMSOL Multiphysics. This combined methodology can calibrate the dielectric properties of the distal femur by measuring the electric potential at different points. The dielectric properties' parameter values of the femur model setup inside COMSOL were modified by the optimization technique. The goal of the optimization was to minimize the differences between the output electric potential in the numerical simulation and the experimental data. The minimum area difference between the experimental measurement and the numerical simulation, the electric potential and the minimum absolute difference between these two data sets have to be elaborated to receive the global optimum.

Calibration methods require extensive experimental data. As the electric field around the implant within the bone stock is the most interesting area, the electric potentials around the implant were mainly measured to reduce the overall computational effort. In total, 24 measuring point results were used in the optimization approach (Figure 6.6 (top)).

Table 6.1 Data space for conductivity and relative permittivity used in the calibration.

Bone type	Conductivity range σ [S/m]	Relative permittivity range ε_γ	Initial conductivity σ [S/m]	Initial relative permittivity ε_γ
Cortical	0.002 to 0.1	2511 to 10^5	0.02004	25119
Cancellous	0.007 to 0.2	$4.0 \cdot 10^5$ to 10^7	0.078902	4020200

The initial dielectric properties (cortical conductivity (CC), cortical relative permittivity (PC), cancellous conductivity (CS), cancellous permittivity (PS)) for the simulation were taken from Gabriel et al. due to the lack of data available for rabbit bone at 20 Hz. Gabriel et al. [105,108,109] reviewed the dielectric properties of biological tissue. They found that the cortical bone conductivity in general is less than 0.1 S/m and the relative permittivity is less

than 10^5 when the frequency is less than 100 Hz. Sierpowska et al. [124] measured the dielectric properties of the trabecular part of bovine femur at 50 Hz, with a conductivity at around 0.125 S/m and a relative permittivity of $5 \cdot 10^6$. Therefore, the data space for conductivity and relative permittivity used in the calibration were set as shown in Table 6.1.

Setting up the iSIGHT model

The distal femur model of the rabbit was created in COMSOL and was integrated into iSIGHT to run the optimization. Figure 6.7 shows the workflow in iSIGHT. Since COMSOL is not one of the supported applications in iSIGHT, a SimCode component (named CallComsol) was used in iSIGHT to execute COMSOL through a command line interface. The modelling in COMSOL was launched through MATLAB batch mode. After the COMSOL modelling had been integrated into iSIGHT, the initial conductivity and relative permittivity (see Table 6.1), which were saved in the input file, and the electric potentials at the measuring points from the initial numerical calculation were parsed for COMSOL modelling. Data matching, a direct application in iSIGHT, was used to compare the results from the numerical simulation to the experimental measurement. The objectives in the optimization algorithm were the sum of the absolute difference and the sum of the absolute area difference.

The optimization workflow entailed using a two-step optimization plan: DOE and the optimization algorithm (see 4.1.2). An estimated global optimization result can be found in the DOE as it screens the whole design space. The '*optimal Latin hypercube technique*' with 150 points was chosen to sample the variables in the whole data space. Furthermore, the multi-objective algorithm '*Non-dominated Sorting Genetic Algorithm (NSGA-II)*' was selected in iSIGHT to calculate the optimum dielectric properties for rabbit distal femur at 20 Hz based on the results of the DOE. When a considerable reduction in the number of optimization iterations to convergence was achieved, the global optimum solution was found.

Figure 6.8 shows the whole automatic optimization process. For each optimization step, the CallComsol model executed COMSOL. In COMSOL, a new rabbit distal femur model with the current dielectric property parameters was created and the present electric potentials at all measuring points were calculated, then the results were saved to the matrix of the numerical data. The data matching component compared the electric potentials at all measuring points from the numerical simulation to the experimental measurement and the results were imported into the optimization algorithm. The new dielectric properties were created automatically according to the optimization algorithm when the output of the calculation in the data matching was not optimal. Consequently the input file was updated and used for the next calculation.
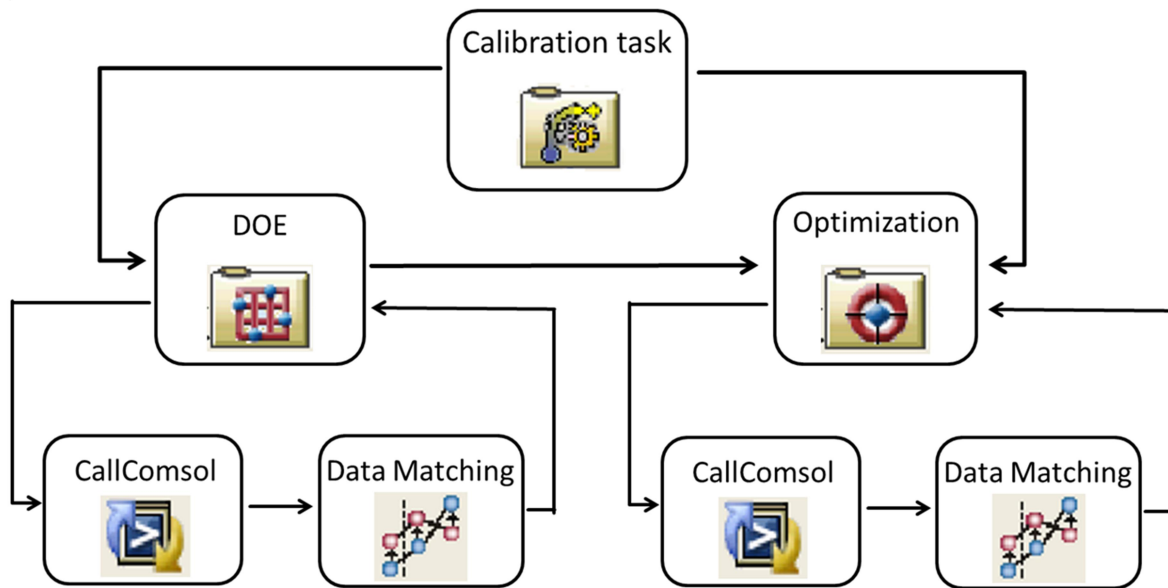
Fig. 6.7. The workflow in iSIGHT.
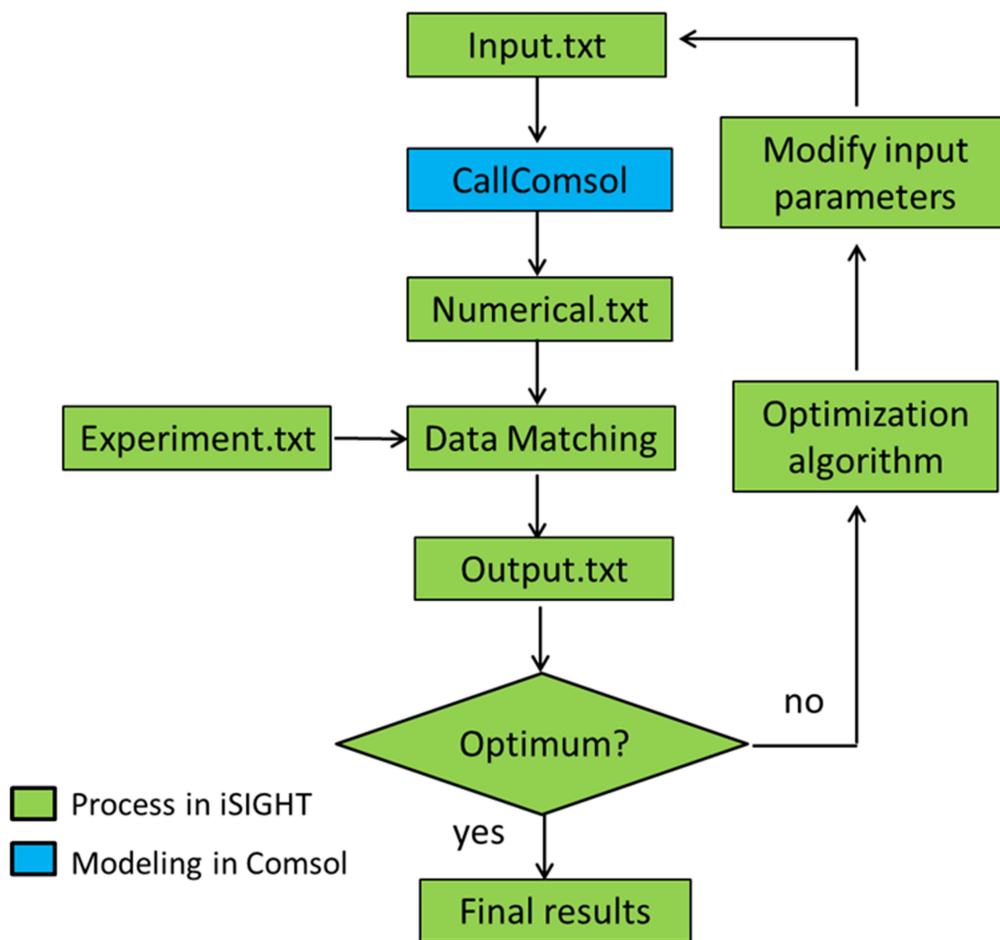
Fig. 6.8. iSIGHT parametric, automatic optimization procedure.

6.2 Results
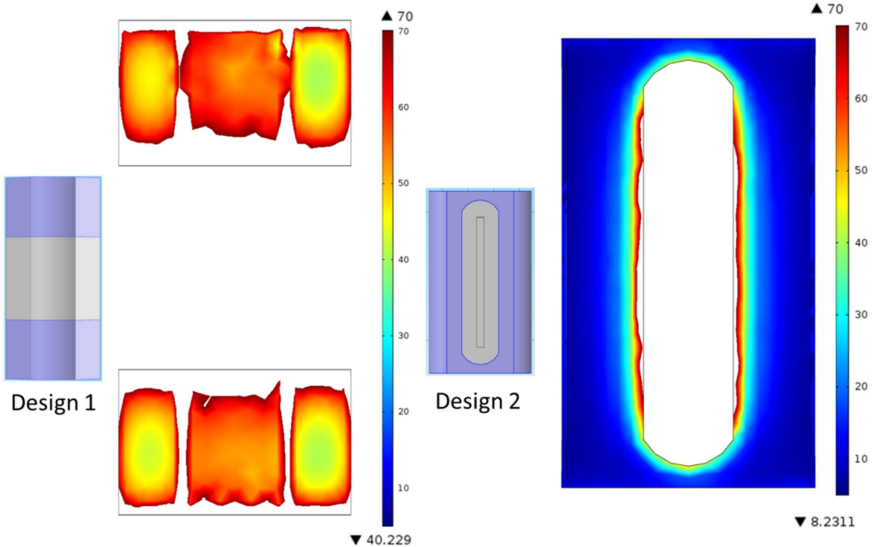
6.2.1 Electro-stimulating implants for animal tests
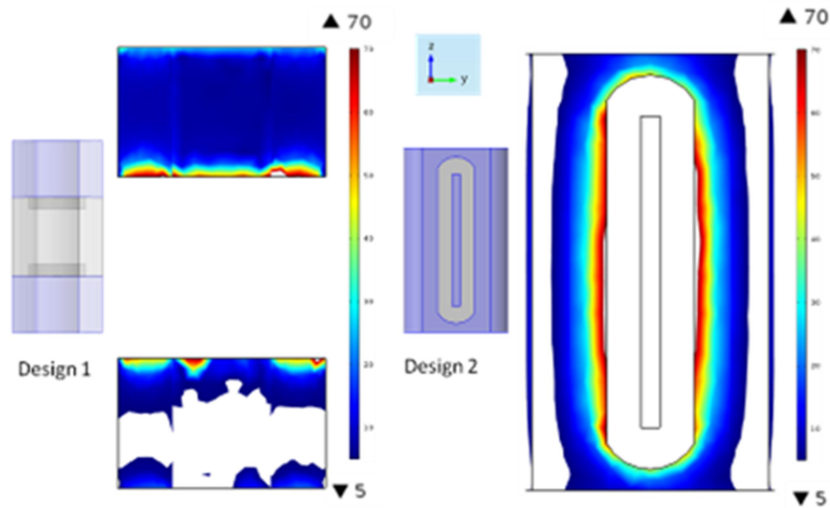
Fig. 6.9 Electric field distribution on both designed implants' electrode surfaces when gaps are blood.

To compare the electric field distribution on the surface of the designed implants, the activated tissue electric field (5-70 V/m) distribution on the surfaces of the implants when the gaps are considered as blood are shown in figure 6.9. With the design 1 implant, the activating electric field is not as homogenous as with the design 2 implant. Although, the activated tissue electric field is distributed on the whole surface of the upper electrode of the design 1 implant, this is not the case on the lower electrode. With implant design 2, the activated tissue electric field distribution on the surface of the electrodes is homogenous and it covers almost the whole implant electrode beside the wire electrode and the round edge. The implant's round edge is not an interesting area for the animal tests due to the reason that the implant was pressed into the hole drilled into the rabbit distal femur using a hammer and the bone is stimulated on the surface of the implant and in the gap between the bone and the implant.

Figure 6.10 shows the electric field distribution on the electric insulators of both designed implants when considering the gaps as blood. The activating electric field is homogenously distributed on the design 1 implant's insulator. In implant design 2, all the areas of the insulator have a higher electric field than 70 V/m and the highest intensity of the electric field (682 V/m) is distributed on the edge of the wire electrode.
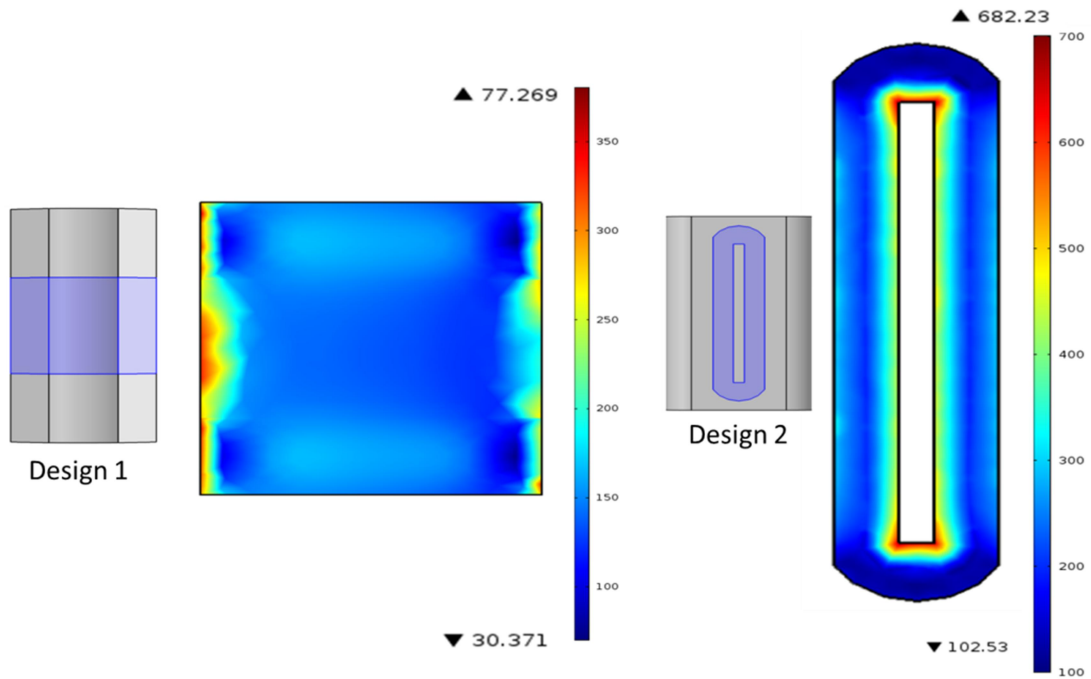
Fig. 6.10 Electric field distribution on both designed implant insulators' surfaces when gaps are blood.

In figure 6.11, the iso-surfaces of the activated tissue electric field (5-70 V/m) distribution in the gaps between the bone and the two implants while considering gaps as blood are shown. In implant design 1, the electric field distribution in the gap is relatively more inhomogeneous than in the case of implant design 2. It is clear to see that in implant design 1 the gaps between electrodes and bone are both in the range from 5 to 70 V/m. But the gap around the insulator is higher than 70 V/m. In implant design 2, homogenous activating electric fields fill all the gaps around the implant. For animal test requirements, this electric field distribution is more ideal for the stimulation of bone.
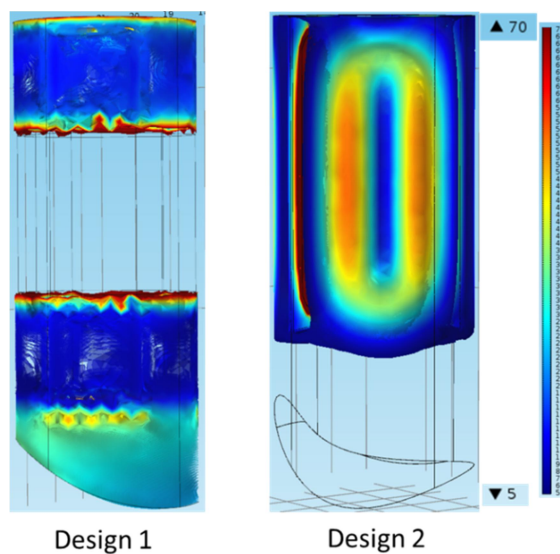
Fig. 6.11 Electric field distribution in the gaps between bone and implant when gaps are blood.

Figure 6.12 shows, when considering the gaps as cancellous bone, how the activating electric field is distributed on both designed implants' electrode surfaces. In implant design 1, only parts of the electrode surfaces are in the activated tissue electric field interval and the minimum intensity of the electric field on the electrode surface shows as 40 V/m. In implant design 2, the activated tissue electric fields are equally distributed on the surface of the implant body electrode but not on the surface of the wire electrode.

Fig. 6.12 Electric field distribution on both designed implants' electrode surfaces when gaps are cancellous bone.
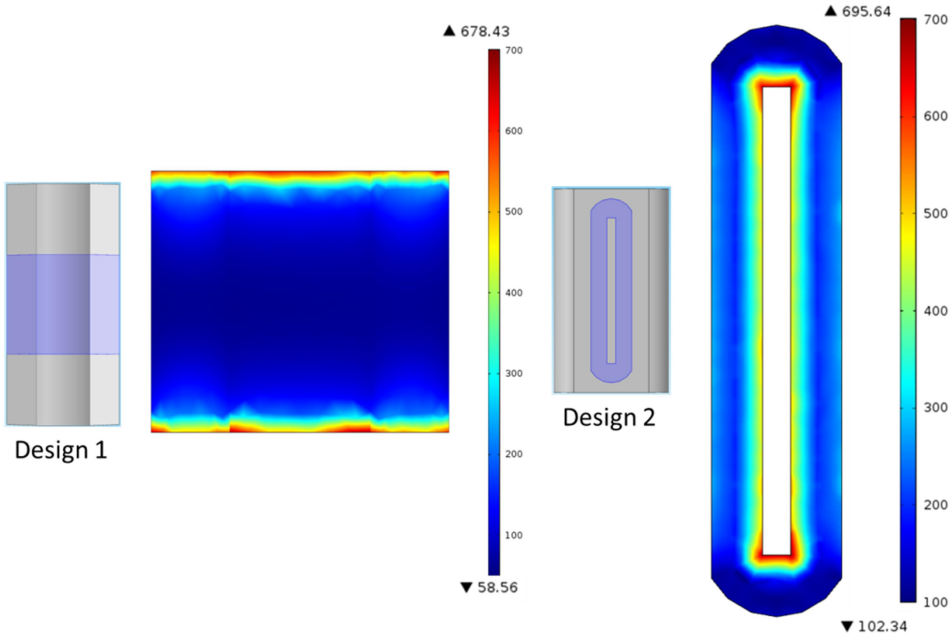
Fig. 6.13 Electric field distribution on both designed implants' insulator surfaces when gaps are cancellous bone.

Figure 6.13 shows, when the gaps are considered as cancellous bone, how the electric field is distributed on the surfaces of both designed implant insulators. In implant design 1, the electric fields on the surface of the insulator are in the range of 58 V/m to 678 V/m. The activated tissue electric fields are distributed in the middle of the insulator surface. In design 2, all the electric fields on the surface of the insulator have a higher intensity (from 102 V/m to 695 V/m) than the activated tissue electric field.
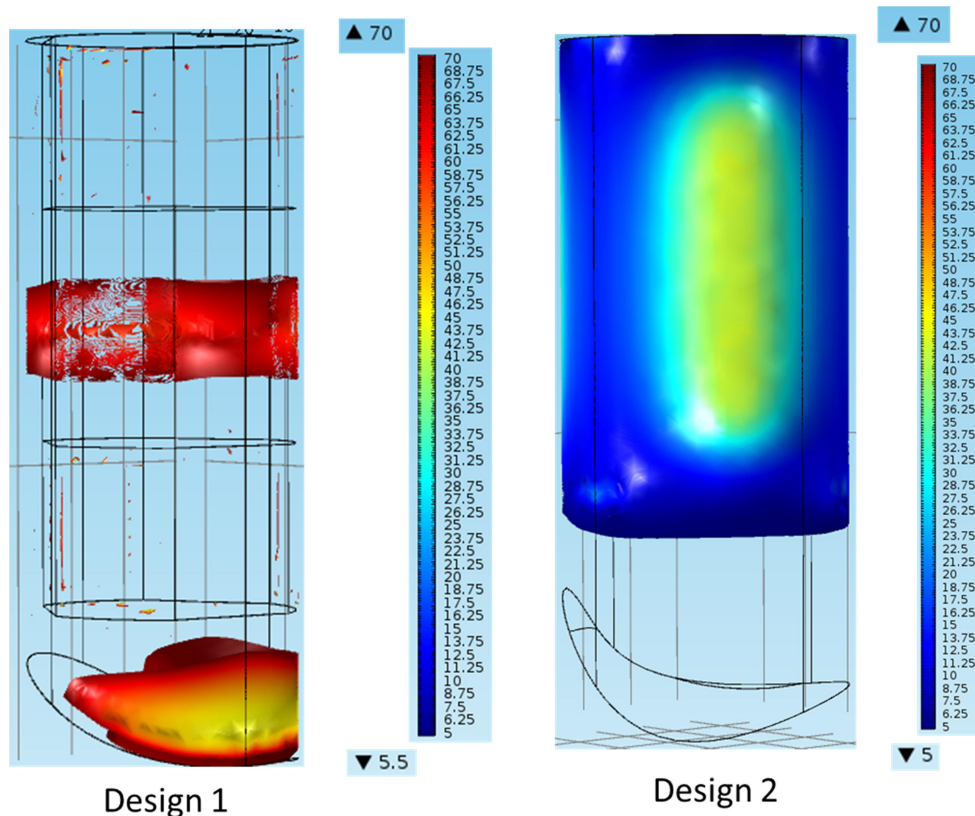
Fig. 6.14 Electric field distribution in the gaps between bone and implant
when gaps are cancellous bone.

In figure 6.14, the activated tissue electric field distribution in the gaps is shown for both designed implants, when the gaps are considered as cancellous bone. From the resulting iso-surfaces, it is clear to see that in implant design 1, only the gaps around the insulator have the desired activated tissue electric field intensity. But this is not the case in implant design 2. Homogenous activated tissue electric fields are distributed in the gaps between bone and implant.

The aim of the implant design for the animal testing is to find an implant that delivers a relatively larger activated tissue electric field on the surface of the implant electrodes and in the gaps between implant and bone. Therefore, as a short conclusion, in both gaps

considerations, blood and cancellous bone, design 2 results in a better activated tissue electric field distribution not only on the surface of the implant electrode but also in the gaps between bone and implant.

6.2.2 Calibration of the dielectric properties of the animal bone

The results of optimizing the conductivity and relative permittivity at 20 Hz for both, cortical and cancellous animal bone, are shown in Table 6.2. Comparing these calibrated rabbit distal femur dielectric properties to bone dielectric properties from the parametrical model [105,108,109], in both bones the conductivity of cortical and cancellous bone are higher and the relative permittivity is relatively lower.

Table 6.2 Optimized conductivity and relative permittivity after calibration.

Bone structure	Optimum conductivity σ [S/m]	Optimum relative permittivity ε_γ
Cortical	0.09615	19522
Cancellous	0.14913	1561507
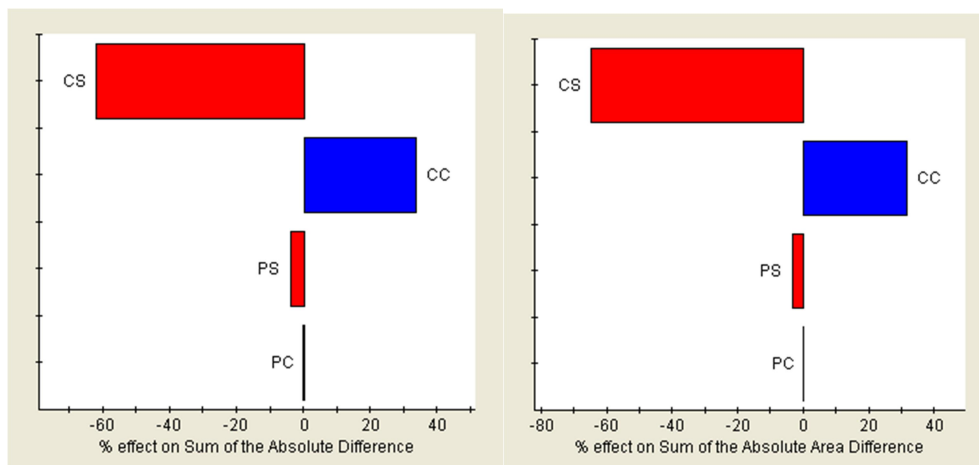
Fig. 6.15 Pareto plots of the effects of the dielectric properties on the sum of the absolute difference (left) and the sum of the absolute area difference (right), cortical conductivity (CC), cortical relative permittivity (PC), cancellous conductivity (CS), cancellous permittivity (PS).

Pareto plots demonstrate the effects of the dielectric properties on the sum of the absolute difference and sum of the absolute area difference between the experimental data set and the numerical simulation data set (Fig. 6.15). One common phenomenon between these two plots was that the conductivity of cancellous bone (CS) and cortical bone (CC) has the most effect on the results (more than 90 %). Only less than 10 % effect can be found from the

relative permittivity on both, cancellous and cortical bone. This means that at a frequency of 20 Hz, the conductivity is the most essential parameter in analysing the electric field distribution in the bone. And the conductivity of cancellous bone has the most effect on the calibration [144] due to the reason that the volume fraction of the cancellous bone is much bigger than the volume fraction of the cortical bone in a rabbit distal femur.

6.3   Discussion

6.3.1   Electro-stimulating implants for animal tests

Implant design 1 and 2 are numerically compared in the rabbit distal femur model. Design 2 has obvious advantages over design 1. No matter if considering gaps as blood or cancellous bone, in both relevant areas, implant surface and the gaps between bone and implant in the rabbit distal femur, with implant design 2 a more homogenous activated tissue electric field (5-70 V/m) distribution can be found. This is not the case with design 1.

Moreover, in implant design 2, a 150 mV peak electric potential on the electrodes is sufficient to result in a homogenous activating electric field distribution in the interesting areas. But in design 2, at least 400 mV need to be applied. Lower power consumption is important to animal testing. It results in longer battery life and produces less heat which leads to less discomfort for the animal because the power supply was inserted under the rabbit leg skin for the animal tests.

From the construction of both implant designs, design 2 also showed advantages compared to design 1. Design 1 has three different parts, two electrodes and one insulator. These three different parts need to be installed. As the size of the parts is small, they are hard to handle. This raises the risk of a short-circuit during the tests. Design 2 has one complete electrode. The wire electrodes can be easily fixed on the slots of each electrode plane. The length of the implant design 2 is 1.5 mm shorter than that of implant design 1. Due to the reason of the relatively small size of a rabbit distal femur, the smaller the implant, the easier the operation.

The numerical simulation of the rabbit femur models with the two designed electro-stimulating implants is based on some simplifications and has limitations (see 4.3). For example, considering a low electrical potential (peak potentials 400 mV and 150 mV) on the surface of the implant electrodes, the influence of electrical double layer (EDL) was not considered in all numerical simulations. In future studies, EDL should be calculated like in [135,136] and new comparisons for two implants should be made. The rabbit distal femur model is simplified only to cortical bone and cancellous bone with blood surrounding it. This simplification is reasonable as in [125] was found that only the attached surrounding tissue has the most effect on the electric field distribution in the bone. Due to the lack of sources for the cortical and cancellous rabbit distal femur bone dielectric properties at 20 Hz, in the

simulation, the computed data from Gabriel et al. [105,109] was used. Although, in the numerical simulation the rabbit distal femur cortical and cancellous bone were considered as homogenous and isotropic, in reality the structure of cancellous bone is porous and includes blood vessels. And the numerical models for both designed implants were not validated and bone dielectric properties were not calibrated.

In the current implant comparison study we only focus on the activated tissue electric field on the surface of the implant electrodes and in the gaps between implant and bone, but the influence of the electric field on the implant insulators has not been involved. In future studies, the cell experiment for bone cell growth on the surface of the insulator has to be carried out and the results have to be considered in implant design.

6.3.2 Calibration of the dielectric properties of the animal bone

A convenient approach is presented for automatic calibration of the dielectric properties of bone tissue at a specific frequency. It combines numerical modelling and experimentation. Calibration is considered to be an optimization problem and is implemented by combining the software tool iSIGHT with COMSOL. These two software products are both common and commercially available. iSIGHT is well known for its strong automatic design exploration and optimization techniques. It is widely used in industry for optimizing product design. COMSOL Multiphysics is a widely used, commercial FEA software. Furthermore, calibrating material parameters with iSIGHT in combination with Computer-aided engineering (CAE) software is also a common method. For example, Zhou et al. [145] identified constitutive parameters for composite deformation at elevated temperatures using iSIGHT and ABAQUS.

The dielectric properties of rabbit distal femur bone at 20 Hz were automatically calibrated as an example. The present study introduced an automatic calibration method for bone dielectric properties at any specific frequency. The motivation for this arises from the complex measurement method for bone dielectric properties and the need to understand electrical stimulation of bone regeneration. Although electrical stimulation used for bone healing is becoming more and more common, only limited sources of bone dielectric properties are available for numerical simulations. Therefore, this study aims to provide a convenient and reproducible method for calibrating bone dielectric properties from a specific frequency base using limited resources [105,108,109].

In contrast with complex electric measurement methods for bone dielectric properties, the presented algorithm represents an automatic calibration approach. Here, iSIGHT in combination with COMSOL is used to calibrate the bone specimen dielectric properties and to achieve the optimum values. The experimental measurement is a common process in validating numerical simulation of electrical bone stimulation. Keeping a consistent coordinate system in both the experiment and the numerical simulation is a key to the

calibration approach. Compared to complex electric measurements of bone dielectric properties, this experiment is relatively easy to implement. However, in Saha et al. [113] many factors influence the measurement of dielectric properties, such as time of exposure, moisture content and temperature. These could also be influencing factors for the presented experiment. To improve the accuracy of the experimental measurement, more experiments under different conditions should be conducted. The results could be compared and used for automatic calibration.

The current calibration process is based on available sources. As only limited sources of bone dielectric properties are available, the data range for calibration is relatively wide. The accuracy of the optimum dielectric properties can be improved when the values of bone specimen dielectric properties are available. Another possibility to improve the accuracy of calibration is to get more measuring points for both experiment and numerical simulation. But this may increase the computational effort. The size of the bone specimen should also be taken into account. Too many measuring points may destroy the bone specimen. Due to the experiment process complexity, there was only one bone specimen relied upon in the bone dielectric properties calibration. To verify the accuracy of the calibration, more bone specimens should be used in calibration in the future. The simplifications and limitations for the numerical simulation are similar to the numerical simulation for the human femoral head (see 4.3).

Combining iSIGHT with COMSOL is not only suitable for calibration of dielectric bone properties. Some electrical stimulation parameters, such as frequency and electric potential, can also be optimized using this method. Moreover, it is also applicable to many other optimization problems in bio-electrics, such as optimum electric implant design for bone electrical stimulation and optimum position of the electric implant in the bone.

7 Summary and Outlook

Electrical stimulation has been used for treatment of bone diseases for several decades. Using the Asnis III s-series screw system is a common treatment for avascular necrosis in the human femoral head using electromagnetic fields. Although it has been shown in a clinical study that 86% of the patients had a significantly improved medical condition after treatment, the influence of the stimulation parameters and the electro-stimulating implant's parameters on this clinical application have not been fully studied. Furthermore, the optimum parameters for this clinical application are still unknown. This thesis analyses the influence of the stimulation parameters and electro-stimulating implants parameters on volume tissue activated (VTA) on bone regeneration and carries out a parameter optimization for bone electrical stimulation. Three aspects have been considered to optimize the parameters, field distribution in the human femoral head, bone cell experiments and animal testing. Finite element analysis (FEA) was used to analyse how the electric field distributions in the bone and the designed in vitro setup models were influenced by the electrical stimulation and electro-stimulating implant's parameters. Combining iSIGHT with a FEA solver (COMSOL Multiphysics) was an approach to automatically optimize the parameters in models.

In human femoral head model, the effect of screw implant parameters, including screw tip design, screw insulator length and screw positioning, on the electric field distribution in the femoral head model was analysed. Screw positioning and screw insulator length brought out similar and significant effects on the VTA in the femoral head but the screw tip design did not. Moreover, an electric field distribution calculation for femoral head with surrounding tissues models was carried out for analysing effect of surrounding tissues on VTA in femoral head. The results showed that the simplification of femoral head surrounding tissues to blood was acceptable as only the attached surrounding tissue brought out the significant effect on VTA in the femoral head. Removing the necrotic lesion from the patient and let the blood fill the lesion gaps before implanting the screw is a correct procedure in surgery due to the lesion as blood having 35%more VTA than lesion as fat in the femoral head.

An automatic optimization approach was carried out for optimizing the electro-stimulation screw implant position in patient's femoral head by combining iSIGHT with COMSOL. After the optimization procedure, the screw's optimum position in the patient's femoral head model brought a 3% VTA gain compared to the original screw position derived from post-operative MRI data. The screw's z-direction positioning (moving in and out of femoral head) yields the highest effect on the VTA in patient's femoral head model.

In an animal testing, an evaluation of two designed electro-stimulating implants for animal bones could be carried out by numerical calculating the electric field distributions caused by the implants in the bone models. Implant design 2 showed obvious advantages compared to

design 1 implant after the numerical analysing in both defined areas, electric field distribution on the surface of implant and in the gap between bone and implant. An automatic calibration procedure was carried out for rabbit distal femur bone dielectric properties at 20 Hz using an optimization approach combining iSIGHT with COMSOL and an experiment. The dielectric properties of rabbit distal femur bone was calibrated and the conductivity of cancellous bone was found to have the highest effect on the calibration due to the volume fraction of cancellous bone being much bigger than the volume fraction of the cortical bone in rabbit distal femur.

In cell experiment, a design for three cell experiment systems was carried out for in vitro testing by numerically calculating electric field distribution in cell experiment's setup models. In system I, the activated tissue electric field was found to distribute in the centre area of scaffold and setup model was successfully validated by one experiment. In system II, triangular outer shape electrodes brought out the similar electric field distribution as the cylinder shaped electrodes. In system III, the optimum potential on the surface of electrode and height of scaffold have been automatically found and the electric potential has much higher effect (70%) than height of scaffold (30%) on the activated tissue electric field area on the surface of scaffold.

In the future, the surgery plan for a bone electrical stimulation therapy will be informed by the results from a numerical simulation in the bone model. Customized electro-stimulating implants for specific patients can be designed using the automatic optimization approach. More parameters can be optimized besides the ones already shown in this thesis, such as electric potential on the surface of implant, number of implants, lesion size and location. To automatically optimize the design of electro-stimulating implant in bone electrical stimulation, CAD software, i.e. Solidworks, can be integrated to the optimization approach. The validation experiment approach presented may be used as a standard process to validate a bone model for further bone electrical stimulation. Automatically calibration bone dielectric properties method will be used for at all frequencies and any bone specimen in order to use to improve bone dielectric properties accuracy in future numerical simulation. Electrical stimulation of bone will be analysed in cell experiments with bone cells to find the limit of the bone stimulation for surgery and in the design of electro-stimulation implants. The present optimization approach can also be used to design the cell experiment's setup. Furthermore, the cell experiment setups should be validated by experiments to ensure the numerical simulation model accuracy.

8 Zusammenfassung und Ausblick

Die elektrische Stimulation wird seit mehreren Jahren in der Behandlung von Knochenerkrankungen eingesetzt. Das Schraubensystem *ASNIS III S-Serie* wird bei avaskulärer Nekrose des Hüftkopfes zur Erzeugung elektromagnetischer Felder innerhalb des Knochens verwendet. Obwohl in klinischen Studien 86% der Patienten eine signifikante Verbesserung zeigten, sind die Einflüsse der Stimulationsparameter und der Parameter des Implantates auf den Behandlungserfolg noch nicht tiefgreifend erforscht. Des Weiteren sind die optimalen Stimulationsparameter für diese klinische Anwendung noch unbekannt. Die vorliegende Arbeit analysiert den Einfluss der Stimulationsparameter und der Implantatparameter auf das aktivierte Gewebevolumen (volume tissue activated, VTA) zur Knochenregeneration und führt eine Parameteroptimierung für die Elektrostimulation des Knochens durch. Drei Aspekte wurden für die Optimierung der Parameter herangezogen: Feldverteilung im Hüftkopf, Knochenzellexperimente und Tierversuche. Um zu analysieren, wie die elektrischen Feldverteilungen im Knochen und die geschaffenen in-vitro Modelle durch die Stimulations- und Implantatparameter beeinflusst werden, wurde die Finite-Element-Methode (FEM) angewandt. Mit der Software-Kombination von *iSIGHT* und einem FEM-Solver (COMSOL Multiphysics) wurde ein Ansatz gewählt, der eine automatisierte Parameteroptimierung im Modell ermöglicht.

Die auf ihren Einfluss auf die elektrische Feldverteilung im generierten Hüftkopfmodell analysierten Implantatparameter beinhalten die Form der Implantatspitze, die Länge der Isolierung und die Position des Implantats im Knochen. Dabei zeigen die Position und Isolatorlänge sowohl signifikante als auch ähnlich große Effekte auf das aktivierte Gewebevolumen im Hüftkopf, die Form der Implantatspitze jedoch nicht. Darüber hinaus wurde die elektrische Feldverteilung für das den Hüftkopf umgebende Gewebe berechnet, um den Einfluss des umgebenden Gewebes auf das aktivierte Gewebevolumen zu analysieren. Die Ergebnisse zeigen, dass es erlaubt ist, die umgebenden Gewebe (Muskel, Fett, Haut) vereinfachend als Blut zu modellieren, da nur das direkt am Knochen anliegende Gewebe einen signifikanten Einfluss auf das aktivierte Gewebevolumen hat. Bei der Implantation wird das nekrotische Gewebe entfernt und Blut füllt die entstehende Lücke. Im Unterschied zu einer fetthaltigen Läsion, führt Blut als direkt umgebendes Gewebe zu einer mehr als 35%igen Steigerung des aktivierten Gewebevolumens im Hüftkopf.

Eine automatisierte Optimierung in Bezug auf die Position des Implantats im Hüftkopf wurde mit der Kombination von iSIGHT und COMSOL durchgeführt. Im Vergleich zur post-operativen Implantatposition beim Patienten anhand von MRI-Daten, wurde durch die Optimierung eine 3%ige Steigerung des aktivierten Gewebevolumens im Hüftkopfmodell errechnet. Der Implantatparameter mit dem größten Einfluss ist die z-Richtung der Position

(entlang der Bohrung).

Für den Tierversuch am Kaninchen wurden zwei Implantatvarianten numerisch evaluiert, indem die elektrische Feldverteilung im Knochenmodell berechnet wurde. Variante 2 zeigte Vorteile gegenüber Variante 1 in den beiden definierten Bereichen bezüglich elektrischer Feldverteilung an der Oberfläche und in der Lücke zwischen Knochen und Implantat. Es wurde eine automatisierte Kalibrierungsprozedur mit dielektrischer Eigenschaft bei 20 Hz durchgeführt, indem in iSIGHT und COMSOL ein Optimierungsansatz mit einem Experiment kombiniert wurde. Die dielektrischen Eigenschaften des Kaninchenknochens wurden kalibriert und die spezifische elektrische Leitfähigkeit der Spongiosa wurde als am einflussreichsten auf die Kalibrierung bestimmt, da im Kaninchenbein Spongiosa viel ausgeprägter als Kortikalis ist.

Für das Zellexperiment wurde die elektrische Feldverteilung in drei Zellexperimentsystemen für die nachfolgenden in-vitro Tests numerisch berechnet. In System I verteilte sich das elektrische Feld im aktivierten Gewebe im Zentrum des Gerüsts. Das Modell konnte durch ein Experiment erfolgreich validiert werden. In System II führten kegelförmige Elektroden zu ähnlichen elektrischen Feldverteilungen wie zylinderförmige Elektroden. In System III wurde das optimale Potential an der Elektrodenoberfläche und die Höhe des Gerüsts automatisiert ermittelt. Das elektrische Potential hat hier einen stärkeren Einfluss (70% Gewichtung) auf die elektrische Feldfläche im aktivierten Gewebe auf der Oberfläche des Gerüsts als die Höhe des Gerüsts (30% Gewichtung).

Zukünftig könnten in die präoperative Planung für eine Elektrostimulationstherapie am Knochen die Ergebnisse der vorliegenden numerischen Simulation am Hüftknochenmodell einbezogen werden. Zudem können durch den automatisierten Optimierungsansatz Elektro-stimulationsimplantate patientenindividuell entworfen werden. Neben den in dieser Arbeit untersuchten Parametern kann z.B. nach dem elektrischen Potential an der Implantat-oberfläche, der Anzahl der Implantate, der Größe der Knochenläsion und deren Lokalisation optimiert werden. Um das Design von Elektrostimulationsimplantaten automatisch zu optimieren, kann eine CAD-Software in den Optimierungsansatz integriert werden. Um das Knochenmodell für weitere Elektrostimulation zu validieren, kann der vorgestellte experimentelle Validierungsansatz als Standardprozess verwendet werden. Die gewählte Methode, die dielektrischen Eigenschaften des Knochens automatisiert zu kalibrieren, kann für alle Frequenzen und Knochenproben verwendet werden, um die Genauigkeit künftiger numerischer Simulationen zu verbessern. Die elektrische Stimulation des Knochens kann in Zellexperimenten untersucht werden, um das obere Limit der elektrischen Stimulation zu begrenzen und im Design des Implantats zu berücksichtigen. Der vorgestellte Optimierungs-ansatz kann beim Design des experimentellen Setups benutzt werden. Des Weiteren sollten

die entwickelten Zellkultur-Setups durch Experimente validiert werden, um die Genauigkeit des numerischen Simulationsmodells sicherzustellen.

9 Publication list

- Su Y, Souffrant R, Kluess D, Ellenrieder M, Mittelmeier W, van Rienen U, Bader R. Evaluation of electric field distribution in electromagnetic stimulation of human femoral head. Bioelectromagnetics. 2014 Dec; 35(8): 547-58.

- Su Y, Kluess D, Mittelmeier W, van Rienen U, Bader R. An automatic approach for calibrating dielectric bone properties combining finite-element and optimization software tools. Computer Methods of Biomechanics and Biomedical engineering. Accepted 12/2015.

- Grunert PC, Jonitz-Heincke A, Su Y, Souffrant R, Hansmann D, Ewald H, Krüger A, Mittelmeier W, Bader R. Establishment of a novel in vitro test setup for electric and magnetic stimulation of human osteoblasts. Cell Biochem Biophys. 2014 Nov; 70(2): 805-17.

- Su Y, Kluess D, Mittelmeier W, Ellenrieder M, van Rienen U, Bader R. Optimised positioning of an electrostimulative implant in the human femoral head by an automatic modelling approach. Medical Engineering & Physics. Submitted 12/2015.

10 Bibliography

[1] Yasuda I. Fundamental aspects of fracture treatment. J Kyoto Med Soc 1953; 4: 395-406.

[2] Sharrard WJ. A double-blind trial of pulsed electromagnetic fields for delayed union of tibial fractures. J Bone Joint Surg Br 1990; 72(3): 347-55.

[3] Borsalino G, Bagnacani M, Bettati E, Fornaciari F, Rocchi R, Uluhogian S et al. Electrical stimulation of human femoral intertrochanteric osteotomies. Double-blind study. Clin Orthop Relat Res 1988; (237): 256-63.

[4] Bassett CA, Mitchell SN, Schink MM. Treatment of therapeutically resistant non-unions with bone grafts and pulsing electromagnetic fields. J Bone Joint Surg Am 1982; 64(8): 1214-20.

[5] Wahlstrom O. Stimulation of fracture healing with electromagnetic fields of extremely low frequency (EMF of ELF). Clin Orthop Relat Res 1984; (186): 293-301.

[6] Steinberg ME, Brighton CT, Corces A, Hayken GD, Steinberg DR, Strafford B et al. Osteonecrosis of the femoral head. Results of core decompression and grafting with and without electrical stimulation. Clin Orthop Relat Res 1989; (249): 199-208.

[7] Aaron RK, Boyan BD, Ciombor DM, Schwartz Z, Simon BJ. Stimulation of growth factor synthesis by electric and electromagnetic fields. Clin Orthop Relat Res 2004; (419): 30-7.

[8] Wolff J. Das Gesetz der Transformation der Knochen. Berlin: 1892.

[9] Tanck E, Homminga J, van Lenthe GH, Huiskes R. Increase in bone volume fraction precedes architectural adaptation in growing bone. Bone 2001; 28(6): 650-4.

[10] Guldberg RE, Caldwell NJ, Guo XE, Goulet RW, Hollister SJ, Goldstein SA. Mechanical stimulation of tissue repair in the hydraulic bone chamber. J Bone Miner Res 1997; 12(8): 1295-302.

[11] Frost HM. Skeletal structural adaptations to mechanical usage (SATMU): 1. Redefining Wolff's law: the bone modeling problem. Anat Rec 1990; 226(4): 403-13.

[12] Frost HM. Skeletal structural adaptations to mechanical usage (SATMU): 2. Redefining Wolff's law: the remodeling problem. Anat Rec 1990; 226(4): 414-22.

[13] Vaananen HK, Horton M. The osteoclast clear zone is a specialized cell-extracellular matrix adhesion structure. J Cell Sci 1995; 108 (Pt 8): 2729-32.

[14] Vaananen HK, Zhao H, Mulari M, Halleen JM. The cell biology of osteoclast function. J Cell Sci 2000; 113 (Pt 3): 377-81.

[15] Weinreb M, Suponitzky I, Keila S. Systemic administration of an anabolic dose of PGE2 in young rats increases the osteogenic capacity of bone marrow. Bone 1997; 20(6): 521-6.

[16] Lammens J, Liu Z, Aerssens J, Dequeker J, Fabry G. Distraction bone healing

versus osteotomy healing: a comparative biochemical analysis. J Bone Miner Res 1998; 13(2): 279-86.

[17] Asahina J, Waranabe M, Sakurai N. Repair of bone defect in primate mandible using a bone morphogenetic protein (BMP)-hydroxyapatite- collagen composite. J Med Dent Sci 1997; 44(3): 63-70.

[18] Neilsen HM, Andreassen TT, Leder T. Local injection of TGF-b increases the strength of tibial fracture in the rat. Acta Orthop Scand 1994; 65(1): 37-41.

[19] Einhorn TA. The cell and molecular biology of fracture healing. Clin Orthop Relat Res 1998; (355 Suppl): S7-21.

[20] Dimitriou R, Jones E, McGonagle D, Giannoudis PV. Bone regeneration: current concepts and future directions. BMC Med 2011; 9: 66.

[21] Aronson J. Limb-lengthening, skeletal reconstruction, and bone transport with the Ilizarov method. J Bone Joint Surg Am 1997; 79(8): 1243-58.

[22] Green SA, Jackson JM, Wall DM, Marinow H, Ishkanian J. Management of segmental defects by the Ilizarov intercalary bone transport method. Clin Orthop Relat Res 1992; (280): 136-42.

[23] Giannoudis PV, Dinopoulos H, Tsiridis E. Bone substitutes: an update. Injury 2005; 36 (Suppl 3): S20-S27.

[24] Walker NA, Denegar CR, Preische J. Low-intensity pulsed ultrasound and pulsed electromagnetic field in the treatment of tibial fractures: a systematic review. J Athl Train 2007; 42(4): 530-5.

[25] Mont MA, Hungerford DS. Non-traumatic avascular necrosis of the femoral head. J Bone Joint Surg Am 1995; 77(3): 459-74.

[26] Inoue S, Horii M, Asano T, Fujioka M, Ogura T, Shibatani M et al. Risk factors for nontraumatic osteonecrosis of the femoral head after renal transplantation. J Orthop Sci 2003; 8(6): 751-6.

[27] Griffith JF, Antonio GE, Kumta SM, Hui DS, Wong JK, Joynt GM et al. Osteonecrosis of hip and knee in patients with severe acute respiratory syndrome treated with steroids. Radiology 2005; 235(1): 168-75.

[28] Hirota Y, Hirohata T, Fukuda K, Mori M, Yanagawa H, Ohno Y, Sugioka Y. Association of alcohol intake, cigarette smoking, and occupational status with the risk of idiopathic osteonecrosis of the femoral head. Am J Epidemiol 1993; 137(5): 530-8.

[29] Mitchell MD, Kundel HL, Steinberg ME, Kressel HY, Alavi A, Axel L. Avascular necrosis of the hip: comparison of MR, CT, and scintigraphy. AJR Am J Roentgenol 1986; 147(1): 67-71.

[30] Steinberg ME, Hayken GD, Steinberg DR. A quantitative system for staging avascular necrosis. J Bone Joint Surg Br 1995; 77(1): 34-41.

[31] Cherian SF, Laorr A, Saleh KJ, Kuskowski MA, Bailey RF, Cheng EY. Quantifying the extent of femoral head involvement in osteonecrosis. J Bone Joint Surg Am

2003; 85(2): 309-15.

[32] Ficat RP. Idiopathic bone necrosis of the femoral head. Early diagnosis and treatment. J Bone Joint Surg Br 1985; 67(1): 3-9.

[33] Gardeniers JW. A new international classification of osteonecrosis of the ARCO Committee on terminology and classification. J Jpn Orthop Assoc 1992; 66: 18-20.

[34] Mont MA, Carbone JJ, Fairbank AC. Core decompression versus nonoperative management for osteonecrosis of the hip. Clin Orthop Relat Res 1996; (324): 169-78.

[35] Mont MA, Fairbank AC, Krackow KA, Hungerford DS. Corrective osteotomy for osteonecrosis of the femoral head. J Bone Joint Surg Am 1996; 78(7): 1032-8.

[36] Aldridge JM, III, Berend KR, Gunneson EE, Urbaniak JR. Free vascularized fibular grafting for the treatment of postcollapse osteonecrosis of the femoral head. Surgical technique. J Bone Joint Surg Am 2004; 86(Suppl 1): 87-101.

[37] Ellenrieder M, Tischer T, Kreuz PC, Frohlich S, Fritsche A, Mittelmeier W. [Arthroscopically assisted therapy of avascular necrosis of the femoral head]. Oper Orthop Traumatol 2013; 25(1): 85-94.

[38] Habel B. Elektrische Stimulation von Zellen und Geweben am besonderen Beispiel von Knochenzellen. 2004. Ref Type: Thesis/Dissertation

[39] Fukada E YI. On the piezoelectric effect of bone. Phys Soc Jpn 1957; 12: 1158-62.

[40] Kesani AK, Gandhi A, Lin SS. Electrical bone stimulation devices in foot and ankle surgery: types of devices, scientific basis, and clinical indications for their use. Foot Ankle Int 2006; 27(2): 148-56.

[41] Friedenberg ZB, Brighton CT. Bioelectric potentials in bone. J Bone Joint Surg Am 1966; 48(5): 915-23.

[42] Gjelsvik A. Bone remodeling and piezoelectricity. II. J Biomech 1973; 6(2): 187-93.

[43] Gjelsvik A. Bone remodeling and piezoelectricity. I. J Biomech 1973; 6(1): 69-77.

[44] Bassett CA. Pulsing electromagnetic fields: a new method to modify cell behavior in calcified and noncalcified tissues. Calcif Tissue Int 1982; 34(1): 1-8.

[45] Soda A, Ikehara T, Kinouchi Y, Yoshizaki K. Effect of exposure to an extremely low frequency-electromagnetic field on the cellular collagen with respect to signaling pathways in osteoblast-like cells. J Med Invest 2008; 55(3-4): 267-78.

[46] Fredericks DC, Nepola JV, Baker JT, Abbott J, Simon B. Effects of pulsed electromagnetic fields on bone healing in a rabbit tibial osteotomy model. J Orthop Trauma 2000; 14(2): 93-100.

[47] Goodwin CB, Brighton CT, Guyer RD, Johnson JR, Light KI, Yuan HA. A double-blind study of capacitively coupled electrical stimulation as an adjunct to lumbar spinal fusions. Spine 1999; 24(13): 1349-56.

[48] Baranowski TJ, Black J. The mechanism of faradic stimulation of osteogenesis.

Mechanistic Approaches to Interactions of Electric and Electromagnetic Fields with Living Systems. 1987; 399-416.

[49] Haddad JB, Obolensky AG, Shinnick P. The biologic effects and the therapeutic mechanism of action of electric and electromagnetic field stimulation on bone and cartilage: new findings and a review of earlier work. J Altern Complement Med 2007; 13(5): 485-90.

[50] Griffin M, Bayat A. Electrical stimulation in bone healing: critical analysis by evaluating levels of evidence. Eplasty 2011; 11: e34.

[51] Aaron RK, Ciombor DM, Simon BJ. Treatment of nonunions with electric and electromagnetic fields. Clin Orthop Relat Res 2004; (419): 21-9.

[52] Brighton CT, Friedenberg ZB, Mitchell EI, Booth RE. Treatment of nonunion with constant direct current. Clin Orthop Relat Res 1977; (124): 106-23.

[53] Bassett CA, Herrmann I. Influence of oxygen concentration and mechanical factors on differentiation of connective tissues in vitro. Nature 1961; 190: 460-1.

[54] Bodamyali T, Kanczler JM, Simon B, Blake DR, Stevens CR. Effect of faradic products on direct current-stimulated calvarial organ culture calcium levels. Biochem Biophys Res Commun 1999; 264(3): 657-61.

[55] Brighton CT, Adler S, Black J, Itada N, Friedenberg ZB. Cathodic oxygen consumption and electrically induced osteogenesis. Clin Orthop Relat Res 1975; (107): 277-82.

[56] Brighton CT, Ray RD, Soble LW, Kuettner KE. In vitro epiphyseal-plate growth in various oxygen tensions. J Bone Joint Surg Am 1969; 51(7): 1383-96.

[57] Cho M, Hunt TK, Hussain MZ. Hydrogen peroxide stimulates macrophage vascular endothelial growth factor release. Am J Physiol Heart Circ Physiol 2001; 280(5): H2357-H2363.

[58] Steinbeck MJ, Kim JK, Trudeau MJ, Hauschka PV, Karnovsky MJ. Involvement of hydrogen peroxide in the differentiation of clonal HD-11EM cells into osteoclast-like cells. J Cell Physiol 1998; 176(3): 574-87.

[59] Gan J, Fredericks D, Glazer P. Direct current and capacitive coupling electrical stimulation upregulates osteopromotive factors for spinal fusions. Orthop J Harvard Med School 2004; 6: 57-59..

[60] Wang Q, Schizen Z, Xie Y. Electrochemical reactions during constant DC current stimulation: an in vitro experiment with cultured rat calvarial cell. Electro Magnetobiol 1995; 14: 31-40.

[61] Brighton CT, Black J, Friedenberg ZB, Esterhai JL, Day LJ, Connolly JF. A multicentre study of the treatment of non-union with constant direct current. J Bone Joint Surg Am 1981; 63(1): 2-13.

[62] Brighton CT, Pollack SR. Treatment of recalcitrant non-union with a capacitively coupled electrical field. A preliminary report. J Bone Joint Surg Am 1985; 67(4): 577-85.

[63] Colson DJ, Browett JP, Fiddian NJ, Watson B. Treatment of delayed- and non-union of fractures using pulsed electromagnetic fields. J Biomed Eng 1988; 10(4): 301-4.

[64] Aaron RK, Steinberg ME. Electrical stimulation of osteonecrosis of the femoral head. Semin Arthroplasty 1991; 2(3): 214-21.

[65] Gan JC, Glazer PA. Electrical stimulation therapies for spinal fusions: current concepts. Eur Spine J 2006; 15(9): 1301-11.

[66] Brighton CT, Wang W, Seldes R, Zhang G, Pollack SR. Signal transduction in electrically stimulated bone cells. J Bone Joint Surg Am 2001; 83(10): 1514-23.

[67] Lorich DG, Brighton CT, Gupta R, Corsetti JR, Levine SE, Gelb ID et al. Biochemical pathway mediating the response of bone cells to capacitive coupling. Clin Orthop Relat Res 1998; (350): 246-56.

[68] Adey WR. Biological effects of electromagnetic fields. J Cell Biochem 1993; 51(4): 410-6.

[69] Diniz P, Shomura K, Soejima K, Ito G. Effects of pulsed electromagnetic field (PEMF) stimulation on bone tissue like formation are dependent on the maturation stages of the osteoblasts. Bioelectromagnetics 2002; 23(5): 398-405.

[70] Bassett CA, Pawluk RJ, Pilla AA. Augmentation of bone repair by inductively coupled electromagnetic fields. Science 1974; 184(4136): 575-7.

[71] Bassett C.A. Biomedical implications of pulsing electromagnetic fields. Surg Rounds 1983; 22-31.

[72] Aaron RK, Ciombor DM, Jolly G. Stimulation of experimental endochondral ossification by low-energy pulsing electromagnetic fields. J Bone Miner Res 1989; 4(2): 227-33.

[73] Ciombor DM, Aaron RK. Influence of electromagnetic fields on endochondral bone formation. J Cell Biochem 1993; 52(1): 37-41.

[74] Aaron RK, Ciombor DM. Therapeutic effects of electromagnetic fields in the stimulation of connective tissue repair. J Cell Biochem 1993; 52(1): 42-6.

[75] Skerry TM, Pead MJ, Lanyon LE. Modulation of bone loss during disuse by pulsed electromagnetic fields. J Orthop Res 1991; 9(4): 600-8.

[76] Tabrah F, Hoffmeier M, Gilbert F, Jr., Batkin S, Bassett CA. Bone density changes in osteoporosis-prone women exposed to pulsed electromagnetic fields (PEMFs). J Bone Miner Res 1990; 5(5): 437-42.

[77] Bassett CA. Beneficial effects of electromagnetic fields. J Cell Biochem 1993; 51(4): 387-93.

[78] Glassman LS, McGrath MH, Bassett CA. Effect of external pulsing electromagnetic fields on the healing of soft tissue. Ann Plast Surg 1986; 16(4): 287-95.

[79] Ieran M, Zaffuto S, Bagnacani M, Annovi M, Moratti A, Cadossi R. Effect of low frequency pulsing electromagnetic fields on skin ulcers of venous origin in humans:

a double-blind study. J Orthop Res 1990; 8(2): 276-82.

[80]   Trock DH, Bollet AJ, Dyer RH, Jr., Fielding LP, Miner WK, Markoll R. A double-blind trial of the clinical effects of pulsed electromagnetic fields in osteoarthritis. J Rheumatol 1993; 20(3): 456-60.

[81]   Otter MW, McLeod KJ, Rubin CT. Effects of electromagnetic fields in experimental fracture repair. Clin Orthop Relat Res 1998; (355 Suppl): S90-104.

[82]   McLeod KJ, Rubin CT. Frequency specific modulation of bone adaptation by induced electric fields. J Theor Biol 1990; 145(3): 385-96.

[83]   McLeod KJ, Rubin CT. The effect of low-frequency electrical fields on osteogenesis. J Bone Joint Surg Am 1992; 74(6): 920-9.

[84]   Akai M, Yabuki T, Tateishi T, Shirasaki Y. Mechanical properties of the electrically stimulated callus. An experiment with constant direct current in rabbit fibulae. Clin Orthop Relat Res 1984; (188): 293-302.

[85]   Law HT, Annan I, McCarthy ID, Hughes SP, Stead AC, Camburn MA, Montgomery H. The effect of induced electric currents on bone after experimental osteotomy in sheep. J Bone Joint Surg Br 1985; 67(3): 463-9.

[86]   Miller GJ, Burchardt H, Enneking WF, Tylkowski CM. Electromagnetic stimulation of canine bone grafts. J Bone Joint Surg Am 1984; 66(5): 693-8.

[87]   Pienkowski D, Pollack SR, Brighton CT, Griffith NJ. Comparison of asymmetrical and symmetrical pulse waveforms in electromagnetic stimulation. J Orthop Res 1992; 10(2): 247-55.

[88]   Kraus W, Lechner F. [Healing of pseudoarthrosis and spontaneous fractures with structure-forming electrodynamic potentials]. Munch Med Wochenschr 1972; 114(42): 1814-9.

[89]   Kraus W. Magnetfeldtherapie und magnetisch induzierte Elektrostimulation in der Orthöpädie (Magnetic induced electrostimulation in orthopadis). Der Orthopäde 1984; 13(2): 78-92.

[90]   Krüger T, Hein W, Plitz W, Ettinger C, Gräfe G, Reichel H. Einfluss der magnetisch induzierten Elektrostimulation (MIES) auf die Klausfestigkeit nach Distraktion der Schafstibia (Callus Stability Following Magnetically induced Electrostimulation (MIES) in the Sheep Tibia). Osteologie 2000; 157-64.

[91]   Ascherl R. Experimentelle Untersuchungen uber den elektrischen Widerstand und den Leitwert am lebenden und toten Knochengewebe unter physiologischen Bedingungen sowie nach pathologischen Veränderungen. 1976. Technische Universität Munich. Ref Type: Thesis/Dissertation

[92]   Kraus W. Zur Biophysik der Knochenbruch — und Wundbehandlung durch funktionelle electrische und magnetische Potentiale [The biophysics of bone fracture treatment and wound treatment by means of functional electric and magnetic potentials (author's transl)]. Langenbeckes 1974; 337: 625-30.

[93]   Blümlein H, McDaniel JM, Perren SM. Effect of the Magnetic Field Component of the Kraus-Lechner Method on the Healing of Experimental Nonunions in Dogs.

Electric stimulation of bone growth and repair. 1978; 41-4.

[94] Gerber H, Cordey J, Perren SM. Influence of magnetic fields on growth and regeneration in organ culture. Langenbecks Arch Chir 1976; 286-91.

[95] Grunert PC, Jonitz-Heincke A, Su Y, Souffrant R, Hansmann D, Ewald H et al. Establishment of a Novel In Vitro Test Setup for Electric and Magnetic Stimulation of Human Osteoblasts. Cell Biochem Biophys 2014.

[96] Mittelmeier W, Lehner S, Kraus W, Matter HP, Gerdesmeyer L, Steinhauser E. BISS: concept and biomechanical investigations of a new screw system for electromagnetically induced internal osteostimulation. Arch Orthop Trauma Surg 2004; 124(2): 86-91.

[97] Steinberg ME, Steinberg DR. Classification systems for osteonecrosis: an overview. Orthop Clin North Am 2004; 35(3): 273-viii.

[98] van Rienen U. Numerical Methods in Computational Electrodynamics. Berlin Heidelberg: 2001.

[99] Maxwell JC. A Dynamical Theory of the Electromagnetic Field. Phil Trans R Soc Lond 1865; 155: 459-512.

[100] Haus HA, Melcher JR. Electromagnetic Fields and Energy. New Jersey: Prentice Hall. 1989.

[101] Jackson J.D. Klassische Electrodynamik. Berlin: 1999.

[102] Bondeson A, Rylander T, Ingelstroem P. Computational Electromagnetics. USA: Springer. 2005.

[103] Cai K, Frant M, Bossert J, Hildebrand G, Liefeith K, Jandt KD. Surface functionalized titanium thin films: zeta-potential, protein adsorption and cell proliferation. Colloids Surf B Biointerfaces 2006; 50(1): 1-8.

[104] Kosterich JD, Foster KR, Pollack SR. Dielectric permittivity and electrical conductivity of fluid saturated bone. IEEE Trans Biomed Eng 1983; 30(2): 81-6.

[105] Gabriel S, Lau RW, Gabriel C. The dielectric properties of biological tissues: II. Measurements in the frequency range 10 Hz to 20 GHz. Phys Med Biol 1996; 41(11): 2251-69.

[106] Schwan HP. Electrical properties of tissue and cell suspensions. Adv Biol Med Phys 1957; 5: 147-209.

[107] Grimnes S, Martinsen QG. Bioimpedance and bioelectricity basics. San Diego: 2000.

[108] Gabriel C, Gabriel S, Corthout E. The dielectric properties of biological tissues: I. Literature survey. Phys Med Biol 1996; 41(11): 2231-49.

[109] Gabriel S, Lau RW, Gabriel C. The dielectric properties of biological tissues: III. Parametric models for the dielectric spectrum of tissues. Phys Med Biol 1996; 41(11): 2271-93.

[110] Cole KS, Cole R. Dispersion and Absorption in Dielectrics I. Alternating Current Characteristics. The Journal of Chemical Physics 1941; 9(4): 341-51.

[111] Cole KS, Cole R. Dispersion and Absorption in Dielectrics II. Direct Current Characteristics. The Journal of Chemical Physics 1942; 10(2): 98-105.

[112] Gabriel S. Modelling the frequency dependence of the dielectric properties to a 4 dispersions spectrum. 1997. Ref Type: Online Source

[113] Saha S, Reddy GN, Albright JA. Factors affecting the measurement of bone impedance. Med Biol Eng Comput 1984; 22(2): 123-9.

[114] Peyman A. Dielectric properties of tissues; variation with age and their relevance in exposure of children to electromagnetic fields; state of knowledge. Prog Biophys Mol Biol 2011; 107(3): 434-8.

[115] Sierpowska J, Hakulinen MA, Toyras J, Day JS, Weinans H, Kiviranta I et al. Interrelationships between electrical properties and microstructure of human trabecular bone. Phys Med Biol 2006; 51(20): 5289-303.

[116] Sierpowska J, Lammi MJ, Hakulinen MA, Jurvelin JS, Lappalainen R, Toyras J. Effect of human trabecular bone composition on its electrical properties. Med Eng Phys 2007; 29(8): 845-52.

[117] Sun W, Starly B, Nam J, Darling A. Bio/CAD modeling and its applications in computer-aided tissue engineering. Computer-Aided Design 2005; 37: 1097-114.

[118] Mankovich NJ, Robertson DR, Cheeseman AM. Three-dimensional image display in medicine. J Digit Imaging 1990; 3(2): 69-80.

[119] Frounchi K, Briand LC, Grady L, Labinche Y, Subramanyan R. Automating image segmentation verification and validation by learning test oracles. Inform Softw Technol 2011.

[120] Kluess D, Souffrant R, Mittelmeier W, Wree A, Schmitz KP, Bader R. A convenient approach for finite-element-analyses of orthopaedic implants in bone contact: modeling and experimental validation. Comput Methods Programs Biomed 2009; 95(1): 23-30.

[121] Gray H. Anatomy of the Human Body. 2000. New York. bartleby.com Ref Type: Online Source

[122] Jorgensen TE. Electrical stimulation of human fracture healing by means of a slow pulsating, asymmetrical direct current. Clin Orthop Relat Res 1977; (124): 124-7.

[123] Prodanovic M, Malesevic M, Filipovic T, Tevtic T, Bijelic G, Malesevic N. Numerical Simulation of the Energy Distribution Biological Tissues During Electrical Stimulation. Serbian Journal of Electrical Engineering 2014; 10(1): 165-73.

[124] Sierpowska J, Toyras J, Hakulinen MA, Saarakkala S, Jurvelin JS, Lappalainen R. Electrical and dielectric properties of bovine trabecular bone—relationships with mechanical properties and mineral density. Phys Med Biol 2003; 48(6): 775-86.

[125] Su Y, Souffrant R, Kluess D, Ellenrieder M, Mittelmeier W, van Rienen U, Bader R. Evaluation of electric field distribution in electromagnetic stimulation of human

femoral head. Bioelectromagnetics 2014; 35(8): 547-58.

[126] Saha S, Williams PA. Electric and dielectric properties of wet human cancellous bone as a function of frequency. Ann Biomed Eng 1989; 17(2): 143-58.

[127] Schittkowski K, NLPQL: A Fortran subroutine for solving constrained nonlinear programming problems. Annals of Operations Research 1985; 5: 485-500.

[128] Miller CE, Henriquez CS. Finite element analysis of bioelectric phenomena. Crit Rev Biomed Eng 1990; 18(3): 207-33.

[129] Isaacson BM, Stinstra JG, Bloebaum RD, Pasquina PF, MacLeod RS. Establishing multiscale models for simulating whole limb estimates of electric fields for osseointegrated implants. IEEE Trans Biomed Eng 2011; 58(10): 2991-4.

[130] Kocbach J, Folgero K, Mohn L, Brix O. A Siimulation Approach to Optimizing Performance of Equipment for Thermostimulation of Muscle Tissue using COMSOL Multiphysics. Biophysics &Bioeng Letters 2011; 4(2): 9-33.

[131] Reichel M, Martinek J. Simulation of the electrical field in equine larynx to optimize functional electrical stimulation in denervated musculus cricoarythenoideus dorsalis. Eur J Trans Myol- -Basic Appl Myol 2014; 24(2): 181-5.

[132] Potratz C, Kluess D, Ewald H, van Rinen U. Multiobjective optimization of an electrostimulative acetabular revision system. IEEE Trans Biomed Eng 2010; 57(2): 460-8.

[133] Andreaus U, Colloca M, Iacoviello D. Optimal bone density distributions: numerical analysis of the osteocyte spatial influence in bone remodeling. Comput Methods Programs Biomed 2014; 113(1): 80-91.

[134] Yang X, Fan Q. Simulation and Optimization of Eddy-Current Senson Based on COMSOL and iSIGHT. Measurement & Control Technology 2011; 30(8): 7-10.

[135] Ekaterian Gongadze. Influence of the surface sturcture of a Biomaterial on the field distribution in the neighbouring biosystem. 2011. University of Rostock.
Ref Type: Thesis/Dissertation

[136] Potratz Carsten. Zur Optimierung electrostimulativer Hüftgelenksimplantate mit externer magnetischer Anregung. 2011. University of Rostock.
Ref Type: Thesis/Dissertation

[137] Williams PA, Saha S. The electrical and dielectric properties of human bone tissue and their relationship with density and bone mineral content. Ann Biomed Eng 1996; 24(2): 222-33.

[138] Schmidt C, Grant P, Lowery M, van Rienen U. Influence of uncertainties in the material properties of brain tissue on the probabilistic volume of tissue activated. IEEE Trans Biomed Eng 2013; 60(5): 1378-87.

[139] Isaacson BM, Bloebaum RD. Bone bioelectricity: what have we learned in the past 160 years? J Biomed Mater Res A 2010; 95(4): 1270-9.

[140] Qu C, Qin QH, Kang Y. A hypothetical mechanism of bone remodeling and

modeling under electromagnetic loads. Biomaterials 2006; 27(21): 4050-7.

[141] Fordyce MJ, Solomon L. Early detection of avascular necrosis of the femoral head by MRI. J Bone Joint Surg Br 1993; 75(3): 365-7.

[142] Nagatani Y, Mizuno K, Saeki T, Matsukawa M, Sakaguchi T, Hosoi H. Numerical and experimental study on the wave attenuation in bone--FDTD simulation of ultrasound propagation in cancellous bone. Ultrasonics 2008; 48(6-7): 607-12.

[143] Mizuno K, Nagatani Y, Yamashita K, Matsukawa M. Propagation of two longitudinal waves in a cancellous bone with the closed pore boundary. J Acoust Soc Am 2011; 130(2): EL122-EL127.

[144] Christian Schmidt. Uncertainty quantification in a computationally optimised volume conductor model for deep brain stimulation. 2013. University of Rostock.
Ref Type: Thesis/Dissertation

[145] Zhou J, Qi L, Chen G. New inverse method for identification of constitutive parameters. Transactions of Nonferrous Metals Society of China 2006; 16(1): 148-52.

11 Tables and figures

107

Acronyms

ARCO	Association Research Circulation Osseous
ASCII	American Standard Code for Information Interchange
BMP	bone morphogenetic protein
CAD	computer aid design
CAE	Computer-aided engineering
CC	capacitive coupling
CT	computed tomography
DC	direct current
DOE	design of experiment
DoF	degrees of freedom
ECM	extracellular matrix
EDL	Electrical double layer
EQS	electro-quasistatic
FEM	finite element method
FIT	finite integration method
GMRES	generalized minimal residual method
IC	inductive coupling
IGES	International Graphics Exchange Standard
IGF	insulin-like growth factor
MRI	magnetic resonance imaging
NURBS	Non-Uniform Rational B-spline
PDGF	platelet derived growth factor
PEMF	pulsed electromagnetic fields
RMS	root mean square
SARS	severe acute respiratory syndrome
STEP	Standard for Exchange of Product
STL	Stereolithography
TGF /ß	transforming growth factor beta
VTA	volume of tissue activated

Theses

1. Clinical application shows that the growth of bone can be affected by a low-frequency electric field.

2. Avascular necrosis, often named osteonecrosis, is a bone disease caused by death of bone cells and primarily affects weight-bearing joints.

3. A suitable low frequency sinusoid electric field in the bone can be generated by Asnis III s-series screw system which consists of one screw with two electrodes and embedded coils and external primary coil outside of bone. Asnis III s-series screw system can only be used to treat early stage of avascular necrosis in femoral head.

4. Electric field distribution caused by Asnis III s-series screw system in bone can be calculated by electro-quasistatic equation.

5. FEA is a favourite approach for the numerical solution of electromagnetic field problems in bone as it can deal with complex bone geometry.

6. Electric properties of bone and electro-stimulating implant, like relative permittivity ϵ_r and electric conductivity σ are crucial parameters for evaluation electric field distribution in the bone caused by electrical stimulation.

7. Bone tissue is an inhomogeneous composite material with fluid-filled pores and it is anisotropic in its structure. The dielectric properties of bone are varied at different frequency range.

8. The results of present numerical simulations underline that the electro-stimulation treatment of bone structures in clinical applications can be influenced by the implant parameters.

9. Comparing to screw tip design, screw positioning and screw insulator length of the Asnis III s-series screw system brought out similar and significant effects on the volume tissue activated (VTA) in the human femoral head

10. Moving the necrotic lesion out from the patient and filling the blood in the lesion gaps before implanting the screw to patient is a correct procedure in surgery due to the reason that the lesion as blood can bring out more than 35% VTA than lesion as fat in the patients femoral head.

11. Combining iSIGHT with a FEA solver (COMSOL Multiphysics) is a convenient approach to automatically optimize the parameters bone electrical stimulation.

12. Moving Asnis III s-series screw implant within femoral head can result in the significant effects in the VTA in patients femoral head model.

13. Bone dielectric properties at any frequency can be automatically calibrated by an optimization approach, combining iSIGHT with COMSOL, using experimental data.

14. For animal tests electric field distribution on the surface of implant and in the gap between bone and implant different designs of electro-stimulating implant showed obviously differences at both defined areas in the numerical simulations.

15. Prior numerical simulation is a necessary step for designing the in vitro setup for cell experiments. It can give an insight of electric field distribution in the cell chamber and it helps cell experiment save the establishing time caused by inappropriate design.

Acknowledgement

I want to express my deep foremost gratitude to my supervisors, friends, and family who helped me with their advice and support during these years. I am truly grateful to my supervisor Prof. Dr. Rainer Bader. Without him this study could not be completed. His invaluable guidance and constant support in all times of need and his advice improved the quality of this work. I sincerely thank Prof. Dr. Wolfram Mittelmeier for his support and Prof. Dr. Ursula van Rienen for her valuable supervision from my master's to this PhD study.

I want to give thanks to my great colleagues at the Biomechanics and Implant Technology Research Laboratory (Department of Orthopaedics) for the wonderful work environment. Special thanks to work group 'Numerical simulation and implant technology' for the professional support. My sincere thanks go to Dr. Catherine Ebner and Carolin Gabler, MSc. for the great atmosphere in the office and many cheerful moments.

I wish to express my gratitude to all my co-workers, Dipl.-Ing. Robert Souffrant, PD Dr. Daniel Klüß, Dr. Martin Ellenrieder, Dr. Philip Grunert and Dr. Anika Jonitz-Heincke.

I am deeply grateful to my parents Zaichao Su and Anxia Zhang and my sister Yujie Su and my brother Yubing Su for their endless trust and love in me. I would also like to thank my parents-in-law Karin and Gerald Paul for their endless love. Finally, I would like to express my sincere gratitude to my loved husband Stephan Paul, my son John Chunlei Paul and my daughter Zoe Chunyal Paul who constantly support me.

Declaration

I, the undersigned, hereby declare that the work contained in this dissertation is my own original work and that I have not previously in its entirety or in part submitted it at any university for a degree.

Rostock,

Yukun Su